SYNTHESIS OF TITANIA NANOPARTICLES AND ITS APPLICATION FOR PHOTOCATALYTIC DEGRADATION OF POLLUTANTS FROM AQUEOUS SOLUTIONS

BY

Mousab Salah Eldeen Mirghani Mohammed

A Dissertation Presented to the

DEANSHIP OF GRADUATE STUDIES

KING FAHD UNIVERSITY OF PETROLEUM & MINERALS

DHAHRAN, SAUDI ARABIA

In Partial Fulfillment of the

Requirements for the Degree of

DOCTOR OF PHILOSOPHY

In

Chemical engineering

May 2012

KING FAHD UNIVERSITY OF PETROLEUM & MINERALS

DHAHRAN 31261, SAUDI ARABIA

DEANSHIP OF GRADUATE STUDIES

This dissertation, written by **MOUSAB SALAH ELDEEN MIRGHANI** under the direction of his dissertation advisor and approved by his dissertation committee, has been presented to and accepted by the Dean of Graduate Studies, in partial fulfillment of the requirements for the degree of **DOCTOR OF PHILOSOPHY IN CHEMICAL ENGINEERING.**

Dissertation committee

Dr. Reyad A. Shawabkeh (Advisor)

Dr. Ibnelwaleed A. Hussein (Member)

Dr. Naim M. Faqir (Member)

Dr. Adnan A. Al-Amer (Member)

Dr. Tahar Laoui (Member)

Dr. Usamah A. Al-Mubaiyedh
Department Chairman

Dr. Salam A. Zummo
Dean of Graduate Studies

27/6/12

Date

DEDICATION

This work is dedicated to my family for their continuous support through the good and bad times. It is also dedicated to my supervisor, Dr. Shawabkeh, and my friends for motivations and continuous support, in many different ways.

ACKNOWLEDGMENT

All thanks to Allah, almighty for his guidance and bless for me to be able to complete this work. In addition, Appreciation is for King Fahd University of Petroleum and Minerals for giving me the chance to attain my PhD degree.

I would like to express my deep gratitude to my supervisor, Dr. Reyad Shawabkeh for his guidance, patience, and support all the time. It has been a great pleasure for me to work with him. Moreover, I would like to thank my committee members, Prof. I. Hussein, Prof. A.Al-Amer, Prof. N. Faqir and Dr. T. Laoui for their recommendations and support and Dr. Usama Al-Mubeiyedh for helping in the kinetics model development and solution.

gratitude's are extended to KACST for funding this project, members of chemical and mechanical engineering departments, graduate studies and my friends and colleagues for their technical support.

TABLE OF CONTENTS

LIST OF TABLES

LIST OF FIGURES

NOMENCLATURE

A	Catalyst surface area (cm^3).
b	Langmuir isotherm coefficient (L/g)
C, C_e, C_o	Bulk, equilibrium and initial concentration of heavy metal, respectively (mg/L)
I	UV - Light intensity (W)
k_f	Mass transfer coefficient (cm/s)
k_{rxn}	Reaction rate constant (cm.g/W.s)
m	Reaction order with respect to UV intensity
m_s	Concentration of sludge in solution (g/L)
M	Catalyst mass (g)
n	Reaction order with respect to solid-phase concentration
q, $q_{e,}$ q_{max}	Solid phase, equilibrium and maximum concentration of heavy metals (mg/g)
R	Particle radius (cm)
S	Stirring speed (rpm)
T	Temperature (^oC)
V	Volume of solution (cm^3)
α	Specific surface area of catalyst (cm^{-1})
ε	Porosity of catalyst
ρ_p	Particle density (g/cm^3)

THESIS ABSTRACT

FULL NAME OF STUDENT	Mousab Salah Eldeen Mirghani Mohammed
TITLE OF STUDY	Synthesis of titania nanoparticles and its applications for photocatalytic degradation of pollutants from aqueous solutions.
MAJOR FIELD	Chemical Engineering
DATE OF DEGREE	April 2012

Sol-gel method was used to synthesize pure and metal-doped TiO_2 nanoparticles. The optimum experimental conditions for synthesis of pure nanocrystalline TiO_2 were found by Analysis of Variance (ANOVA). These experimental parameters include the amount of water, type of acid, acid concentration and ultrasonication duration. Three transition metals including tungsten, vanadium and iron were selected for doping of titanium dioxide at the optimum conditions.

All types of catalysts were characterized by Scanning Electron Microscopy (SEM), which has shown spherical shape of particles for the samples obtained at the optimum conditions. the average diameter of these particles was found to be ranging from 6-14 nm as measured by Particle Size Analyzer (PSA). X-Ray Diffraction (XRD) analysis was carried out in order to investigate the phase of catalysts, which was found to be mainly anatase for all samples calcined at 450^oC. The percentage of metals doped on titanium dioxide was measured by Elementary Dispersive Spectroscopy (EDS), which is found to be 2.7%, 1.8% and 1% for tungsten, vanadium and iron, respectively, and the effect of incorporating these transition metals onto

titanium dioxide was resulted in the significant increasing of the surface are as measured by (BET).

The photocatalytic activities of these catalysts were investigated by measuring the degradation of methylene blue from aqueous solutions. It was reported that, doping of these transition metals has increased the catalyst maximum uptake 11.5 mg/g for pure titanium dioxide to 17.4 mg/g for V-doped titanium dioxide, 25.6 mg/g for Fe-doped titanium dioxide and 20.8 mg/g for W-doped titanium dioxide. These metal-doped titanium dioxide were further applied for removal of Pb(II), Zn(II), and Cd(II) from aqueous solutions, and it was found that, the highest removal percentage of Pb(II) was achieved by W-doped titanium dioxide, while Fe-doped titanium dioxide and V-doped titanium dioxide performed better for removal of Zn(II) and Cd(II) respectively. The kinetics of photocatalytic degradation of these heavy metals was carried out, where the maximum degradation percentages were found to be 4^{o}C, at dosage of 1 g of catalyst, stirring speed of 600 rpm, and initial concentration of 25 ppm.

ملـخص الرســـالة

الاســـــــــــم: **مصعب صلاح الدين ميرغني.**

عنوانالرسالة: **إنتاج حبيبات التيتانيوم النانويه وتطبيقاتها في إزالةالتلوث من المحاليل المائية.**

التخصـــــص: **الهندسة الكيميائية.**

تاريخالتخـرج: **ابريل 2012.**

تم إنتاج حبيبات اكسيد التيتانيوم النانويه بواسطة عملية المحاليل الجلاتينيه وتم الحصول علي الظرف الامثل للانتاج بواسطة تحليل المتغيرات وتم تطعيم حبيبات التيتانيوم النانويه بثلاث عناصر انتقالية وهي التنقستون، الفاناديوم،والحديد.

تم تحليل جميع الحفازات بواسطة المسح الالكتروني الذي اظهر مشكلا كرويا للحبيبات بقطر يتراوح بين6-14 نانوميتر، والذي قيس بواسطة جهاز تحليل الحجم. تم عمل التحليل بواسطة الاشعة السينية لتبين نوع الطور، بينما اظهر تحليل تشتيت الطاقه كمية المواد في كل عينة، وقد وجد انه في حدود 2.7% للتنقستون، 1.8% للفاناديوم، و 1% للحديد.

تم التحقق من النشاط الحفزي الضوئي لجميع المواد المنتجة بواسطة إزالةالمثلين الازرقمن الماء، ووجد أن إضافة العناصر الانتقالية قد زاد من فاعلية الحفاز في الازال' من 11.5% للحفاز النقي الي 17.4% للحفاز المطعم بالفاناديوم ، و 25.6% للحفاز المطعم بالتنقستون ، و20.8% للحفاز المطعم بالحديد.

جميع هذه المواد تم استخدامها لازالة الرصاص، الزنك، والكادميوم من المحاليل المائية، وتم التحقق من النشاط الضوئي في ظروف عملية مختلفة تشمل درجة الحرارة، كمية الحفاز المضاف، التركيز الابتدائي، وسرعة التحريك الدائرية.

CHAPTER 1

INTRODUCTION

In recent years, semiconductors have gained major attention in a vast number of physical and chemical applications such as devices manufacturing and modern electronics. This is because of the unique properties of these materials, including the band gab energy, surface area, pore volume and optical properties.

Among semiconductors, titanium dioxide, which is a white pigment with band gab energy of 3.2 eV, that has been used intensively in many industrial applications such as optical coating, optoelectronic devices manufacturing, catalysts support and photocatalysis. This wide range of applications comes as a result of its efficient catalytic activity, photosensitivity, non-toxicity and physical and chemical stability. When irradiated with UV light with energy higher than its band gab, it ejects an electron from the valence band to the conduction band on its surface, which reacts with electron accepter. This ejection of electrons creates a hole (h+) in the valence band that leads to formation of highly reactive hydroxyl radicals by (h+). In addition, titanium dioxide has many superior characteristics such as UV shielding capability which makes it an excellent prominent photocatalyst.

Generally, the photocatalytic activity of titanium dioxide is affected by the surface area, pores size and volume, the phase of the solid material and the band gab energy. Therefore, in order to enhance this photocatalytic activity, it is inevitable to increase the surface area and pore volume

of titanium dioxide, where it is hard to control the band gab energy. Thus, nano-level synthesized titanium dioxide can offer a significant improvement of photocatalytic performance.

Several synthetic routes including chemical vapor deposition, hydrolysis, micro-emulsion, template hydrothermal, sputtering and sol–gel synthesis are utilized for the synthesis of nanocrystalline titanium dioxide, and the choice of any of these methods depends on the required properties of the final catalyst and its applications[1-3].

The most commonly used techniques for synthesis of titanium dioxide and other semiconductors are:

- Chemical vapor deposition (CVD): in this process, a substrate is exposed to precursor s with higher relative volatility to allow the decomposition on the surface of substrate to produce the desired materials. The main advantage of this process is the ability to produce ultra high purity materials with a very small particle size. The main drawback of CVD is the low yield.
- Sputtering: In this technique, bombardment by energetic particles is used to eject atoms from the solid target materials in a vacuum chamber to produce semiconductors. It is a very efficient method to synthesis nano film with uniform thickness, but it is a high cost process due to the sophisticated equipments required.
- Flame synthesis: This process utilizes a high temperature – or plasma - exposure of precursors to produce small size nano particles. It is commonly used for nano coating due to the mobility of the products as they were achieved by bombardment through the flame.

Because of the drawbacks of these processes, which are the high cost and equipments, the sol-gel technique emerges as the most promising technique due to its simplicity and ability to control the

final catalyst properties. This can be attained by adjusting the process parameters such as the ratio of precursor to acid and solvent, solution temperature and sonication time.

To make the crystalline titanium dioxide more photocatalytically active, it is required to modify it to enhance both its surface area and photoactive wave length range. To do so, the modifications may include the incorporation of other transition metals oxides into titanium dioxide matrix to promote the catalyst surface in both physical and chemical ways . The doped transition metals onto the surface of titanium dioxide improves its photocatalytic activity be reducing the band gab energy, hence, make it more active towards the visible range. In addition, these metals prevent the surface agglomeration by acting as physical promoters and may also increase the selectivity toward different materials in many applications. This is due to the higher affinity and physical interaction achieved by incorporating these metals.

1.1 Applications of titanium dioxide

Many studies have immerged concerning the applications of photocatalysis in the field of environmental degradation of chemical pollutants including organic and inorganic materials as well as dyes. Toxic metals, which include heavy metals, are individual metals and metal compounds that negatively affect the human and animal health. At trace levels, many of these elements are necessary to support life[1-4]. However, at elevated levels they may build up in biological systems, and become a significant health hazard.

Among the class of heavy metals that are classified by Environmental Protection agency (EPA) and Agency for Toxic Substances & Disease Registry (ATSDR), the top priority list of hazardous substances for removal from water includes lead, cadmium and zinc . These heavy metals are carcinogenic and have severe effects on the vital human organs including lungs,

kidneys and blood vessels. The maximum allowable limits of these metals vary according to the local regional regulations, but in general, they are limited to less than 20 ppm in most local regulation. Therefore, removal of these heavy metals from aqueous solution is required to maintain the water quality standards.

Several technological methods could be employed for treatment of water form heavy metals. Among these methods are chemical precipitation, ion exchange, membrane separation and adsorption[5, 6]. These methods are either costly, energy consuming or produce sludge that requires further treatment. Photocatalytic application on the other hand has gained major attention in this field as offers an efficient removal to a majority of pollutants with low cost of processing as well as other features including chemical stability and non-toxicity[7, 8].

In addition to the conventional eliminating of toxic metals from industrial waste effluents, the application of the light driven processes that can occur on irradiated semiconductor photocatalysis gained an interest for the recovery of precious metals. These metal are reduced on the surface of the semiconductor particle which is subsequently extracted from the slurry by mechanical and/or chemical means [9].

In polymer technology, titanium dioxide is also used as a filler to different polymeric materials such as poly vinyl chloride (PVC), polyolefins, polystyrene (PS) and acrylonitrile butadiene styrene (ABS) copolymer. The addition of this titanium dioxide to polymers will improve their physical and mechanical properties induced by TiO_2. This will occur without loss of ease processing, light weight, and often ductile nature of neat polymer. Traditionally, the polymer composites were reinforced with micron-sized TiO_2. Recently, processing techniques have been developed to allow the size of TiO_2 to go down to nanoscale.

More recent development in photocatalysis is the development of semiconductor nanofibers. These nanofibers have advantages over the regular semiconductors as they have large surface areas and high reactivates. It can decrease the band gap of TiO2 from 3.2 eV to less than 2.32 eV, which demonstrate higher photo-conversion efficiency by absorbing visible light at wavelengths below 535 nm.

1.2 Objectives and scope of work

The main objective of this work is to produce titanium dioxide nanoparticles and investigate its applications for photocatalytic reduction of toxic heavy metals from aqueous solution. Nanocrystalline titanium dioxide will be synthesized using modified Sol-Gel process with continuous ultrasonication. Furthermore, titanium dioxide will be impregnated with different transition metals to improve its photocatalytic activity, these metals include iron, vanadium and tungsten.

The produced pure and metal doped titanium dioxide will be applied for removal of lead, zinc and cadmium from aqueous solution. Therefore, it is expected to accomplish the following:

- Synthesis of pure and M-doped titanium dioxide nanoparticles.
- Test of photocatalytic activity of titanium dioxide by degradation of Methylene Blue.
- Application of the developed nanoparticles for reduction of Pb^{2+}, Cd^{2+}, and Zn^{2+} from aqueous solution.

- Study the kinetics of photocatalytic degradation of these metals based on different experimental conditions, such as initial concentration, temperature, catalyst mass and stirring speed.
- Development of a photocatalytic reaction model that simulates the kinetics of Pb^{2+}, Cd^{2+}, and Zn^{2+} removal from aqueous solution.

The literature survey related to this work is presented in chapter 2. Chapter 3 discusses the materials and methods used in this work, while chapter 4 represents the results and discussion. The isotherms and kinetics experiments and modeling are included in chapter 5, followed by conclusion and recommendations, which are presented in chapter 6.

CHAPTER 2

LITERATURE REVIEW

2.1 Methods for synthesis of Titanium dioxide

Synthesis of titanium dioxide (TiO_2) has been studied intensively using different techniques such as such as solid phase synthesis (sputtering), gas phase synthesis (flame synthesis), and liquid phase processes (precipitation and sol-gel). In liquid phase method, the procedure involves the hydrolysis of titanium precursor by acid and water, followed by the condensation of hydroxides to produce hydrated titanium dioxide, which is thermally treated to form the solid particles. However, the properties of the final oxide, including the particle shape and size, depend on many parameters, including:

- Type of synthesis method, as the choice of specific technique affects the yield and activity of titanium dioxide.
- Type of precursor, which affect the period of synthesis, type of residues which may deposit on the oxide surface. Many titanium-contained salts can be used as a precursor, such as titanium (VI) isopropoxide, tetrabutyl titanate and titanium n-butoxide.
- Type and concentration of acid, as it defines the hydrolysis duration and particles size.
- Amount of water, which has a direct effect on the aggregates size and yield.
- As ultrasonication is effective in reducing the particle size, exposing the reaction mixture for a longer ultrasonication period of time may generate heat, which results in a reagglomeration.

Several research efforts were done in order to enhance the properties of catalysts applications. These efforts involve the optimization of experimental conditions, such as temperature, initial concentration of reactants, reaction time, as well as modifying the processes used for synthesis, such as incorporation of ultrasonication.

Youji Li, et al. [2010], have studied the preparation of cerium-doped titanium dioxide films via sol-gel method. In their experiments The TiO_2 sol was prepared from titanium tetraisopropoxide as a precursor, 1.5 ml titanium tetraisopropoxide was added to another solution of 15 ml ethanol and few drops of HCl at room temperature. The solution was then vigorously stirred for 30 min at and various amounts of solutions of 8% PPG were added in order to obtain a transparent and light yellow PPG containing sol. After that, 0.1 M cerium containing solution was added to the sol to obtain both PPG and Ce containing sol of TiO_2. The solution was later spread on a glass of pyrex -with a rate of 1800 rpm- using a spin-coating technique. At a later stage, the coated glasses were dried at 40 °C in the oven for 1 h followed by calcination at range of temperatures for 1 h to produce cerium-doped titanium dioxide macro-porous films (CTMs), titanium dioxide macro-porous films (TMs) or cerium-doped titanium dioxide films (CTs)[10].

Sol-gel method was used by Yan Yu, et al, [2012] for the synthesis of nanocrystalline titanium dioxide where tetrabutyl titanate was used as a precursor. The effects of temperature on the crystalline phases of TiO_2 were investigated, as well as the properties and photocatalytic activity of TiO_2. The experimental finding of this study is that, the transformation of TiO_2 from anatase to rutile began at 725 °C[11].

Another study for the preparation was conducted by Shujie Pang, et al, [2009] for silica nanoparticles coated with Lanthanide doped titanium dioxide. In this study, titanium n-butoxide

(Ti $(OC_4H_9)_4$, TBOT), was used as a main precursor for catalyst preparation where a salt of lanthanide was added into the reaction mixture. A stock solution of 4 mL of TBOT mixed with 100 mL of ethanol was used as a source for the coating material. In a typical experimental run, 0.10 g silica nanosparticles dispersed in 25 mL of alcohol (ethanol) were mixed thoroughly with a certain quantity of lanthanide salt dissolved in 0.38 g water with 4.0 mL of precursor. More ethanol was added later to complete the total volume of mixture to 50 mL. The mixture was then refluxed and kept under stirring for further 12 h. The final spheres were then separated centrifugally and washed –under ultrasonication- with ethanol.

A gas phase synthesis of titanium dioxide nanoparticles was conducted by E. Popovici, et al, [2012]. In this study, a liquid precursor is evaporated above the boiling point, a lower than the decomposition temperature, which is 500^{o}C. The nanoparticles were synthesized by laser pyrolsis. The produced catalyst was characterized by SEM, XRD, and the mean particle size was found to be 15 nm[12].

Preparation of TiO_2 nanoparticles in solutions of glycerol was investigated by Tran Trung, et al, [2002], where TiO_2 nanoparticles were synthesized from titanium isopropoxide. Titanium isopropoxide was added drop wise to another stock solution containing alcohol and nitric acid at 10^{o}C, followed by stirring in a nitrogen environment for additional 3 h. Then, all the solutions were heated at 60 ^{o}C for 5 h to ensure the gelling reaction was totally completed[7].

The growth kinetics of titanium dioxide nanoparticles was shown by Gerko Oskam et al, [2002]. Anatase particles were prepared via precipitation from a homogeneous solution using titanium (IV) isopropoxide as precursor in aqueous solution acidified with nitric acid to pH 1 using a water-to-titanium mole ratio of about 200. Upon addition of titanium (IV) isopropoxide to the

aqueous solution, a white suspension was immediately formed. Subsequently, the suspension was peptized at 85 °C in order to disperse the aggregates into primary particles and small aggregates (<20 nm). During this step, evaporation of 2-propanol during hydrolysis and some water results in condensation of the colloid. The resulting colloid was light blue, translucent, and was stable for several weeks. Particle growth was achieved by heating the resulting colloid to temperatures ranging from 160°C to 220°C for up to 300 h in a titanium pressure vessel. In atypical run, 15 mL of Ti-$(O\text{-}iPr)_4$ was added carefully –drop wise- to 185 mL of deionized water contains 1.3 mL of concentrated HNO_3 to control the solution pH under vigorous stirring at room temperature. The suspension was then kept at 85 °C with continuous stirring in an open Erlenmeyer flask for further 12 h until a final volume of mixture of 50 mL was reached. The colloid was then heated gradually - elevated temperature- in a closed titanium pressure vessel for a range of 4 to 300 h. Particle growth under these conditions was noticed in a milky-white colloid where a TiO+ concentration was noticed to be about 80 g/ L.

Production of titanium dioxide in continuous process is of a great interest for mass production. A study by M. Hussain, et al, [2010] is the Synthesis, characterization, and photocatalytic application of TiO2 nanoparticles. In their work, Titanium tetra-isopropoxide was implemented as a precursor, due to its fast hydrolysis kinetics. Two solutions of the precursor in isopropyl alcohol and – the other solution- water in isopropyl alcohol were prepared in separated vessels under inert (nitrogen) flux to control the precursor reactivity with humidity. HCl was added to the second solution as a hydrolysis and de-agglomeration agent.

The properties of (TiO_2) with size varies from micrometer to nanometer level have been studied intensively, one of these studies conducted by Hanna L. et al, [2009] which is Size-dependent toxicity of metal oxide particles (comparison between nano- and micrometer size), in biology,

showed that, the bigger micrometer particles of TiO_2 caused more damage of DNA compared to the smaller, nanoparticles, this trend can be explained by the internal crystal structures. The incorporated iron oxides in the matrix showed low or no toxicity and no clear difference between the macro and nano particle sizes. Furthermore, it is found that, nanoparticles of these materials are not always more toxic than micrometer particles, so, it can be summarized that, the size of (TiO_2) does not play a significant role in term of toxicity.

Zhigang Chen, et al, [2012], have investigated the preparation of titanium dioxide by eggshell membrane. tetrabutyl titanate was used as titanium resource while ethanol was used as solvent. The catalyst was characterized by SEM, XRD and BET which revealed anatase form of titanium dioxide[13].

The summary of the conditions and materials used for titanium dioxide preparation, including the types of precursors, solvents, hydrolysis agents and characterizations equipments is given in Table 2.1.

Table 2-1: Summary of the conditions and materials used in titanium dioxide preparation.

Reference	**Precursor**	**solvent**	**Hydrolysis agent**	**finishing**	**Characterization**
Youji Li, et al [2010]	Titanium Tetraisopropoxide	Ethanol	HCl	Drying: 40^{o}C, 1 h. Calcinations: 1 h	SEM, XRD, XPS, BET, UV-spectroscopy
Shulie Pang, et al. [2009]	Titanium n-butoxide	-	HCl, HF	-	SEM, TEM, IR
Tran Trung, et al. [2002]	Titanium Tetraisopropoxide	Nitric acid	Acetic acid	Drying: 60^{o}C, 5 h. Calcinations: 100-400^{o}C, 10 h	SEM, XRD, EDX, UV-spectroscopy
Amar Kumbhar, et al. [2005]	Titanium n-butoxide	Ethanol	Acid free	Drying: 100^{o}C, 10 h. Calcinations: 450^{o}C, 5 h	SEM, TEM, XRD, EDX, UV-spectroscopy
Manjumol, et al [2009]	Titanium oxysulphate	Nitric acid	Ammonium hydroxide	Drying: 50^{o}C, 24 h. Calcinations: 800^{o}C, 3 h	SEM, XRD, UV-spectroscopy
Gerko Oskam et al, [2002].	Titanium Tetraisopropoxide	Nitric acid	Nitric acid	Drying: 85^{o}C, 4-300 h.	TEM, XRD
M. Hussain, et al, [2010]	Titanium Tetraisopropoxide	Isopropyl alcohol	HCl	Calcinations: 400^{o}C, 3 h	XRD, EDX, BET, FTIR.

2.2 Applications of metal-doped titanium dioxide

To make the crystalline titanium dioxide more active for photocatalytic applications, it is required to enhance both its surface area and photoactive wavelength range. In order to achieve that, the modifications may include the incorporation of other transition metals oxides into titanium dioxide matrix to promote the catalyst surface in both physical and chemical ways[14-17]. Several processes were investigated for the doping of titanium dioxide such as sputtering, flame synthesis and laser ablation. Among these methods, sol-gel process has gained wide attention for the synthesis of pure and metal doped titanium dioxide due to its inexpensiveness in term of equipments, and the ability to control the process parameters easily.

Degradation of malachite green by silver-doped commercial titanium dioxide was studied by Sandip Saha, et al, [2012]. In this study, 1 and 2 mol% of Ag was doped into titanium dioxide by liquid impregnation method. The catalyst was further characterized and then applied for the degradation of malachite green. It is found that, the degradation was zero-order kinetics over the whole range of concentration (25 to 125 mg/l), and it occurs via step-wise N-demethylation[18].

Iron is one of the most used promoter which can be doped with titanium dioxide to enhace its photocatalystic activity. Amar Kumbhar, et al [2005], have prepared iron doped titanium dioxide nanoparticles. Titanium (IV) n-butoxide was used as a precursor, and Iron(III) nitrate nonahydrate ($Fe(NO_3)_3.9H_2O$) –dissolved in solutions- was used as a main source of iron. Iron (III)-doped titanium dioxide photocatalyst was prepared by a modified sol-gel process under continuous ultrasonication. In a typical run, 200 ml of titanium (IV) n-butoxide alkoxide was mixed with 15 ml ethanol and then allowed to complete hydrolysis at room temperature with addition of 1 ml of water. The resulting solution was immediately turned to white sol, which indicates the formation of hydrolyzed titanium dioxide nanoparticles. Certain amount of a

solution of an inorganic precursor ($Fe(NO_3)_3.9H_2O$) in ethanol(typically 1% solution) was added drop wise to the hydrolyzed titanium dioxide solution. The reaction mixture was then allowed to proceed further to condensation for 30 min. As the concentration of the $Fe(NO_3)_3.9H_2O$ was increased, the color of the reaction mixture was changed from a milky-yellow solution to dark-milky brown. pure titanium dioxide was prepared by the same procedure without the addition of $Fe(NO_3)_3.9H_2O$. The overall amount of water and ethanol is kept constant for both pure titanium dioxide and doped titanium dioxide reactions.

Lanthanide is also used as a doping agent, K. A. Manjumol, et al [2009] have synthesized lanthanum-doped nano titanium dioxide photocatalyst via aqueous sol–gel method for multifunctional ultra-filtration membranes. The precursor used for the synthesis of titanium oxide was titanium(IV) oxy-sulphate. The membranes were prepared by thermal treatment at temperatures ranging from 600 to 900 ^oC for 3 h.

Jintao Tian, et al, [2008], studied Preparation and characterization of several metal-oxides including TiO_2 nanofilms using sol–gel process. The prepared oxides were characterized using SEM, XRD, as well as EDS. The results showed that the synthesized pure TiO_2 was in the shape of nanoparticles and the film has no cracks. Weak crystallization was also noticed for the composite film of Ti/Zn ratio of 3/1 and 1/1 as well[16].

Titanium oxides can be doped with different materials other than transition metals to enhance its properties for different applications. Pinggui Wu, et al, [2009] have studied the photocatalytic inactivation of bacteria under Visible-light-induced by complex photocatalyst of palladium oxide and nitrogen-doped titanium dioxide. Sol-Gel method was used in this study, and they have found that, the photocatalytic activity was dependent on both, the type of dopants materials and

light intensity. The characterization showed that visible light photocatalysis on PdO-TiON caused severe damage on the bacteria cell wall as well as the cell membrane.

One of the materials that can be doped with titanium oxides is zeolite. Masato Takeuchi and et al [2009], have studied the Enhancement of the photocatalytic activity of TiO_2 nanoparticles using mechanical blending with hydrophobic mordenite (MOR) zeolite. They found that, the blended TiO_2/MOR revealed higher photocatalytic activity compared to the pure nanocrystalline TiO_2. Because of the fact that, silica zeolite powders are generally highly transparent under UV light regions, UV light was effectively irradiated into the inside whole parts of the TiO_2 nanoparticles without any loss of UV light intensity. Furthermore, the siliceous MOR zeolite powders effectively adsorb any gaseous molecules and then feed them into the surfaces of the mixture of TiO_2 nanoparticles, resulting in the observed enhancement of the photocatalytic activity. The optimum amount of the zeolite nano powders to be mixed for the enhancement of the photocatalytic activity of the nanocomposite of TiO_2 mixed with MOR system was noticed to be 80–95 wt%[15].

Hamidreza Farnoush, et al, [2012] have synthesized nano titanium dioxide for wire coating by chemical precipitation. In this work, the precipitated nano particles were characterized by SEM, FTIR, Fe-SEM as well as XRD. It was found that, the wire coating by nano titanium dioxide has increased the corrosion resistance and the bonding strength between coating and substrate[19].

Zhice Zhang, et al, [2009], have studied the Photocatalytic activity of N-doped nano titanium dioxide as well as titanium nitride. The TiO_2 nanopowder was synthesized in a continuous hydrothermal flow synthesis (CHFS) process. The structures of the resulting nano materials were investigated by X-ray diffraction (XRD) and Raman spectroscopy. N-doped anatase TiO_2 and phase pure titanium nitride (TiN) were obtained by controlling the post synthesis heat treatment

conditions. It was reported that TiN started appearing when the TiO_2 was treated at 800 °C, and that pure phase TiN was reported at 1000 °C after 5 h[17].

K. Bhattacharyya, et al, [2009], have carried out the Microstructural characterization of the V-doped nano-titanium dioxide. It is found that, the average particle size of these materials was about 11.5 nm, as calculated by the XRD peak broadening and TEM. Small angle X-ray scattering (SAXS) was also used for the measure of the particle size vanadium-doped titanium dioxide samples. The SAXS conditions were determined assuming semi-spherical particle shape. The SAXS results were in the same range with the particle size as obtained by TEM[20].

Another study of modified (TiO_2) was the synthesis and characterization of S-doped TiO_2 nanoparticles, effect of calcination temperature and evaluation of photocatalytic activity, which is held by M. Hamadanian, A. Reisi-Vanani, A. Majedi [2009]. In this study, S-doped TiO_2 photocatalyst that has high activity in the range of visible light was synthesized by modified sol–gel process adding thiourea as sulfur source. The synthesized catalyst was characterized using XRD, FT-IR, DRS, SEM-EDX and TEM analysis. The pure and S-doped TiO_2 nanoparticles were calcined at 500 °C and found to have only anatase phase. Effects of calcinations temperature revealed the formation of rutile phase which started at temperature between 650 to 700°C for pure TiO_2 and 750°C for S-doped TiO_2. The photocatalytic activity of these materials were examined by photodegradation of methyl orange (MO) in aqueous solution under visible, and UV light and it was found to be a function on the amount of S doped into titanium dioxide. The most activities were observed for samples of 0.05% and 0.1% S-doped TiO_2 under visible as well as UV light, respectively. Results showed for pure titanium dioxide samples, which calcined at 650 and 550 °C under visible and UV-light are the best performance catalysts, respectively.

Also for 0.05% S-doped titanium dioxide, calcined at 500^{o}C was the best catalyst compared to the other samples under UV and visible light[21].

Furthermore, TiO_2 thin films doped with Pd and Eu for optically and electrically active TOS–Si heterojunction was carried out by means of Danuta Kaczmarek, et al [2009]. In this work, a thin films of titanium dioxide doped with Eu (0.9 wt %) and Pd (5.8 wt%) were incorporated in silicon and glass substrates from Ti–Eu–Pd used as a target by modified magnetron sputtering method. XRD measurements revealed main nano-crystalline structure that has rutile phase of TiO_2 in the prepared thin films[22].

Guohui Tian, et al, [2009], have studied the enhancement of photocatalytic activity of S-doped titanium dioxide and zirconia nanoparticles under visible light. The synthesized materials were characterized by XRD, nitrogen adsorption desorption isotherm, TEM, X-ray photo-electron spectroscopy (XPS), UV–vis diffuse reflectance spectra (DRS), Fourier transform infrared spectra (FT-IR) and electron paramagnetic resonance (ESR). It was found that, the modifications by ZrO_2 could effectively reduce phase transformation, enhance visible-light absorption, and possess more functional group on the surface, mainly hydroxyl groups. The photocatalytic activity of the synthesized composite was higher than that of unmodified S-doped TiO_2. It was also found that, different parameters affect the overall photocatalytic activity of the catalyst, which are specific area, particle size, pores structure and surface functional groups in the catalyst[16].

Orhan Murat Kalfa, et al, [2009], have studied the synthesis of nano-level composite of B_2O_3/TiO_2 as a solid-phase extractor and its application for separation of cadmium. The characterization of the synthesized material was done by X-ray diffractometer methods (XRD), scanning electron microscope (SEM), and transmission electron microscope (TEM). The specific

surface area of the material was also measured and found as 3.4 m^2/g. Analytical parameters such pH of the sample solution, overall sample volume, volumetric flow rate of sample solution, output volume and concentration of the column solid-phase extraction (SPE) procedure were also examined. It is found that, under optimum conditions, the recovery of cadmium was found to be 96±3 wt% at 95% confidence level[23].

M. V. Shankar, et al, [2009], studied the One-pot synthesis of peroxo-titanium dioxide nanopowder and dual photochemical oxidation in aqueous methanol solution. A sol–gel hydrothermal method was used to synthesize peroxo-titanium dioxide powders, they have investigated the photo-oxidation performances in alcoholic (methanol) solution under visible-light irradiation. Three kinds of powders were introduced using a precursor sol contains TiO_2 and H_2O_2 with different dispersion mediums including NH_3, NaOH, and water, all samples were characterized using SEM, TEM, and XRD. They found that, the relatively high photochemical oxidation activity of titanium dioxide prepared with NH_3 is due to the visible light active functional peroxo species on TiO_2 surface[24].

Michael Z. Hu, et al, [2009], studied the Synthesis and characterization of anodized titanium oxide nanotube arrays, which is a nanocomposite material that shows potential for different applications. The synthesis using acid free aqueous solution was described. The anodized titanium dioxide films samples which are amorphous, anatase, and rutile, on titanium foils were characterized with scanning electron microscopy SEM, X-ray diffraction (XRD), and Raman spectroscopy. It was found that the anatase crystalline structure utilizes light to current more efficiently and is therefore, chosen as a better photocatalytic catalyst for hydrogen production via photoelectrochemical splitting of water[25].

The photocatalytic reactivity of titanium oxides depends on the process used in production. Bin Gao, et al, [2009] have investigated the (CNTs-TiO_2) nanocomposites synthesized by conventional and novel surfactant wrapping sol–gel methods showed enhanced photocatalytic activity. Both, MWCNTs (multi walled), and the composites were characterized by different analytical techniques including TEM, XRD, BET. The photocatalytic activities of these materials were noticed from the results of the photocatalytic degradation of methylene blue (MB). The optimum CNTs/TiO_2 ratio in the composites prepared by conventional sol–gel method was found to be ranging from 1.5 wt% to 5 wt%, under the experimental conditions. The maximum enhancement in photocatalytic activity was found to be 12.8% compared to the pure TiO_2 sample.

Srimanta Raya, Jerald A. Lalmanb, Nihar Biswas, [2009] statistically modeled phenol photocatalytic degradation by titanium dioxide nanoparticles. It is found that small catalytic particle size incorporated in the final yield has significant role in the photocatalytic degradation process, with the maximum degradation achieved at an approximate catalyst size of 10 nm. The overall photocatalytic degradation rate constants followed an Arrhenius trend with activation energy reported to be 13.55 kJ/mol.K for the 10 nm titanium dioxide particles[26].

Besides well known Sol-Gel process, other alternative processes are undergoing heavy investigations. Anal K. Jha, et al [2009], have considered the preparation of TiO_2 nanoparticles via micro-organisms. X-ray and TEM analyses were performed to investigate the formation of titanium dioxide nanoparticles. Well separated nanoparticles as well as aggregates having the size of 8 to 35 nm were found. Concentric Scherrer rings in the selected area electron diffraction patterns indicated that the nanoparticles are having all possible orientations[27].

Ahmad Rahimpour, et al, [2012], have studied the properties of TiO_2 deposited nano-composite PVDF-SPES membranes. In this study, the surface of poly vinylidene fluoride (PVDF) and sulfonated polyethersulfone (SPES) blend membrane was modified by incorporating titanium dioxide nanoparticles which has been activated by UV. The membranes were mainly characterized by FTIR, SEM, and AFM. It has been found that, the surface contact angle of this composite membrane was noticed to be y decreased by incorporation of nano titanium dioxide[28].

Le Chen, et al, [2009], have studied the Photoreduction of carbon dioxide by titanium dioxide nanocomposites synthesized through reactive direct current magnetron sputter deposition. Mixed phase titanium dioxide films were synthesized by direct current (DC) magnetron sputtering and then, characterized by X-ray diffraction (XRD), atomic force microscope (AFM), scanning electron microscope (SEM) and transmission electron microscope (TEM). The results revealed sputtered mixed phase film (70% anatase, 30% rutile), which deposited at low angle proved to be far better than the other films as measured by the initial rate and reduction with carbon dioxide.

Another sol-gel method was used by Xiaoliang Shi, et al, [2009] in the enhanced of photocatalytic activity of titanium dioxide by nut shell carbon. X-ray diffraction, field emission scanning electron microscopy (FESEM), Brunauer–Emmett–Teller surface area (BET), pore size distribution, ultraviolet–vis light absorption spectrum, and photoluminescence spectrum were carried out in order to characterize the composite catalyst. It has been reported that, the photocatalytic activity of NSC nano titanium dioxide composites were enhanced significantly, and the BET surface area of NSC nano titanium dioxide composites were approximately 15 times larger than P25[29].

Lei Sun, et al, [2009], have studied the effect of synthesis conditions on photocatalytic activities of nano titanium dioxide thin films where the resulting films were characterized by X-ray diffraction (XRD), field emission-scanning electron microscopy (FE-SEM), atomic force microscopy (AFM), as well as Fourier transform-infrared (FT-IR) spectra. The thin film which was prepared under the optimal conditions was found to be compact anatase nanoparticles with an average particle size of approximately 17.2 nm, and an average roughness of 3.653 nm. The 1-hour photocatalytic degradation efficiency of methyl orange (MO) in aqueous solutions as well as toluene in gaseous phase was 98.9 and 100%, respectively. The factorial analysis results of degradation efficiencies showed that the calcination temperatures have significant role in determining the photocatalytic activities of the prepared titanium dioxide thin films.

Although the synthesis and applications of titanium dioxide have been widely covered, there is still more research needs to be performed in order to enhance the surface size and morphology of the nanoparticles. In addition, there is still a need to correlate the required properties of titanium dioxide to correspond its required applications on toxic heavy metals reduction, as most of the applications are focused on nano coating and incorporating titanium dioxide in composites of other materials. Furthermore, the techniques used in its synthesis are commonly complicated and expensive; hence, more research is still needed for the relatively simple process of sol-gel, which can be further enhanced by combining it with continuous ultrasonication. Moreover, some transition metals can be promising in the enhancement of photocatalytic activity of titanium dioxide, these metals include tungsten, vanadium and iron.

CHAPTER 3

MATERIALS AND METHODS

3.1 Materials

All materials were analytical grade reagents, used without further purification. Water was obtained from a Milli-Q water purification system (Millipore). All used glassware were Pyrex, washed with soap and deionized water and dried in an oven at 105 ^{o}C. Details of these materials showing their purity and manufacturer are given in Table 3.1.

Table 3-1: List of chemicals and providers.

Material	purity	provider
Titanium (IV) isopropoxide	99.99%	Sigma-Aldrich
Hydrochloric acid	10 % (V/V)	Sigma-Aldrich
acetic acid	99.7 %	Sigma-Aldrich
isopropyl alcohol	99.9 %	Sigma-Aldrich
ethanol	99.5 %	Loba Chemicals
methanol	99.9 %	Sigma-Aldrich
Methylene blue	99 %	Loba Chemicals
Lead carbonate	99.5 %	Loba Chemicals
zinc nitrate	99.5 %	Loba Chemicals
Iron(III) nitrate nonahydrate	99.9 %	Sigma-Aldrich
ammonium metavanadate	99.9 %	Sigma-Aldrich
tungsten oxide	99.995 %	Sigma-Aldrich

3.2 Synthesis of pure titanium dioxide

Titanium dioxide nanoparticles were synthesized using sol-gel technique using different alcohol types and hydrolyzing agents. In a typical run, 5 ml of titanium isopropoxide (99.99%) was added to 25 ml of alcohol at 5 ^{o}C with vigorous stirring. Three different types of alcohols; ethanol, methanol, and isopropyl alcohol were verified. The resulting solution turned white (Sol) as a result of formation of hydrolyzed Titanium dioxide particles. Another mixture of 25 ml of alcohol with 0.5 ml of hydrolysis agent (either hydrochloric acid or Acetic acid) and/or 5 ml of water was prepared and added drop wise to the Sol to prevent the sudden formation of the gel, which may lead to incomplete reaction or produce bigger particle size. The mixture was stirred for one hour, followed by ultrasonication for different period of times to prevent any agglomeration of the catalyst to form bigger clusters. The product was dried in an oven for 12 hours at 75^{o}C, followed by crushing and calcinations at 300- 450^{o}C for 4 hours. The range of calcinations temperature was carefully chosen to avoid the formation of rutile phase, which appears at calcination temperatures higher than 500^{o}C. A schematic demonstration of sol-gel process is given in Figure 3.1.

Analysis of Variance (*ANOVA*) was used to optimize the reaction parameters for each type of acid and alcohol. Sixteen runs with varied levels of water content, acid concentration, and alcohol volume and calcinations temperature were studied in order to identify the optimum conditions for the size and shape of the produced Titanium dioxide as shown in Table 3.2 and Table 3.3.

In this analysis, the effect of main parameters is shown at the lower and higher levels for all runs as A, B, C and D, while the interactions between these parameters is shown as AB, AC, AD, BC, BD and CD. These interactions are also represented in the lower levels, which denoted by 1 and the higher levels, denoted by 2, (i.e. interaction of AB at 1 means the acid concentration is 0 and the water volume is 0, while AB at 2 means the acid concentration is 1.5 M and the water volume is 1 ml).

The "blocking" technique was implemented to eliminate some interactions that cannot be useful from experimental point of view such as the main interactions at the lower level of all parameters, which means 0 acid concentration, 0 ml of water, and 0 ml of alcohol. This combination means there is no reaction to take place. Generally, the blocking was done taking the following into account:

- Elimination of runs representing the lower levels of all parameters together as it will result in no reaction to take place.
- Effect of calcination temperature was considered for the first runs, then eliminated from the latter runs as it will affect the phase of catalyst only, regardless of the conditions used to produce it.
- When the concentration of acid is at the lower level (0 ml), the amount of acid was added to the amount of water in order to keep the overall water/titanium ratio fixed, hence eliminate the effect of hydrolysis time.

Table 3-2: *ANOVA* conditions for synthesis of titanium dioxide nanoparticles

Factors	**Name**	**Level 1**	**Level 2**
A	Acid Concentration (M)	0	1.5
B	Water Volume (ml)	0	1
C	Alcohol volume (ml)	0	1
D	Calcinations Temperature (^{o}C)	300	450

Table 3-3: Typical runs and interaction between the *ANOVA* parameters for levels 1 and 2.

Runs	**A**	**B**	**C**	**D**	**AB**	**AC**	**AD**	**BC**	**BD**	**CD**
1	1	1	1	2	2	2	1	2	1	1
2	2	1	1	1	1	1	1	2	2	2
3	2	1	1	2	1	1	2	2	1	1
4	1	1	1	1	2	2	2	2	2	2
5	1	2	1	1	1	2	2	1	1	2
6	2	2	1	1	2	1	1	1	1	2
7	1	2	1	2	1	2	1	1	2	1
8	2	2	1	2	2	1	2	1	2	1
9	1	1	2	1	2	1	2	1	2	1
10	2	1	2	1	1	2	1	1	2	1
11	1	1	2	2	2	1	1	1	1	2
12	2	1	2	2	1	2	2	1	1	2
13	2	2	2	2	2	2	2	2	2	2
14	1	2	2	1	1	1	2	2	1	1
15	2	2	2	1	2	2	1	2	1	1
16	1	2	2	2	1	1	1	2	2	2

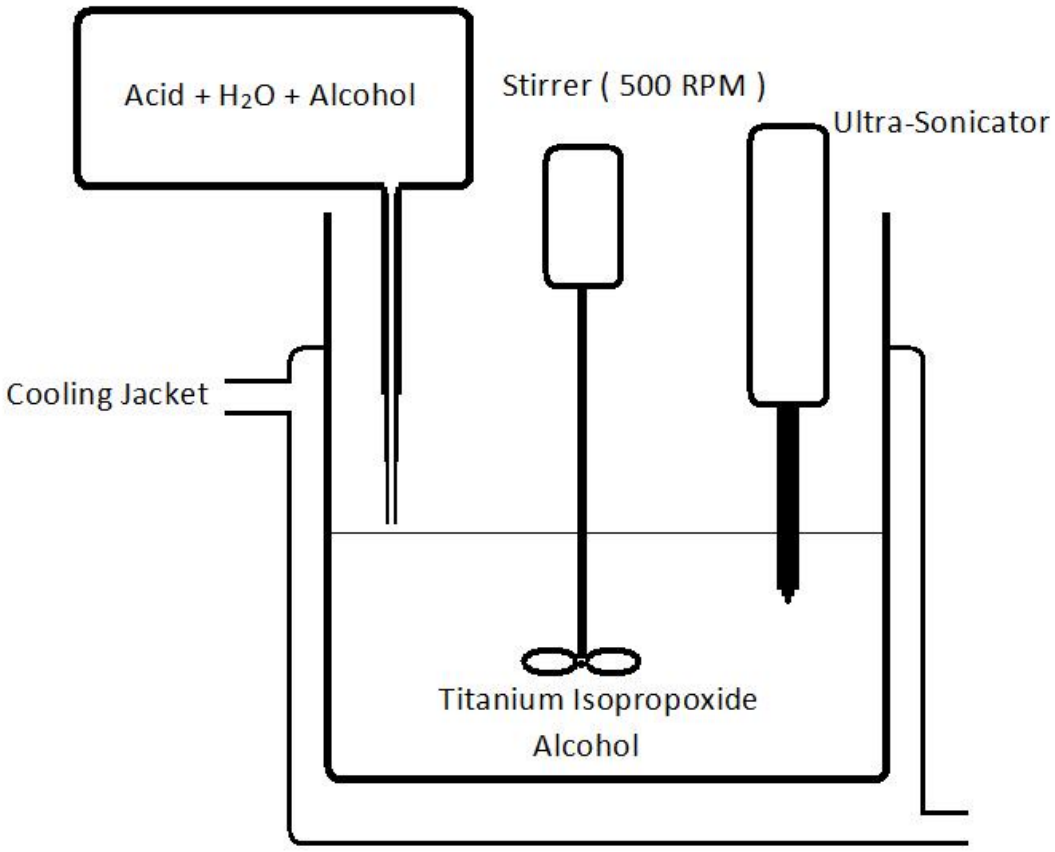

Figure 3-1: Demonstration of sol-gel process.

3.3 Synthesis of metal-doped titanium dioxide

For the synthesis of metal-doped titanium dioxide, the same procedure for synthesis of pure titanium dioxide was followed where water was replaced by a solution of the target metal prepared by dissolving the appropriate amount of its original salt in deionized water. Different solution concentrations of metal ranging between 1000 ppm to 7000 ppm, were used to vary the amount of tungsten doped on titanium dioxide, this verification was done while fixing the amount of acid at 0.5 ml, amount of methanol at 25 ml and amount of titanium (IV) isopropoxide at 5 ml.

3.4 Characterization and microstructural analysis

The produced catalyst was characterized for its shape and morphology using scanning electron microscopy (SEM) (JOEL JSM-6460 LU). Where the sample was placed in a semiconductor wafer and electrically grounded to avoid the electrostatic charge accumulation. The sample was then coated with a conductive material by low vacuum sputter coating.

The surface area was measured using Brunauer, Emmett, and Teller technique (BET) (MICROMERITICS- ASAP 2020), in which, the sample was place in a sealed tube and degassed under 80^{o}C for 20 hours using two vacuum pimps. After that, liquid nitrogen was introduced, and the properties of the samples were measured according to the amount of nitrogen deposited on the surface of the sample.

The crystalline phase and structure were determined using X-Ray diffraction technique (XRD), where the sample was bombarded by electrons produced by heating a filament, and the X-ray spectra was produced when the electrons dislodged the inner shell electrons of the targeted sample. The particle size distribution was determined using particle size analyzer (PSA)

(Microtrac-Zetatrac, MICROMERTICS-S3500). Where the sample was heated to 90oC to remove humidity, then, a compressed air stream is used both as a carrier and a dispersing agent for the dry powder, and the sample was exposed to a laser beam. The particles size was measured according to the properties of the dispersed light.

The amounts of tungsten, vanadium and iron doped into the catalyst matrix were determined using Energy-dispersive X-Ray spectroscopy (EDS) (OXFORD INCAx-SIGHT), attached to the SEM equipment at three different spectra, in which, the resolution at 5.9 KeV was 137 eV. Table 3-4 summarizes these characterization techniques.

Table 3-4: List of characterization and microstructural analysis equipments.

Analysis	**Equipment**	**Model**
• Particles shape • Estimated size	Scanning electron microscopy (SEM)	JOEL JSM-6460 LU
• Catalyst phase	X-ray Diffraction (XRD)	2700 X-Ray analysis Ins.
• Elementary analysis	Elementary dispersive spectroscopy (EDS)	OXFORD INCAx-SIGHT
• Surface area • Average pore diameter	Brunauer, Emmett, and Teller (BET)	MICROMERITICS- ASAP 2020
• Particles size distribution	Particle size analyzer (PSA)	Microtrac-Zetatrac, MICROMERTICS-S3500
• Concentration of MB	UV-Vis	Shimadzu
• Concentration of heavy metals	Atomic absorption spectrometer (AAS)	Thermo-Scientific

3.5 Photocatalytic equilibria and maximum degradation

3.5.1 Adsorption isotherms experiments

The photocatalytic activity of pure and metal-doped titanium dioxide were investigated by the degradation of Methylene blue (MB) and heavy metals using different concentrations ranging from 10 to 100 ppm. All concentrations were prepared from stock solutions prepared by dissolving 100 mg of target solutes (MB, lead carbonate and zinc nitrate) separately in deionized water. The pH of the adsorbate solution was verified at 4, 6 and 10 using standard buffer solutions. Blank solutions were also prepared in the same manner for comparison. Both blanks and catalyst contained samples were exposed to UV light that has wavelength of 254 nm in dark environment with continues shaking for 24 hours to ensure the equilibrium at room temperature. The concentrations of both MB and heavy metals were measured for all samples using UV-vis spectrophotometer and atomic absorption spectrometer respectively. The difference between the initial and final concentrations of samples was measured and the percentage of degradation was calculated accordingly.

3.6 Analysis of Variance (ANOVA)

Analysis of variance (ANOVA) was used to optimize the experimental parameter for the kinetics of photocatalytic reduction of heavy metal. In this analysis, two levels and four factors (k) were defined, and the total number of runs was given by 2^k, accordingly. The parameters to be optimized and the values of each level are given in Table 3.5, where the detailed experimental conditions of the 16 runs are given in Table 3.6.

Table 3-5: parameters and levels for ANOVA.

Factors	Name	Level 1	Level 2
A	Temperature (T)	4	25
B	Initial concentration (ppm)	10	25
C	Catalyst mass (g)	0.5	1
D	Stirring speed (rpm)	100	600

3.6.1 Kinetics of photocatalytic reduction

Kinetics experiments were conducted in a 2-L Pyrex beaker with a glass jacket to control the temperature. A mechanical stirrer with a controllable speed was mounted on the top. The setup was exposed to UV light that has wavelength of 254 nm in dark environment. In a typical run, 1.7 L of target heavy metal containing solution with specific concentration was prepared by dissolving the appropriate amount of its salt in deionized water; the solution temperature was adjusted by controlling the temperature of circulating water in the jacket. The pH of solution was kept at 6 throughout the experiment. The change of metal concentration was monitored by taking samples each period of time using syringes with double layered filters to ensure the cut of the reaction immediately after taking the sample. Metal concentration in each sample was measured using atomic absorption spectrometer (AAS).

The kinetics experiments were designed to study the effects of temperature, initial concentration of target metal solution, mass of catalyst and stirring speed on the removal of toxic heavy metals from aqueous solutions by metal-doped titanium dioxide. Detailed experimental conditions are given in Table 3.6.

Table 3-6: Experimental conditions for kinetics of heavy metals removal by Metal-doped Nanocrystalline titanium dioxide.

EXP No	Parameter	SPEED (rpm)	MASS ADDED(g)	C_0 (mg/L)	T (^oC)
E1	Effect of T	100	0.5	25	4
E2		100	0.5	25	25
E3		600	0.5	25	4
E4		600	0.5	25	25
E5	Effect of C_o	600	1	25	4
E6		600	1	10	4
E7		600	1	25	25
E8		600	1	10	25
E9	Effect of mass	100	0.5	10	25
E10		100	1	10	25
E11		100	0.5	25	25
E12		100	1	25	25
E13	Effect of Speed	100	0.5	10	4
E14		600	0.5	10	4
E15		100	1	10	4
E16		600	1	10	4

3.6.2 Types of adsorption isotherms

In order to measure the maximum loading of heavy metals on the catalyst surface,q_e, several isotherm model were used for fitting the experimental data, where , q_e is given by:

$$q_e = \frac{C_e - C_o}{m/V}$$

In this equation, q_e is the pollutant concentration on the catalyst surface at equilibrium, C_e is the pollutant concentration on the liquid, C_o is the initial concentration, m is the catalyst mass and V is the liquid volume.

There are three common isotherm models to evaluate q_e, which are:

Langmuir model given by

$$q_e = \frac{bC_e q_{max}}{1 + bC_e}$$

Where q_{max} (mg/g) is Langmuir constant related to the maximum adsorption capacity and *b* is Langmuir isotherm coefficient (L/mg)

Freundlich model, given by

$$q_e = kC_e^{\frac{1}{n}}$$

Where *k* and *n* are Freundlich isotherm parameters, which are functions of temperature as the heterogeneity of the surface energy is considered in this model.

Redlich-Peterson model, given by

$$q_e = \frac{AC_e}{1 + BC_e^{\,g}}$$

Where *A*, *B* and *g* are Redlich-Peterson isotherm parameters.

The choice of isotherm model to be coupled with the kinetic model depends on the best fit to experimental data.

3.7 Kinetics modeling

The rate of migration of pollutant molecules from the liquid bulk in the reactor to the catalyst surface is described by the reactor mass balance equation:

$$\frac{dC}{dt} = -\frac{A}{V} k_f \left(C - C_w\right) \tag{1}$$

In this case, the transport of pollutants takes place across a thin liquid film surrounding the catalyst particle where C and C_w are the liquid phase concentrations of the contaminant (mg/cm^3) at the liquid bulk and at the catalyst surface sides of the film, respectively. k_f is the liquid film convective mass transfer coefficient, V is the liquid volume in the reactor (cm^3) and A is the total external surface area of the liquid films surrounding the catalyst particles (cm^2). Assuming thin spherical films, the catalyst total external surface area per unit volume of liquid is approximated by the following equation:

$$\frac{A}{V} = \frac{3}{R} \frac{m_c}{\rho_c} \tag{2}$$

where R is catalyst particle radius (cm), m_c is concentration of catalyst sludge in the reactor (mg/cm^3) and ρ_c is catalyst density (mg/cm^3).

Further to the transport step across the liquid film, the pollutant molecule follows an adsorption step onto the catalyst surface that is described by Langmuir isotherm model, as it is the only model to describe it among the mentioned models:

$$q|_{r=R} = \frac{q_{max} b C_w}{1 + b C_w} \tag{3}$$

Where $q|_{r=R}$ is the solid phase concentration of the contaminant (mg/g) at the catalyst surface in equilibrium with C_w, q_{max} is Langmuir constant (mg/g) related to the catalyst maximum adsorption capacity and b is Langmuir isotherm coefficient (cm^3/mg). Consequently, pollutants diffuse inside the pores of the catalyst and undergo a reaction driven by UV light. The variation

of pollutants concentration inside the catalyst particles, q (mg/g), is given by the diffusion equation:

$$\frac{\partial q}{\partial t} = D_e\left(\frac{\partial^2 q}{\partial r^2} + \frac{2}{r}\frac{\partial q}{\partial r}\right) - k_{rxn}\, I\, q \tag{4}$$

where D_e is the effective diffusivity of molecules (cm^2/s), krxn is the photocatalytic reaction rate constant (cm/s) and I is the of UV light intensity inside the catalyst (W/cm2) that varies with the radial location r as given by Beer-Lambert expression [2]:

$$I = I_0 * 10^{-\alpha(R-r)} \tag{5}$$

where α is the UV attenuation coefficient (cm^{-1}) and I_o is the UV light intensity at the catalyst surface $r = R$. In equation (4) the photocatalytic reaction is assumed to be first order with respect to UV light attenuation I and the solid concentration q.

Starting with a specified initial contaminant concentration in the liquid phase, C_o, and a contaminant-free fresh catalyst during the reactor startup the following initial conditions can be specified for the differential equations (1) and (4):

$$t = 0 \qquad C = C_0, \quad q = 0 \tag{6}$$

Moreover, given the symmetry at the center of the catalyst particle and a balance of the contaminant convective and diffusive fluxes at the surface of the catalyst particle, the following boundary conditions can be specified:

$$r = 0 \qquad \frac{\partial q}{\partial r} = 0 \tag{7-b}$$

$$r = R \qquad -\rho_s D_e \frac{\partial q}{\partial r} + k_f \left(C - C_w\right) = 0 \tag{7-c}$$

Before proceeding with the analysis of the model equations it must be noted that the adsorption model given by Langmuir-Hinshelwood isotherm as described in eq. (3) must be rearranged to solve for C_w:

$$C_w = \frac{q|_{r=R}}{b\left(q_{max} - q|_{r=R}\right)} \tag{8}$$

Consequently, the result from eq, 8 is substituted into eq. (1) and (7-c). This in turn results in an implicit nonlinear coupling between eq. (1) and eq. (4) for which a numerical solution will be implemented and discussed in the following section.

Model solution

The resulting mathematical model represents a nonlinear system of coupled differential equations. In particular, the initial value problem (IVP) given by eq. (1) were solved simultaneously along with the partial differential equation (PDE) (4) and boundary conditions (7). As described previously in section 2.5, the coupling arises due to the nonlinear relationship between C_w and $q|_{r=R}$ as given by the rearranged Langmuir-Hinshelwood adsorption model in eq. (8).

The numerical solution is performed in this study using first-order Backward Euler method for time integration. In this case, for each time step Δt, the right hand sides of equations (1) and (4) are evaluated implicitly at $t + \Delta t$. Moreover, the spatial discretization of the radial coordinate r is performed using Chebyshev pseudo-spectral collocation technique (Canuto et al. 1988)[30]. In

this case, the radial domain ($0 \le r \le R$) is mapped to the Chebyshev domain ($1 \le x \le -1$) as follows:

$$r_i = \frac{(1 - x_i)R}{2} \tag{9}$$

Where x_i are the collocation points defined by Chebyshev-Gauss-Lobatto quadrature (Canuto et al. 1988):

$$x_i = \cos\left(\frac{\pi\, i}{N}\right),\ i = 0, 1, ..., N \tag{10}$$

Where N is the total number of collocation points. In this numerical procedure the unknown variables in eq. (4) and boundary conditions (7-b) and (7-c) are expanded in following manner:

$$\frac{C(t+\Delta t) - C(t)}{\Delta t} = -\frac{A}{V} k_f \left(C(t+\Delta t) - \frac{q_N(t+\Delta t)}{b(q_{\max} - q_N(t+\Delta t))} \right) \tag{11}$$

$$\sum_{j=0}^{N} D_{ij}^1 q_j(t+\Delta t) = 0,\ i = 0 \tag{12}$$

$$\frac{q_i(t+\Delta t) - q_i(t)}{\Delta t} = D_e \left(\sum_{j=0}^{N} D_{ij}^2 q_j(t+\Delta t) + \frac{2}{r_i} \sum_{j=0}^{N} D_{ij}^1 q_j(t+\Delta t) \right) -$$

$$k_{rxn}\, I_i\, q_i(t+\Delta t),\ i = 1, 2, ..., N-1 \tag{13}$$

$$-\frac{\rho_p D_s}{R} \sum_{j=0}^{N} D_{ij}^1 q_j(t+\Delta t) + k_f \left(C(t+\Delta t) - \frac{q_N(t+\Delta t)}{b(q_{\max} - q_N(t+\Delta t))} \right) = 0,\ i = N \tag{14}$$

Where D^1 and D^2 are the first and second Chebyshev collocation derivative matrices of dimensions NxN (Canuto et al. 1988), respectively, which are modified according to the domain mapping in eq. (9).

The resulting equations (11-14) represent a system of N+2 nonlinear algebraic equations which are solved iteratively for each time step using Newton-Raphson method. Computation results that will be presented in this work are usually performed using N = 8 and Δt = 0.1 min. Occasionally, we have used N = 16 and smaller time steps to ensure convergence. All the results that to be presented in this work are converged with respect to spatial and temporal discretizations.

CHAPTER 4

CHARACTERIZATION OF PURE AND M-DOPED TiO_2 NANOPARTICLES

The synthesis of Titanium dioxide takes place via two steps, first, the hydrolysis of titanium isopropoxide by acid according to reaction (4.1):

$$(RO)_3 - Ti - O - R + H_2O \xrightarrow{H^+} (RO)_3 - Ti - O - H + R - OH \quad (4.1)$$

The second step involves the condensation of produced hydroxides to produce hydrated titanium dioxide which is described by reaction (4.2):

$$2(RO)_3 - Ti - O - H \rightarrow (RO)_3 - Ti - O - Ti - (RO)_3 + H_2O \quad (4.2)$$

The produced hydrated titanium dioxide is thermally treated to produce titanium dioxide nanoparticles, and the shape and size of the catalyst depends mainly on the ratio of titanium to water, and generally, the higher water content leads to fast hydrolysis of titanium isopropoxide and hence, large aggregates.

4.1 Characterization and microstructural analysis

4.1.1 Characterization of Pure titanium dioxide

Several factors were tested for the formation of nanoparticles such as sonication time, acid and alcohol types and concentrations, and water content. ANOVA was applied to optimize these parameters for a minimum particle size of TiO_2.

To further investigate the effect of ultrasonication time, the gel was exposed to an ultrasonic bath for three different periods of time (15, 30 and 60 min). The reaction mixture was fixed at 5 ml H_2O, 50 ml methanol without using acid. Figure 4.1 illustrates that the size of the nanoparticles is decreased with increasing the ultrasonication time. This is due to the effect of de-agglomeration of ultrasonic waves on the reaction mixture to prevent bigger chain formation of Ti-O-Ti. However, additional sonication time shows little effect, which will lead to increase the reaction temperature which may lead to back agglomeration of the particles. Sato et al. [31] showed that the increase in ultrasonic irradiation would decrease the viscosity and particle size of the suspension. Further increase in irradiation time after 30 minutes showed no effect in the size and distribution of the nanoparticles. Termnak et al. [32] showed that the aggregates that are strongly bound to each other which are difficult to be break by ultrasonic treatment, for weakly bound aggregates, the ultrasonic treatment would be able to break the aggregates and then smaller aggregates should be detected.

Figure 4.2 shows that the effect of water addition on the size of the produced nanocrystalline titanium dioxide. As the amount of water increases, the particle size is also increased which is due to the fast gel formation that may lead to higher agglomeration of catalyst particles to form bigger sizes. This is due to the nucleophilic attack of water on titanium (IV) isopropoxide which may lead to suppress the fast condensation of titanium (IV) isopropoxide species to yield titanium dioxide nanocrystals. In addition, the hydrolysis rate is low for less amount of water, which is due to the lower presence of alkoxy groups from water. This leads to a smaller particle size as a result of the less formation of Ti-O-Ti chains through alcoxolation[8, 33, 34].

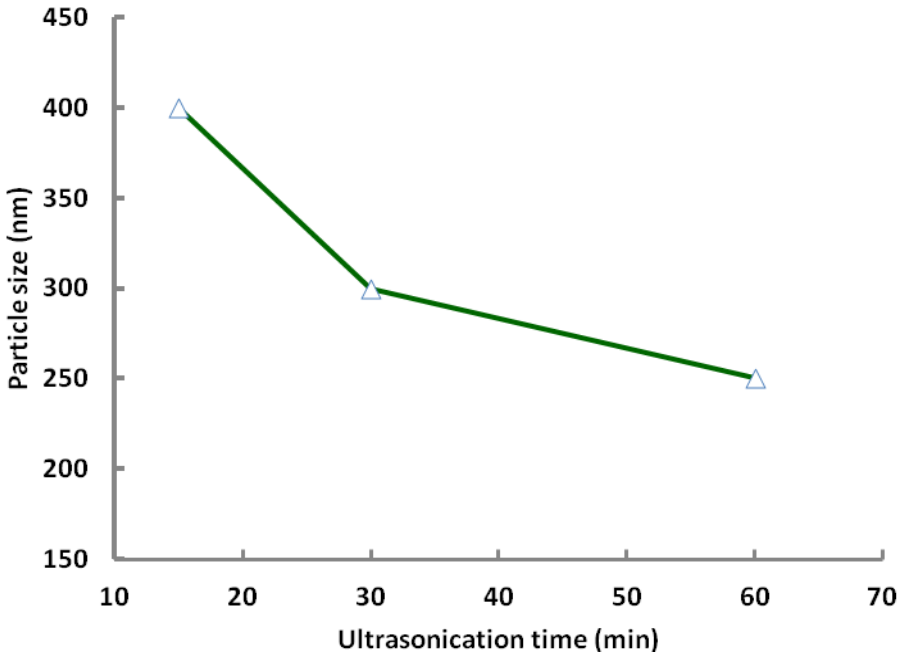

Figure 4-1: Variation of average particle size with ultrasonication time.

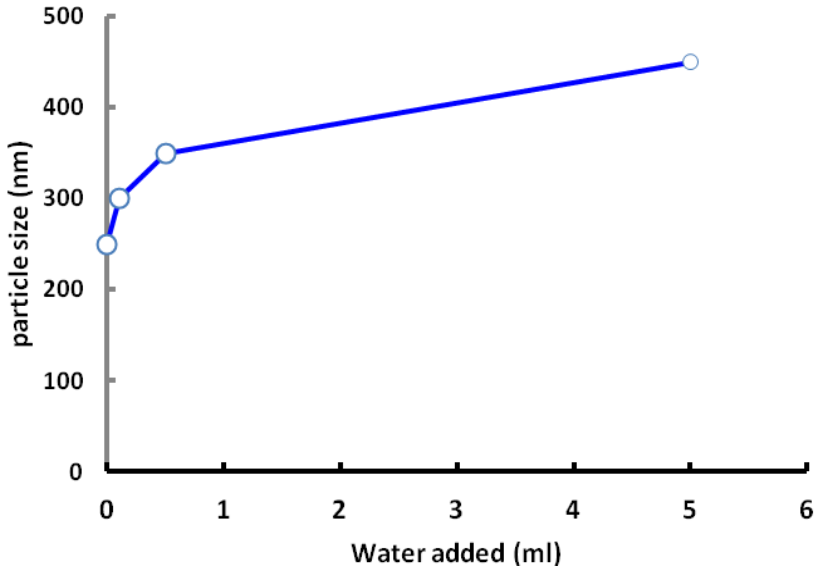

Figure 4-2: Variation of average particle size with the amount of water added.

On the other hand, the acid type and concentration plays a major role as a hydrolysis agent for the formation of nano Titanium dioxide. Two acids were examined for the formation of nano-TiO_2, which are organic acid (HAc) and Inorganic one (HCl). When acetic acid was used with ethanol a spheroid shape was produced, however, irregular shape was formed in the presence of hydrochloric acid (Figure 4.3). The lower acid concentration contributes to the better formation of spheroid shape. This finding was also apparent when isopropanol was used with HAc to produce lower particle size (Figure 4.4). Similar trends were observed by Gerko Oskam, et al, for the synthesis of TiO_2 from titanium (IV) alkoxide,

Furthermore, when methanol was used for the synthesis of nanocrystalline titanium dioxide, the presence of hydrochloric acid illustrated better formation of spheroid shape than that of using acetic acid, while the sample that treated in the absence of acid was the best in shape (Figure 4.5).

In general, the catalyst produced by using methanol and hydrochloric acid has given the smallest particle size while the one that produced using ethanol and isopropanol was further agglomerated to form bigger crystals. This trend is due to the slow hydrolysis of titanium (IV) isopropoxide in the cases of ethanol and isopropanol which can form dimeric species of titanium (IV) isopropoxide and further hydrolyzed to form trimeric species and so on. Moreover, it is clear that the higher acid concentration provides bigger particle sizes and non-spherical shape which is attributed to the decrease in the degree of crystallinity that leads to the development of Ti-O-Ti chain in bigger size and defects (Figure 4.6).

(a) mol HAc without addition of water

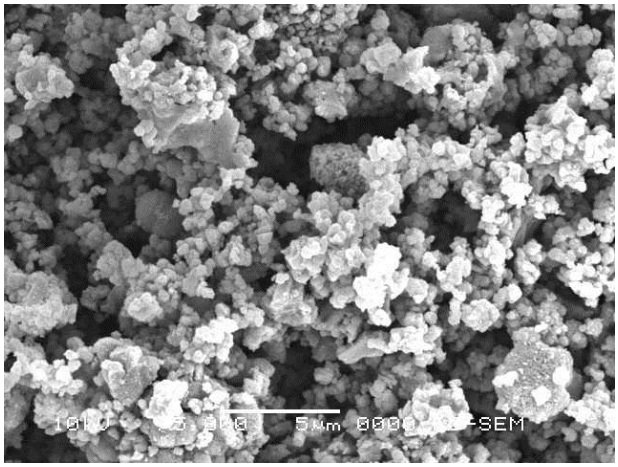

(b) mol HAc without addition of water

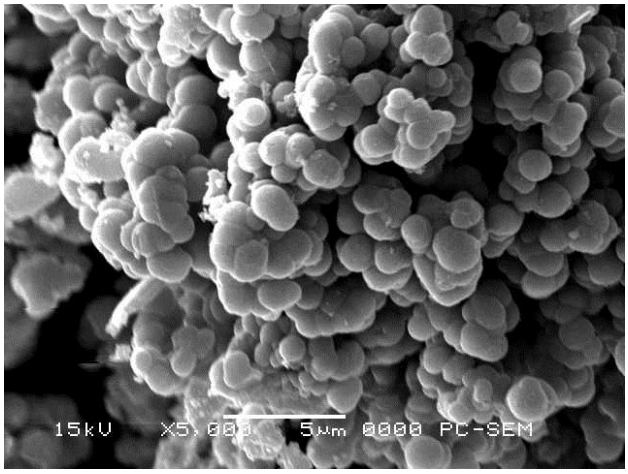

(c) 0.5 ml water without acid

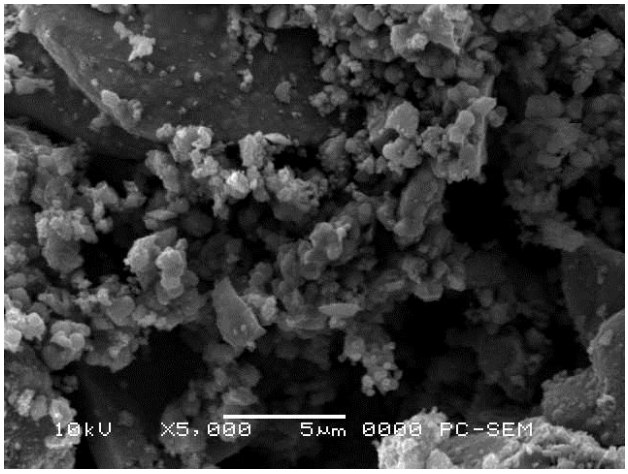

(d) 6.5×10^{-4} mol HCl- no addition of water

Figure 4-3: SEM morphology for TiO_2 nanoparticles produced using ethanol

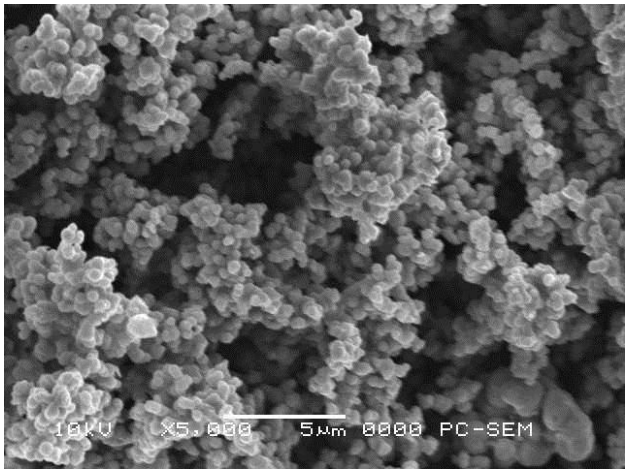

(a) 0.5 ml water without acid

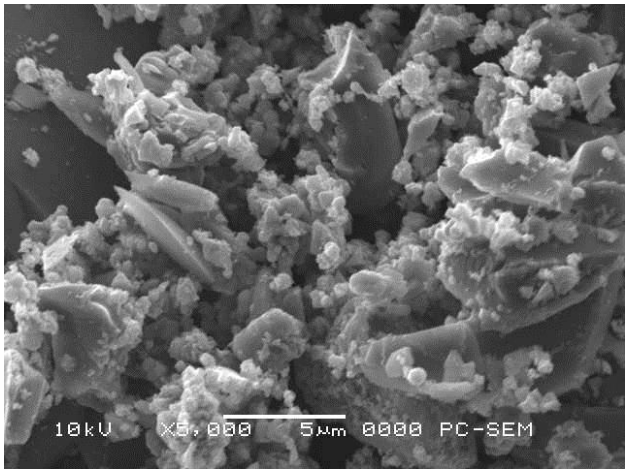

(b) 6.5×10^{-4} mol HAc with 0.5ml water

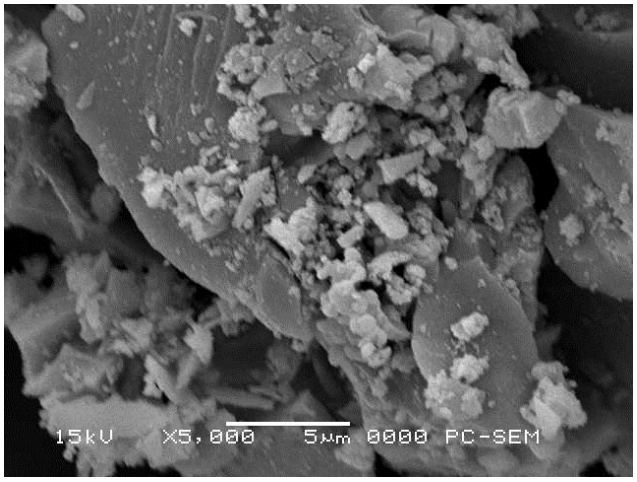

(c) 1.3×10^{-3} mol HAc- no addition of water

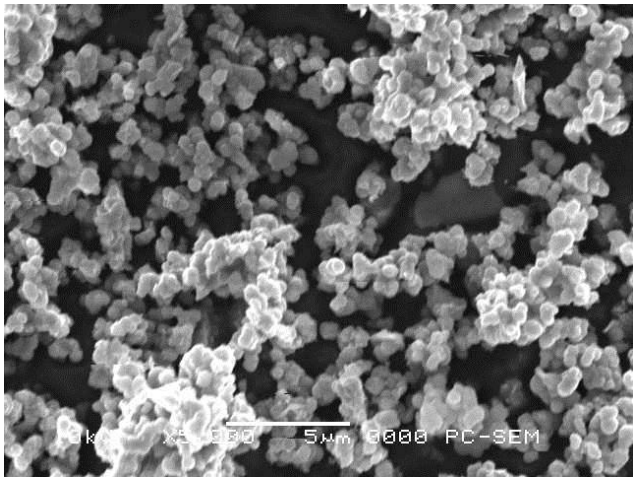

(d) 1.3×10^{-3} mol HCl with 0.5 ml water

Figure 4-4: SEM morphology for TiO_2 nanoparticles produced using methanol

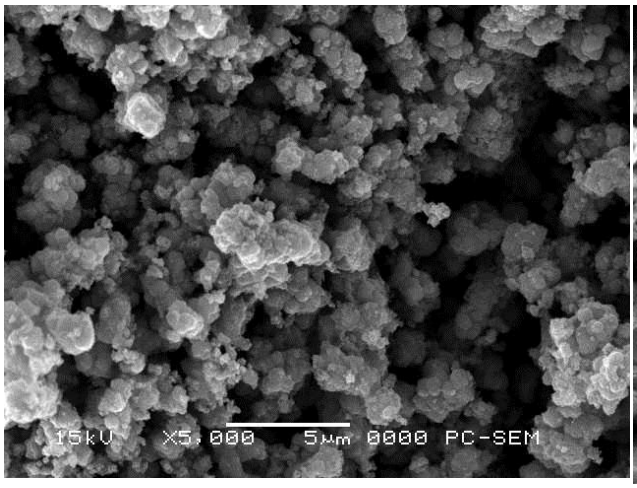

(a) 0.5 ml water without acid

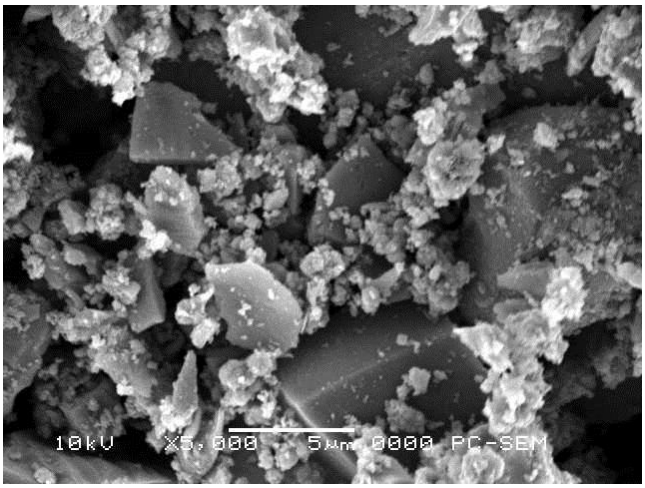

(b) 1.5×10^{-4} mol HCl with 0.5ml water

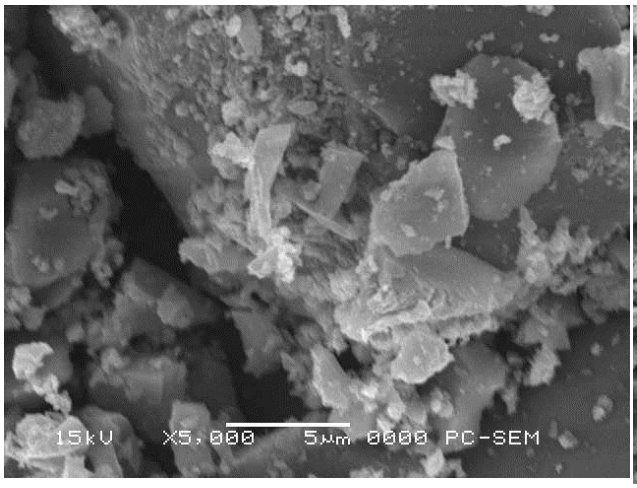

(c) 6.5×10^{-3} mol HCl without water

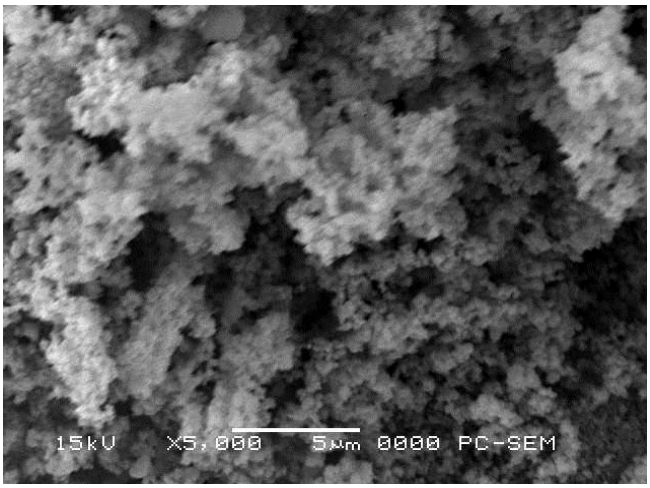

(c) 6.5×10^{-4} mol HAc without water

Figure 4-5: SEM morphology for TiO_2 nanoparticles produced using propanol

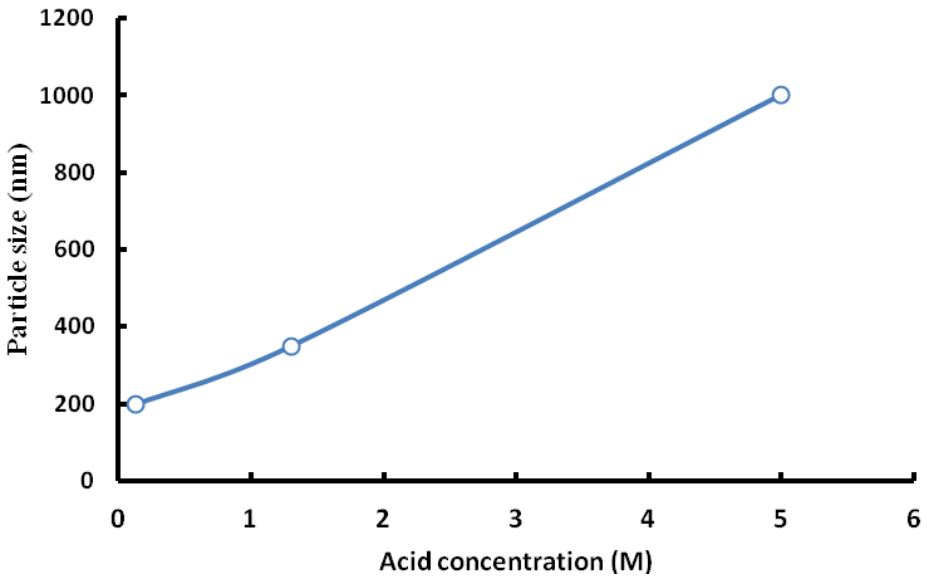

Figure 4-6: Variation of average particle size with the acid concentration.

XRD analysis of the produced sample that calcined at 350^{o}C is shown in Figure 4.7. It is cleared that several peaks appeared at 25^{o}, 36^{o}, 37^{o}, 38.5^{o}, 48^{o}, 54^{o}, 55^{o}, 62.5^{o} and 69^{o} 2θ which were due the presence of polycrystalline anatase structure that was confirmed by (101), (103), (004), (112), (200), (105), (211) and (220) at diffraction peaks, respectively [35]. Moreover, a weak peak located at 28° 2θ coming from the (110) face of rutile phase was found. When the samples were further calcined at 450^{o}C, Figure 4.8, some of the major anatase crystalline peaks were diminished which indicates the formation of anatase crystalline to rutile one[36-39].

This analysis is supported by the findings of Hussain, M, et al, and the work of Tran Trung, et al, where glycerol-containing solutions were used to prepare titanium dioxide. The found that, the catalyst was mainly formed of anatase phase of titanium dioxide, with minor presence of rutile phase when the sample was calcined at a relatively high temperature.

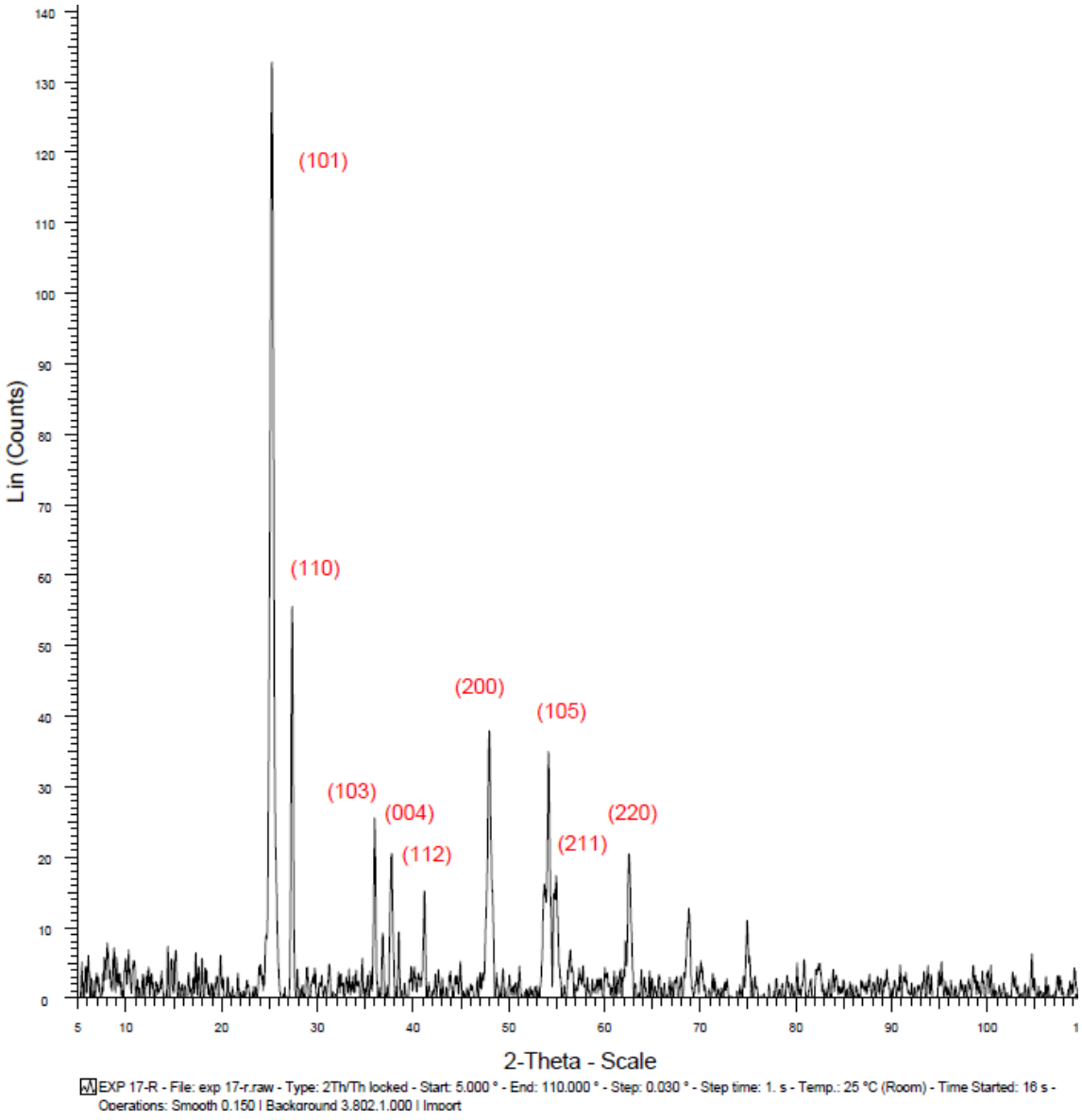

Figure 4-7: XRD pattern of polycrystalline TiO_2 nanoparticles obtained at 350 ^{o}C

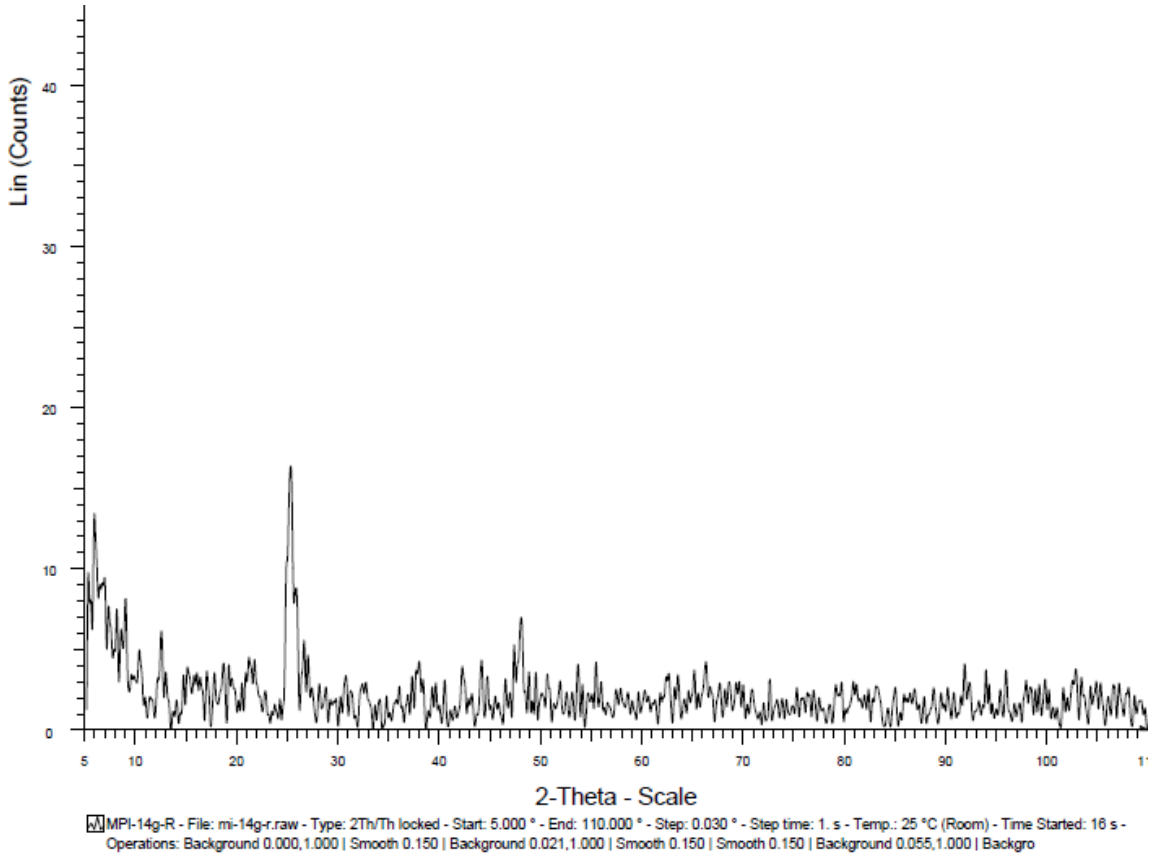

Figure 4-8: XRD pattern of polycrystalline TiO_2 nanoparticles obtained at 450 ^{o}C

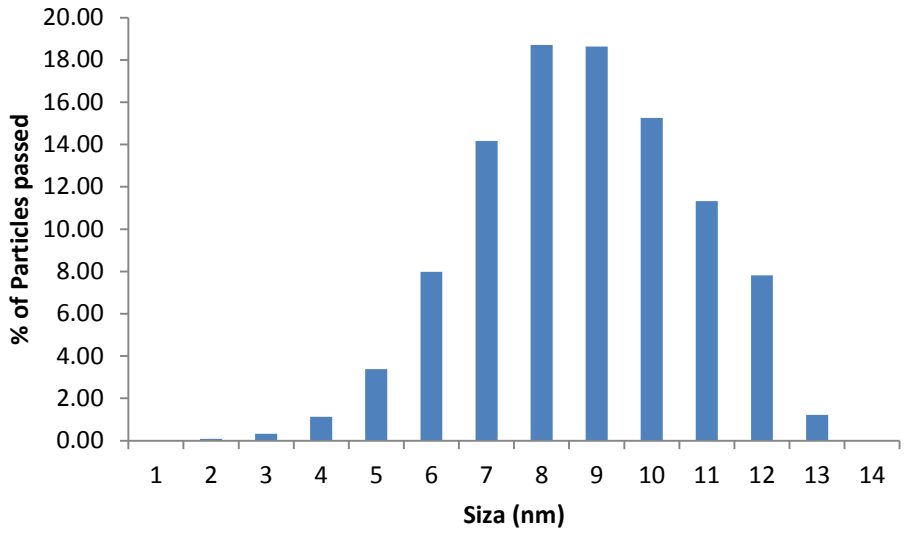

Figure 4-9: Particle size distribution

Particle size analysis (PSA) was done to measure the exact particle size and particle size distribution. Figure 4.9 shows that 53% of the sample is of less than 6 nm particle size and 98% is less than 10 nm. The homogeneity of the particle size indicates that, most of the sample is anatase form of titanium dioxide due to the fact that, rutile phase particles are much bigger in size and this could be noticed only if the amount of rutile is considerable.

The BET analysis is illustrated in Figure 4.10. It is revealed that, the surface area of the catalyst is 112.59 m^2/g using Langmuir isotherm. Compared to the conventional surface area of titanium dioxide which is mostly between 30 – 120 m^2/g, it can be noticed that, this catalyst has a high surface area. The small average particle size (6-10 nm) size and weak agglomeration are responsible for this high surface area of the particles. Nitrogen adsorption–desorption isotherm showed that the catalyst is mesoporous from the shape of the isotherm due to the high surface area.

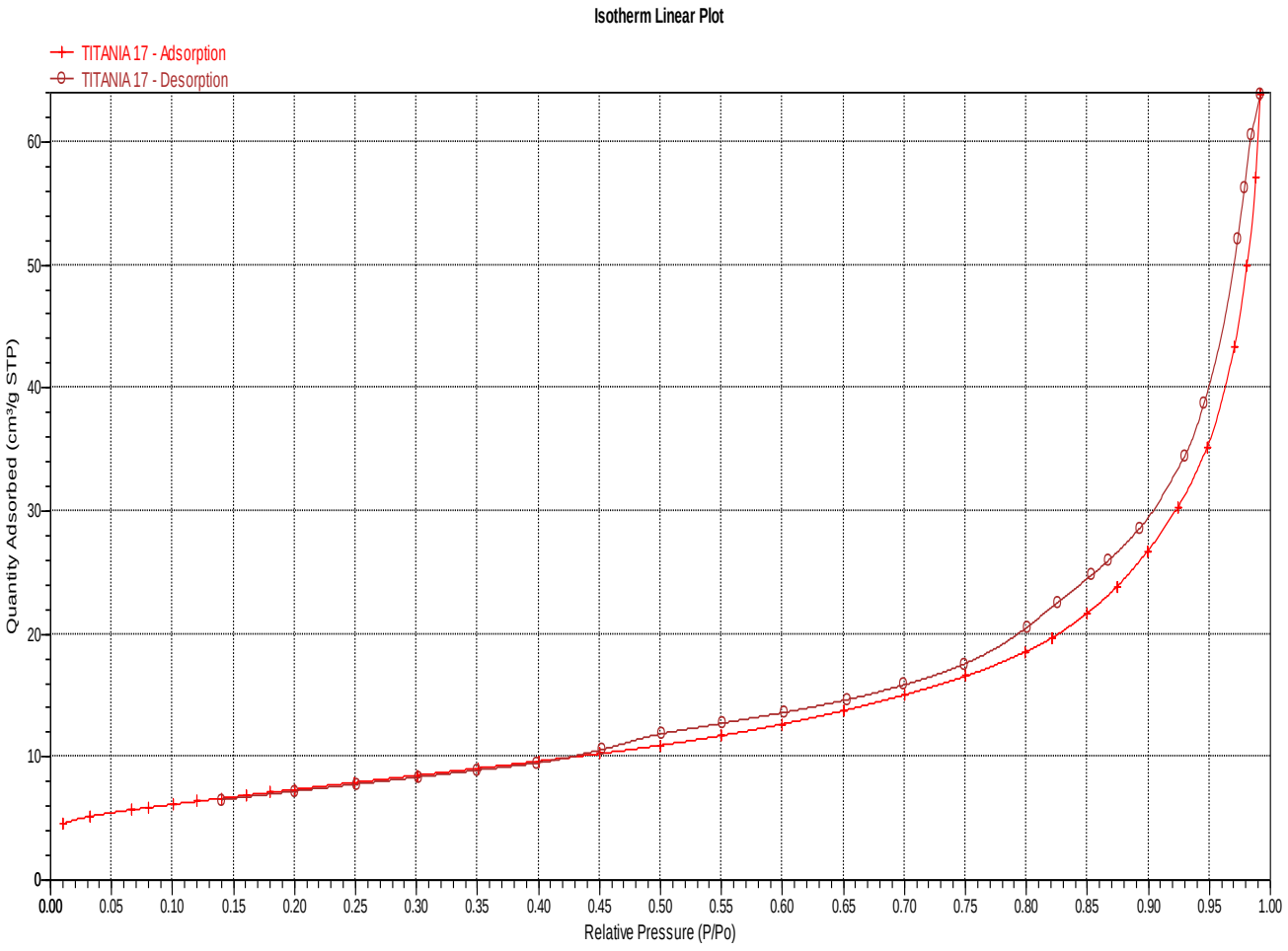

Figure 4-10: BET isotherm of adsorption desorption of nitrogen

4.1.2 Characterization of Metal-doped titanium dioxide

Figure 4.11 illustrates the SEM micrograph of Fe-doped titanium dioxide before calcination (a) and after calcination (b). It can be clearly seen that, the overall structure of the catalyst is spherical, the aggregates observed in the calcined sample is due to the crystallization which takes place during calcination process as well as the incorporation of iron into the catalyst matrix. This is due to the changes in the shape by the formation of iron-oxygen bonding and hence lattice distortion[27].

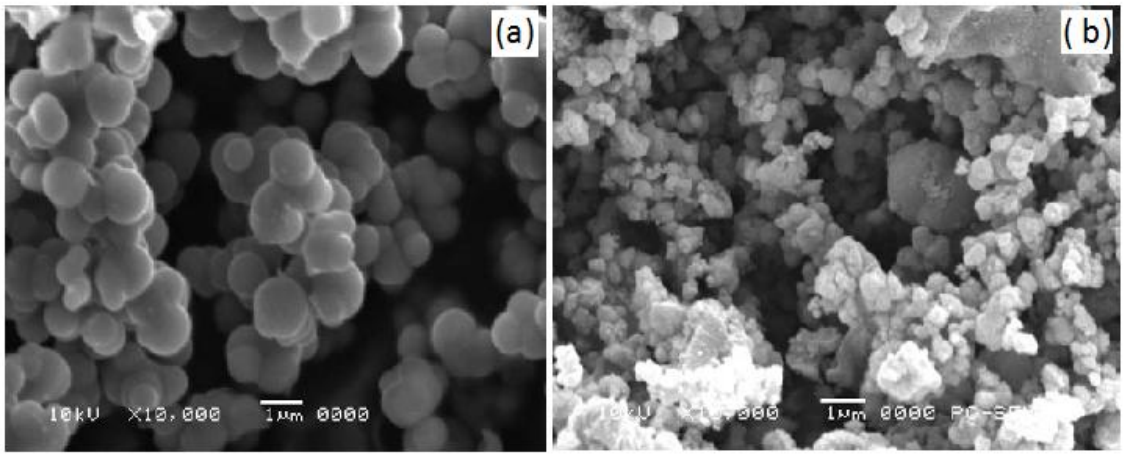

Figure 4-11: SEM image of Fe-doped TiO_2, (a) before calcination, (b) after calcination

Figure 4.12 shows the SEM image of V-doped titanium dioxide produced at different precursor to water ratio. It can be seen that, at high precursor to water ratio (less amount of water), the catalyst particles have spherical shape involves smaller particles, however, the exact particle size distribution using particle size analysis (PSA) is found to be in the range of 3-11 nm as shown in Figure 4.12. When the amount of water increased (Figure 4.12 (c)), one can notice the tendency

to form bigger aggregates from smaller particles, which is known as Ostwald ripening, is due to the coarsening and aggregation which competes the nucleation during hydrolysis, and the extent of this aggregation is a direct result of titanium to water ratio, where the higher ratio (higher than 5) gives smaller particle size. Never the less, low amount of water may lead to the combustion of residual hydrocarbon during calcination process, and hence coke may present in the final catalyst[1, 40].

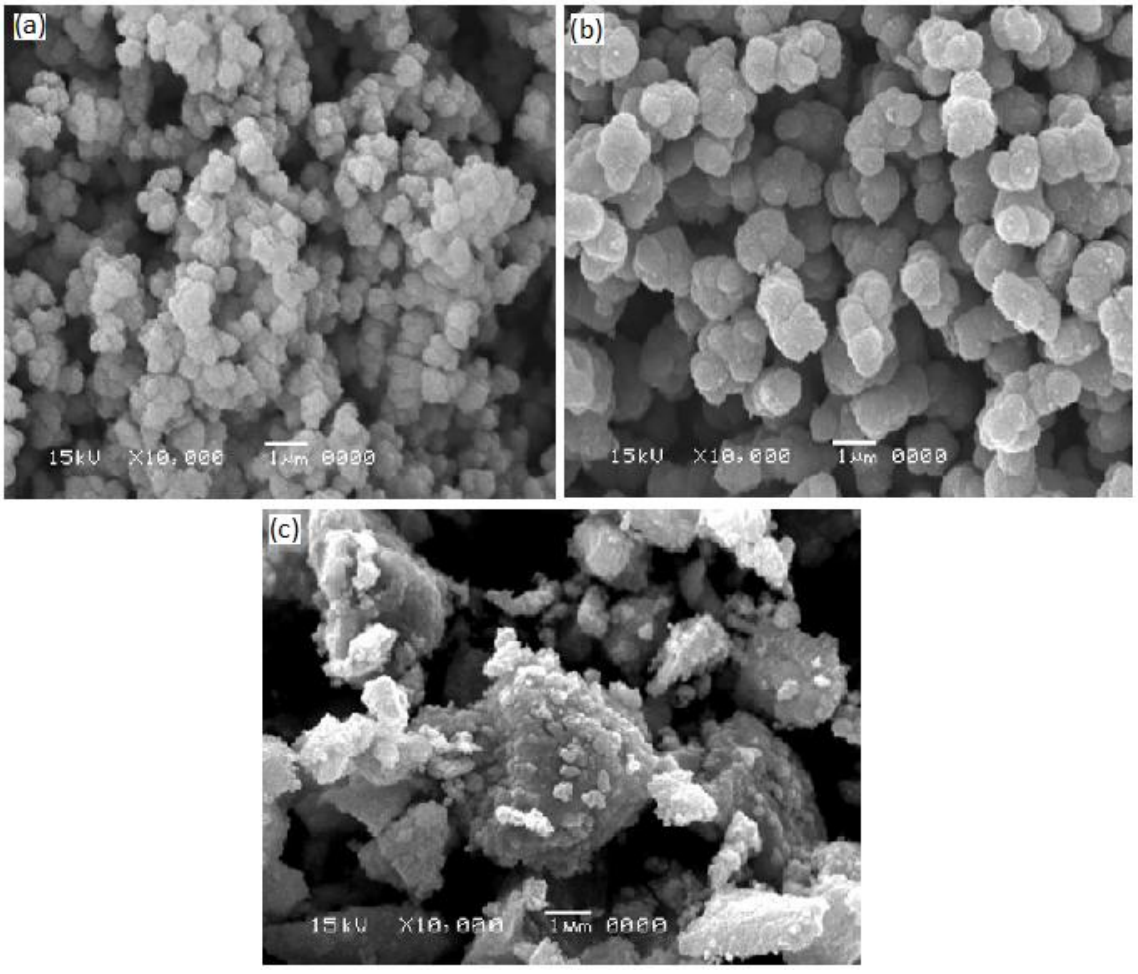

Figure 4-12: SEM image of V-doped titanium dioxide: (a) precursor to water ratio is 10, (b) precursor to water ratio is 5, (c) precursor to water ratio is 1.

The SEM analysis for W-doped titanium dioxide is shown in Figure 4.13 (b) alongside with that of pure titanium dioxide, which is shown in Figure 4.13 (a) for comparison. It can be noticed that, both catalysts have spherical shape with tendency to form more aggregates in case of pure titanium dioxide (a). This tendency, which is known as Ostwald ripening, is due to the coarsening and aggregation which competes with nucleation during hydrolysis, which is a function of titanium to water ratio. This ratio is higher in the synthesis of pure titanium dioxide than W-doped titanium dioxide where some water was replaced by sulfuric acid to complete the dissolving of tungsten oxide. However, the higher acidity of tungsten solution cannot be excluded as the tungsten oxide is mildly acidic and sulfuric acid was added as well.

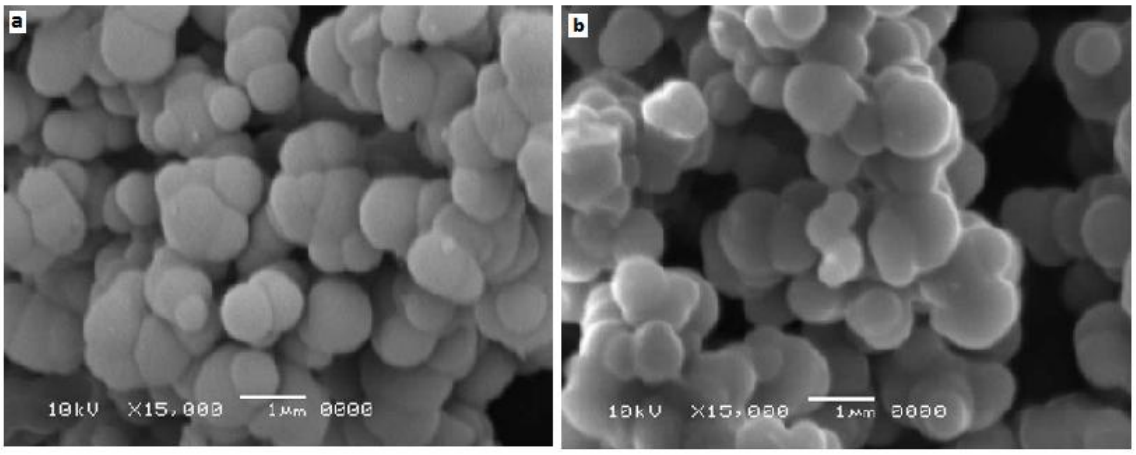

Figure 4-13: SEM micrographs of (a) pure titanium dioxide and (b) W-doped titanium dioxide.

Generally, there are three phases of titanium dioxide, which are anatase, rutile, and brookite which. Anatase is the most active phase and can be converted to rutile when thermally treated at 500^{o}C. The XRD pattern of 1.7 wt% vanadium doped titanium dioxide is shown in Figure 4.14, as the peaks are indicated at planes (101), (004), (200), (105), and (220) at 2θ of 25^{o}, 36^{o}, 48^{o}, 54^{o}, 62^{o} respectively. It can be seen that, the phase of titanium dioxide is mainly anatase, which is confirmed by (101) peak at at 2θ of 25^{o}. The additional peaks indicate the presence of rutile phase of titanium dioxide and crystalline (lattice) distortion caused by the incorporation of vanadium due to the difference in atomic radius of vanadium (134 pm) and titanium (147 pm) as stated by Pauling principle [24, 25, 41].

The XRD pattern of Fe-doped Titanium dioxide (Figure 4.15) shows the presence of smaller particles of titanium dioxide nanomaterial. The anatase phase of TiO_2 can be seen as the value of 2-theta angle is around 25^{o} some amount of rutile phase of titanium dioxide can be observed as well at 2-theta angle is around 30-o. The broadening observed at higher values of 2 theta angle indicates the imperfection of crystals caused by the presence of some defects on the reflective planes. This can be avoided by decreasing the calcination temperature [8]. On the other hand, the shift in 2-theta angle indicates the incorporation of iron into titanium dioxide because of the distortion of lattice [11,12].

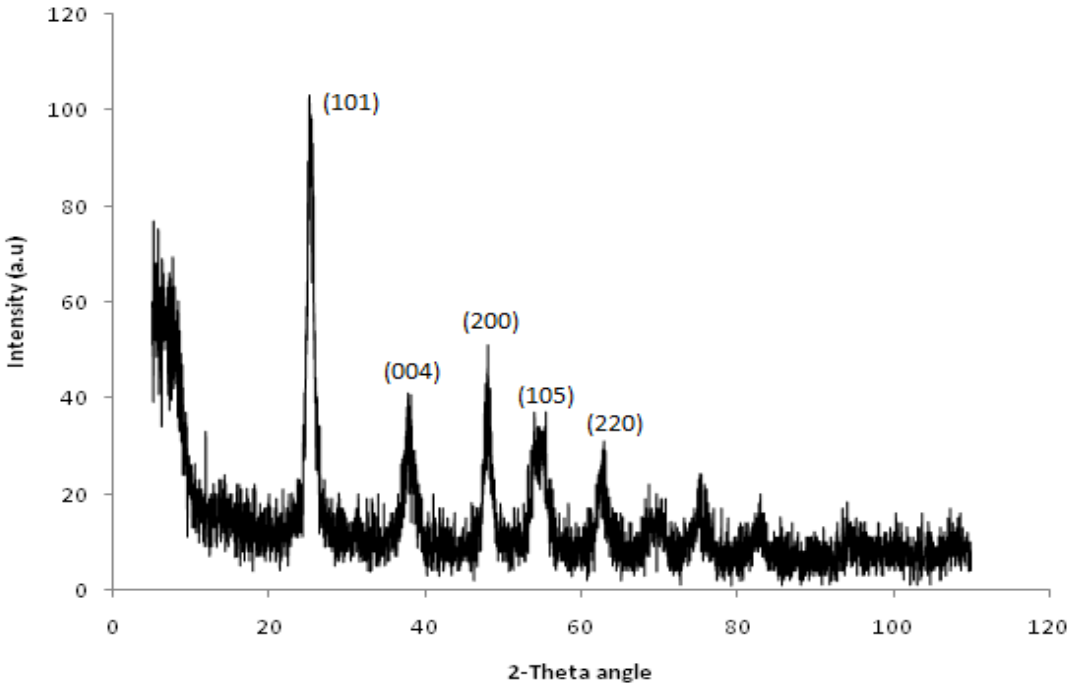

Figure 4-14: XRD pattern of as-prepared vanadium doped titanium dioxide

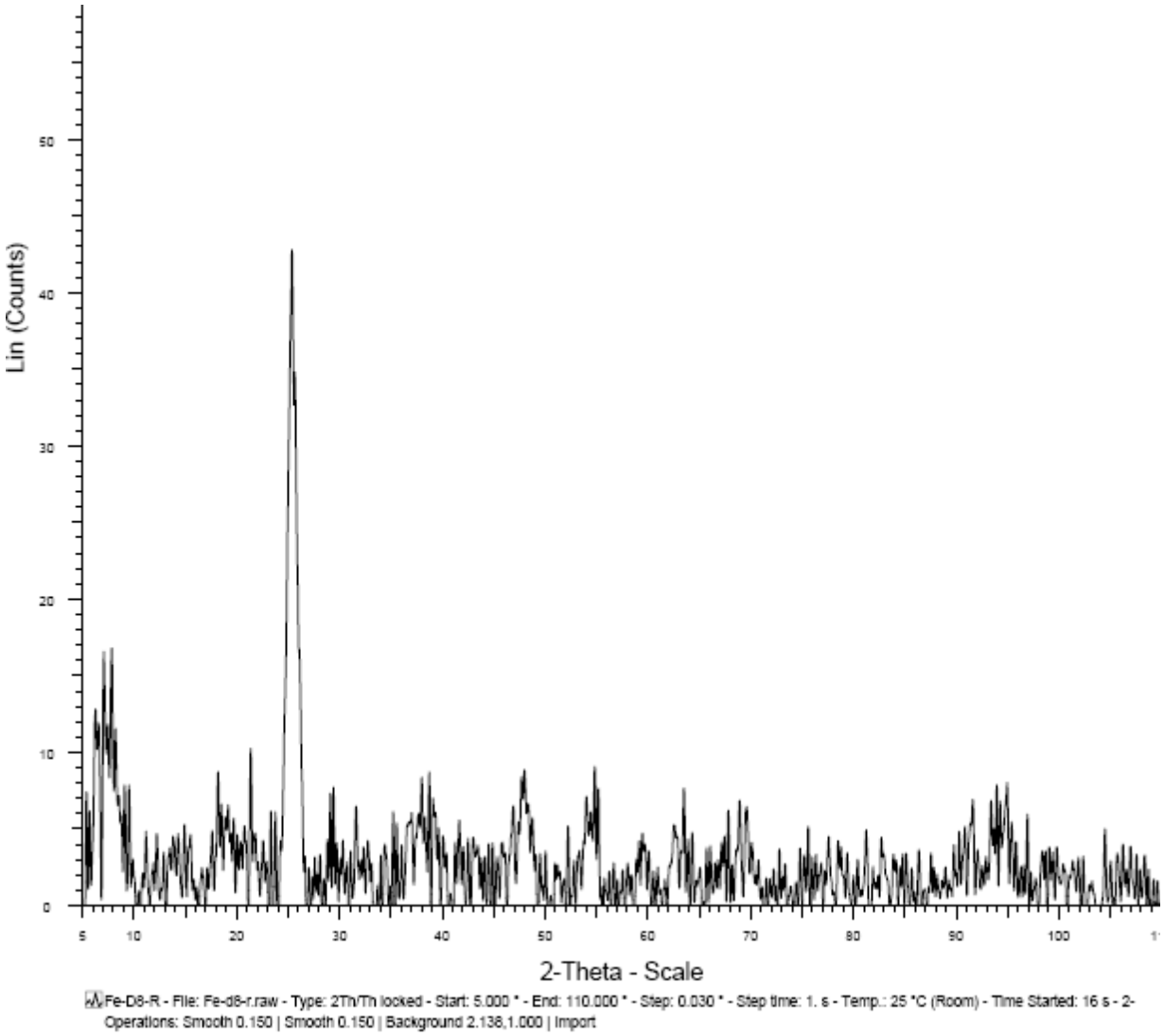

Figure 4-15: XRD pattern of Fe-doped Titanium dioxide.

The XRD pattern of W-doped titanium dioxide calcined at 500^{o}C is shown in Figure 4.16. It can be noticed that the catalyst is mainly in anatase form as indicated by the sharp peak (101) at the value of 2-theta angle of 25^{0}.The later peaks indicated the phase change towards rutile as a result of the calcination temperature of 500^{o}C (rutile phase is usually present when the calcination temperature is between 500^{o}C to 700^{o}C). The lattice distortion is a direct result of the incorporation of tungsten oxide into the matrix of titanium dioxide due to the diffusion of tungsten in the crystal lattice resulting in the crystal grain growth[20, 29, 42].

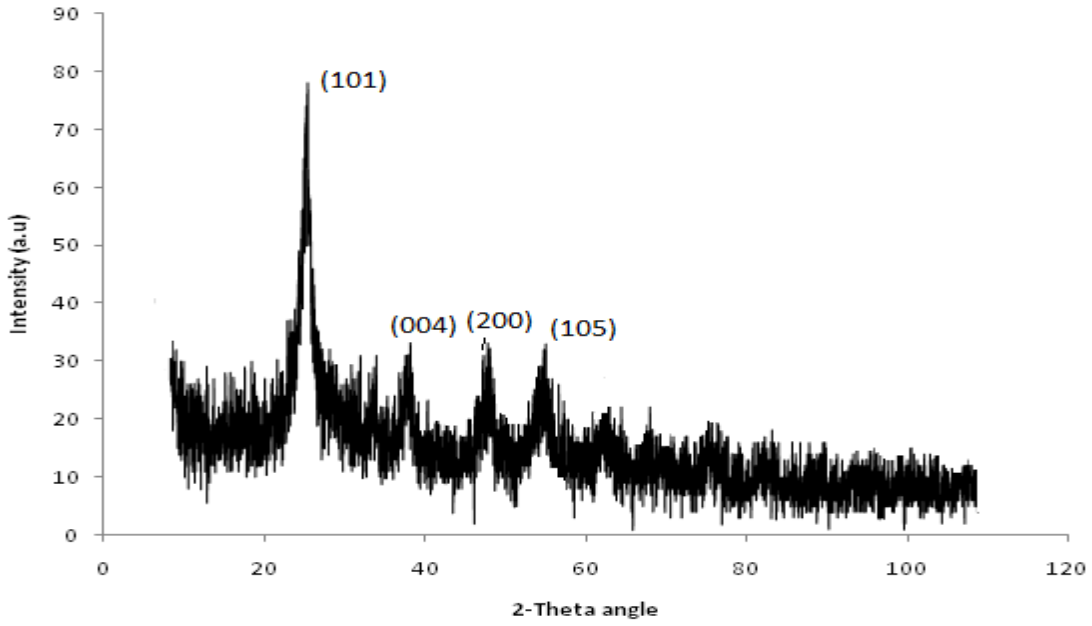

Figure 4-16: XRD pattern of W-doped titanium dioxide.

The amount of vanadium doped on the surface of titanium dioxide is measured using energy dispersive spectroscopy (EDS). The percentage of vanadium on the catalyst was verified using different initial concentrations of vanadium solution, and the result of this variation is shown in Figure 4.17. It is noticed that, at concentrations higher than 4000 ppm, the amount of vanadium doped into titanium dioxide tends to remain constant at 1.7 wt%, this is due to the saturation of titanium dioxide surface with vanadium oxide formed by chemical oxygen-metal bond. The EDS graph of vanadium doped titanium dioxide prepared 5000 ppm is shown in Figure 4.18, where minor amount of Cl is present in the catalyst, coming from the HCl acid used in synthesis.

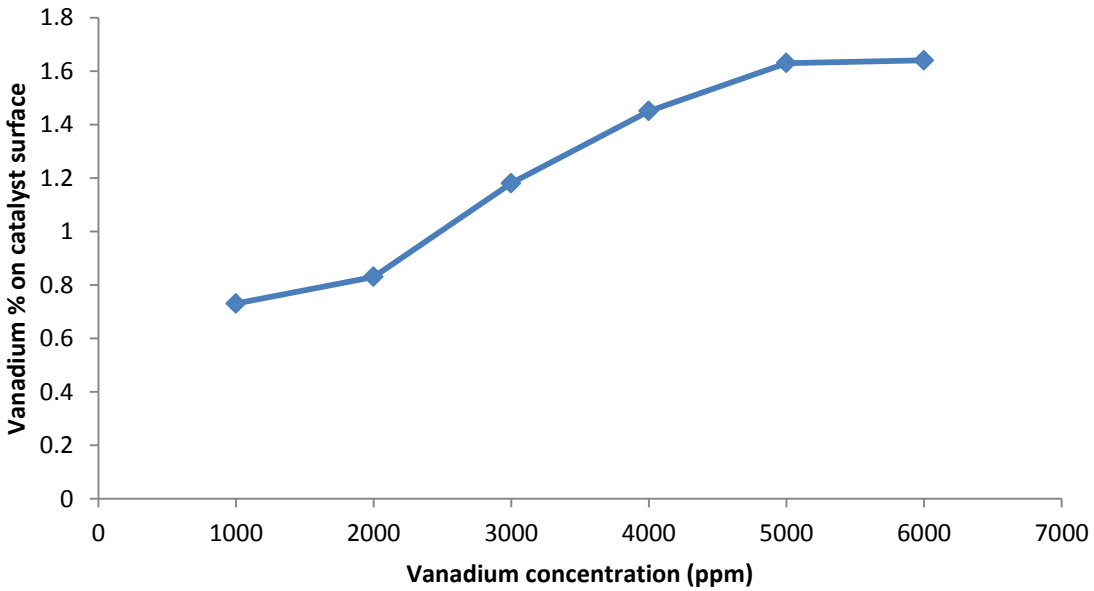

Figure 4-17: Percentage of vanadium doped on titanium dioxide as the concentration of vanadium on solution increased from 1000 to 6000 ppm.

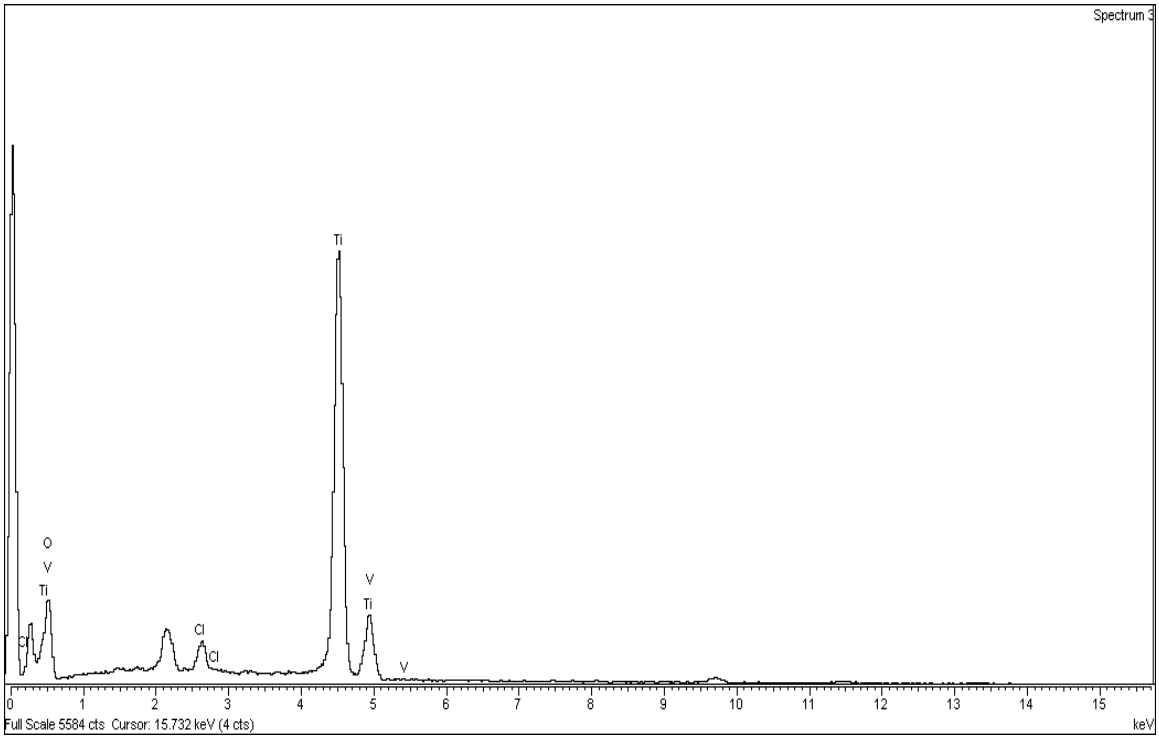

Figure 4-18: Energy dispersive spectrocsopy (EDS) of vanadium doped titanium dioxide.

It can be seen from Figure 4.19 that, at higher concentration of iron solution, the percentage of iron doped on the surface of titanium dioxide remains constant, this can be attributed to the prevention of incorporation of iron (III) ions into titanium dioxide matrix as a result of the formation of surface bound iron oxide phases [6,7]. Figures 4.20 and 4.21 show the graphs of EDS of selected samples and the presence of iron doped into titanium dioxide, as well as, minor amount of Cl from the acid used which is HCl.

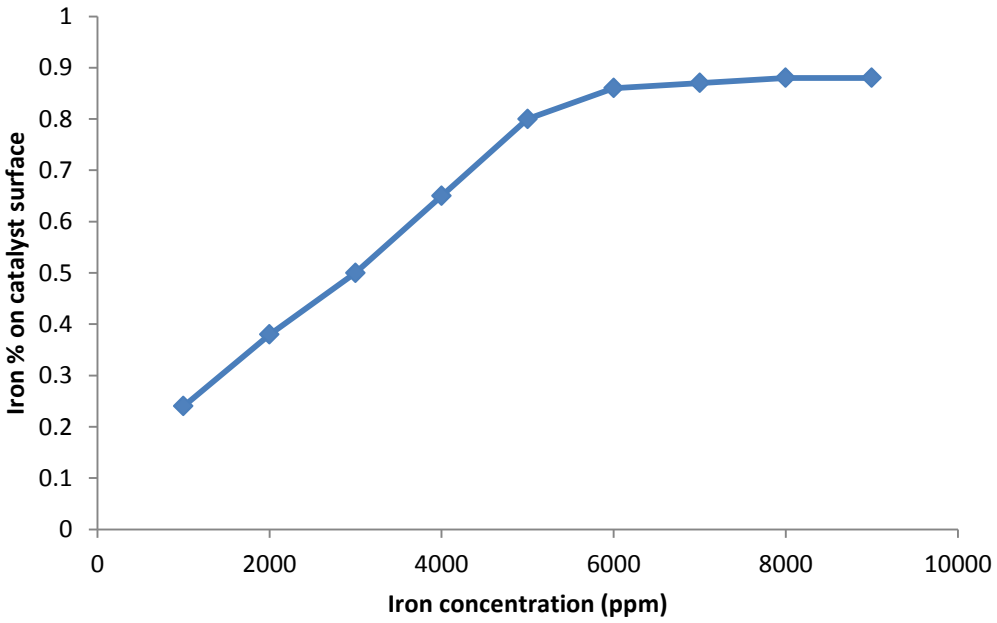

Figure 4-19: Percentage of iron doped as the iron concentration increased

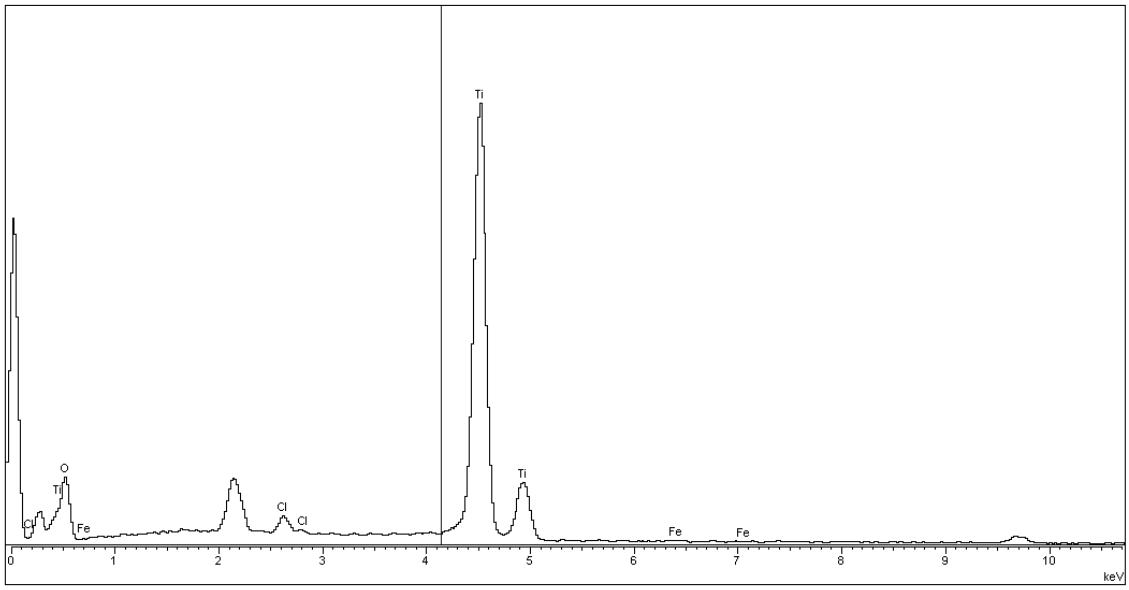

Figure 4-20: EDS graph of sample 1 of Fe-doped titanium dioxide

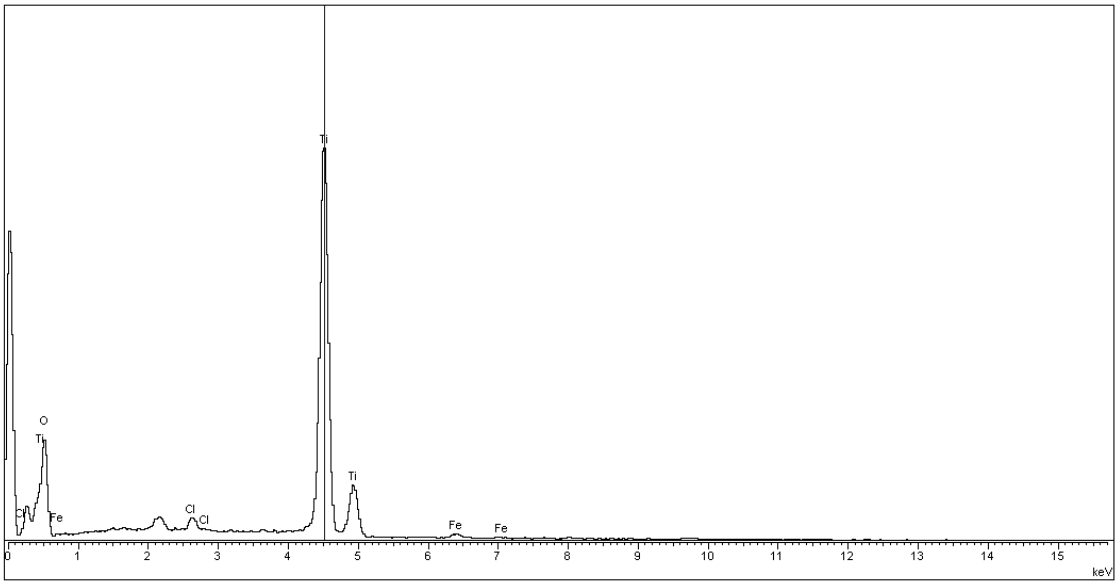

Figure 4-21: EDS graph of sample 9 of Fe-doped titanium dioxide

In addition to that, EDS analysis was carried out in order to measure the exact percentage of tungsten doped in titanium dioxide, the results are shown in Figure 4.22 for different samples prepared using different concentrations of the original solution contains tungsten. It can be noticed that, at low concentrations of tungsten (lower than 3000 ppm) no or minor amount of tungsten was measured. This percentage was increased with increasing solution concentration of tungsten until it reached 2.7 wt% at concentration of 6000 ppm. Minor amount of carbon present in the final sample as shown in Figure 4.23 is due to the high calcination temperature. In addition, trace sulfur was noticed in the catalyst samples, which is expected from sulfuric acid that was used to have complete dissolution of tungsten oxide in water.

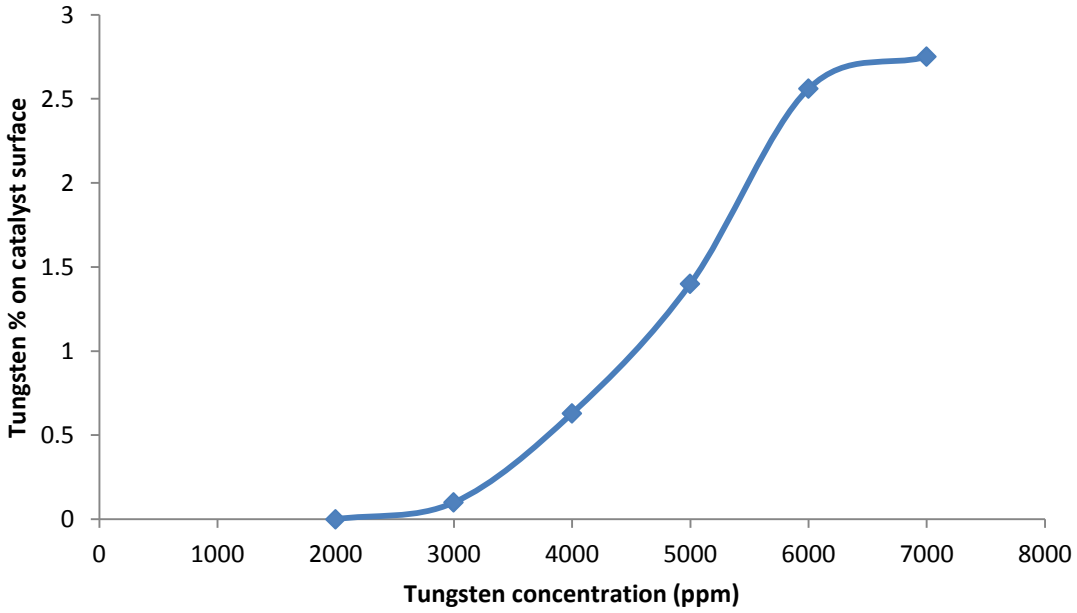

Figure 4-22: Loading of Tungsten on Titanium dioxide as a function of the concentration of initial solution of Tungsten.

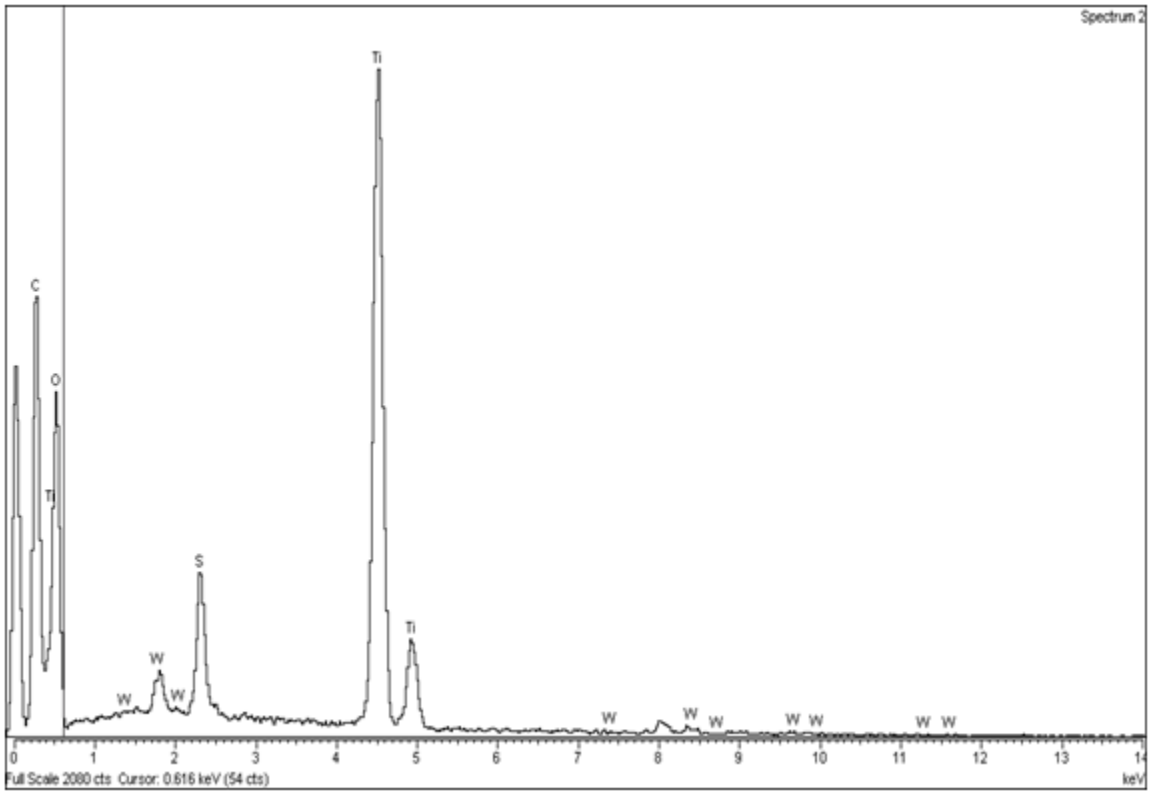

Figure 4-23: Energy Dispersive spectroscopy (EDS) of W-doped Titanium dioxide.

BET analysis of pure and vanadium doped titanium dioxide was carried out, and the results are shown in Table 4.1. It can be seen that, the surface area of pure and vanadium doped titanium dioxide are almost similar (62.9 m^2/g of pure titanium dioxide and 66.1 m^2/g for vanadium doped titanium dioxide). This similarity is because of, there is no separate growth of metal oxide on the surface of titanium dioxide, moreover, vanadium oxide is well dispersed on the surface which is confirmed by the absence of any characteristic peak of vanadium on the XRD patterns observed. The results also indicated similar Langmuir surface area as well as similar pore size[20].

Table 4-1: BET analysis of pure and V-doped titanium dioxide.

property	**Pure titanium dioxide**	**V-doped titanium dioxide**
BET surface area	62.9336 m^2/g	66.1237 m^2/g
Langmuir Surface Area	88.1457 m^2/g	93.2200 m^2/g
Single point desorption total pore volume of pores less than 19.377 Å width at p/p° = 0.140464200	0.023739 cm^3/g	0.024800 cm^3/g
Adsorption average pore width (by BET model)	61.5828 Å	57.318 Å

Furthermore, BET analysis was done for W-doped titanium dioxide as shown in Table 4.2. It is found that the catalyst surface area was increased significantly from 62.9 m^2/g for pure titanium dioxide to 152.3 m^2/g for W-doped titanium dioxide. This increment is attributed to the separate growth of metal oxide on the catalyst surface, which acts as structural promoter to prevent surface agglomeration. In addition to that, the higher particles separation of W-doped titanium dioxide -as shown by SEM- has a direct impact in this higher area.

Table 4-2: BET analysis of pure and W-doped titanium dioxide.

property	**Pure titanium dioxide**	**W-doped titanium dioxide**
BET surface area	62.9 m^2/g	152.27 m^2/g
Langmuir Surface Area	88.15 m^2/g	213.29 m^2/g
Single point desorption total pore volume of pores less than 19.377 Å width at p/p° = 0.140464200	0.0238 cm^3/g	0.0577 cm^3/g
Adsorption average pore width (4V/A by BET)	61.583 Å	56.111 Å

CHAPTER 5

ADSORPTION ISOTHERMS AND KINETICS OF PHOTODEGRADATION OVER TiO_2 NANOCATALYST

5.1 Adsorption isotherms

5.1.1 Adsorption of Methylene blue (MB) as a test of photocatalytic activity

The photocatalytic activity of pure and W-doped titanium dioxide was investigated by measuring the percentage of MB degraded. Figure 5.1 shows that, the catalyst activity was increased significantly by incorporating tungsten into titanium dioxide which has increased the catalyst maximum uptake from 10 mg/g in the case of pure titanium dioxide to 20 mg/g for W-doped titanium dioxide. This is attributed to the more efficient distribution of energy levels of valence and conduction bands of TiO_2 and WO_3 (WO_3 has a band gab of 2.8 eV) compared to that of pure TiO_2 which is 3.2 eV.

The effect of MB solution pH on the catalyst uptake was investigated for solution with pH of 4, 6 and 10 using W-doped titanium dioxide where the degradation is shown in Figure 5.2. It was noticed that the catalyst is more efficient at higher pH as a result of the dimerization of MB, which may take place alongside with the formation of chemical bonding of the hydroxyl group on the catalyst surface during adsorption period. In addition, the catalyst surface may attract the positive charge of nitrogen in MB[1-3, 43-45].

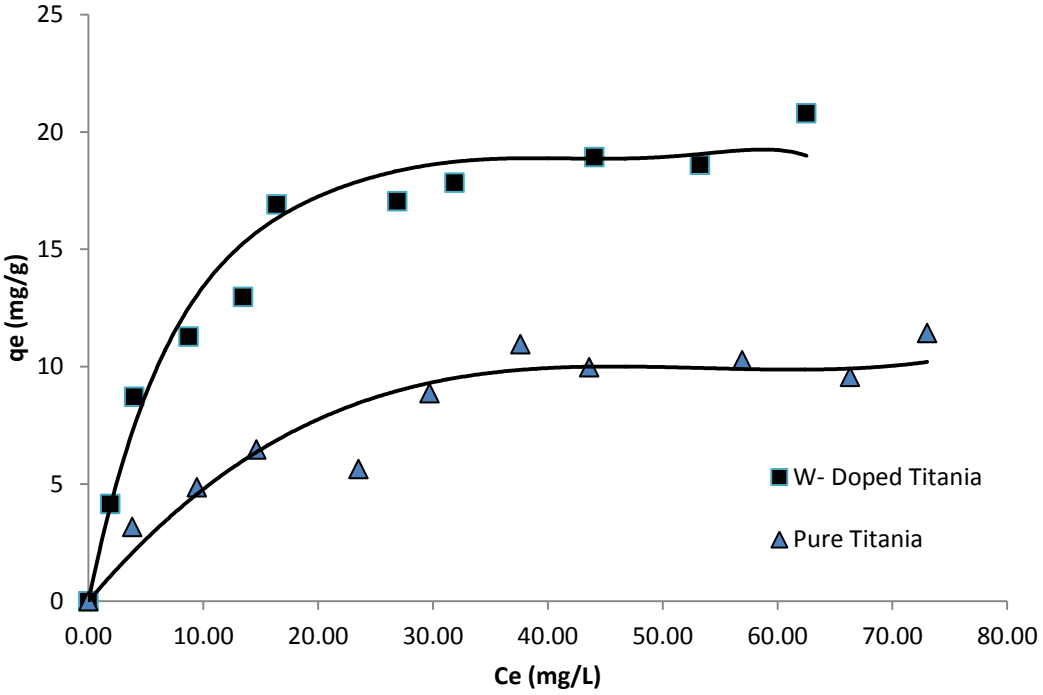

Figure 5-1: Degradation of MB using pure and W-doped titanium dioxide.

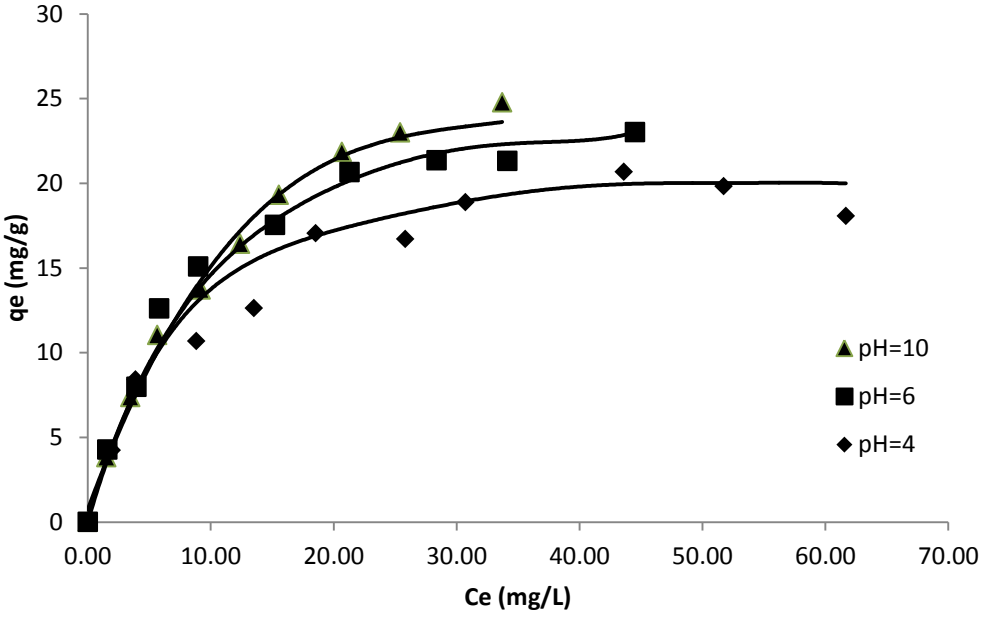

Figure 5-2: Degradation of Mb using 2.7 wt% W-doped Tiatania.

The effect of incorporation of vanadium into titanium dioxide matrix on the degradation of MB was investigated and the results are shown if Figure 5.3. It can be seen that, doping of vanadium into titanium dioxide has increased the catalyst uptake significantly from 10 mg/g to 17 mg/g. This enhancement of photocatalytic performance of titanium dioxide can be attributed to the increment on the surface barrier which leads to less space in the charge region, this large electric field makes the electron hole pair more separated and hence, more efficient.

Figure 5.4 shows the effect of different solution pH on the degradation of MB using V-doped titanium dioxide. It can be seen that, the catalyst uptake increased from 14 mg/g at pH 4 to 16 mg/g at pH 6, and 20 mg/g at pH 10. This increment can be attributed to the fact that, at higher pH, dimerization of MB may take place during the period of adsorption and the reaction of negatively charged hydroxyl group with MB in solution, in addition to that, physical interaction may occur between the negative charge of catalyst surface and the nitrogen charge on MB[45].

When titanium dioxide was doped with iron, the same trend as tungsten and vanadium was observed, where the photocatalystic has been enhanced when measured by the photocatalytic degradation of Methylene blue using both pure and Fe-doped titanium dioxide as shown in Figure 5.5. the effect of pH has been studied as well as shown in Figure 5.6.

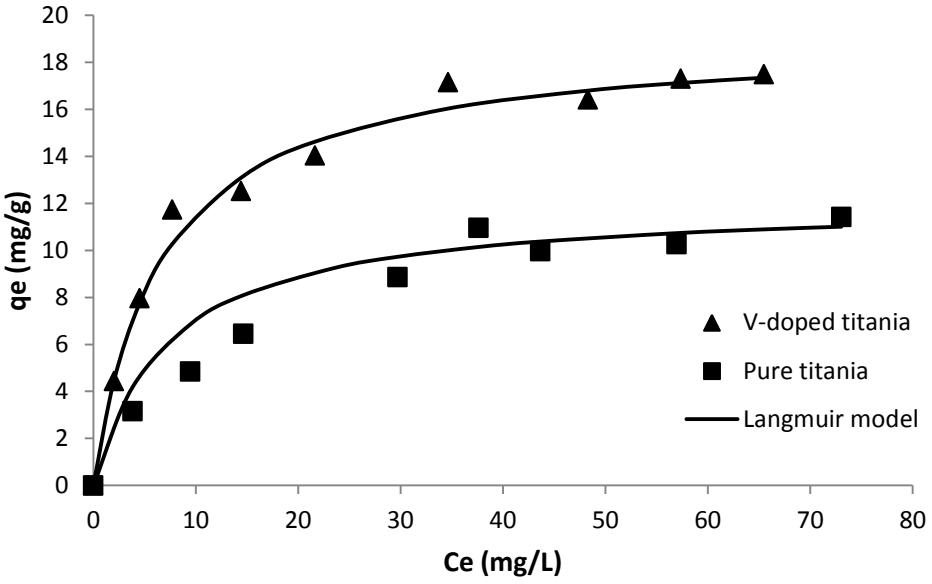

Figure 5-3: Isotherms of photocatalytic degradation of MB using pure and V-doped titanium dioxide.

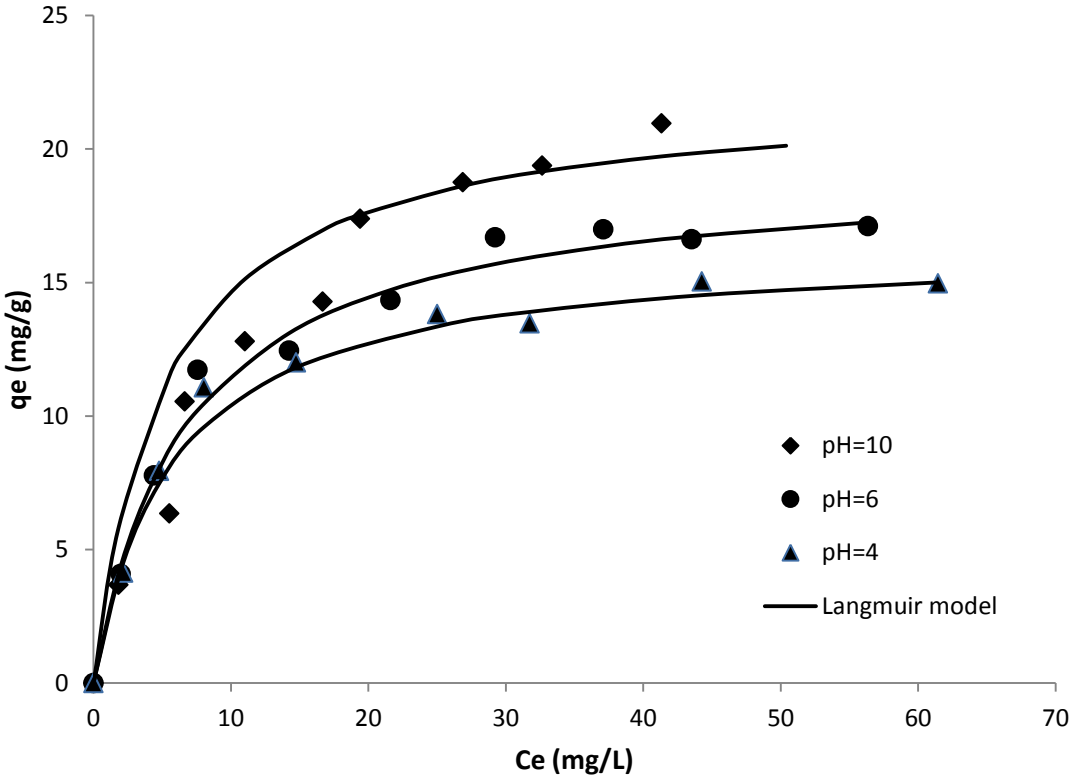

Figure 5-4: Isotherms of photocatalytic degradation of MB at different pH using V-doped titanium dioxide.

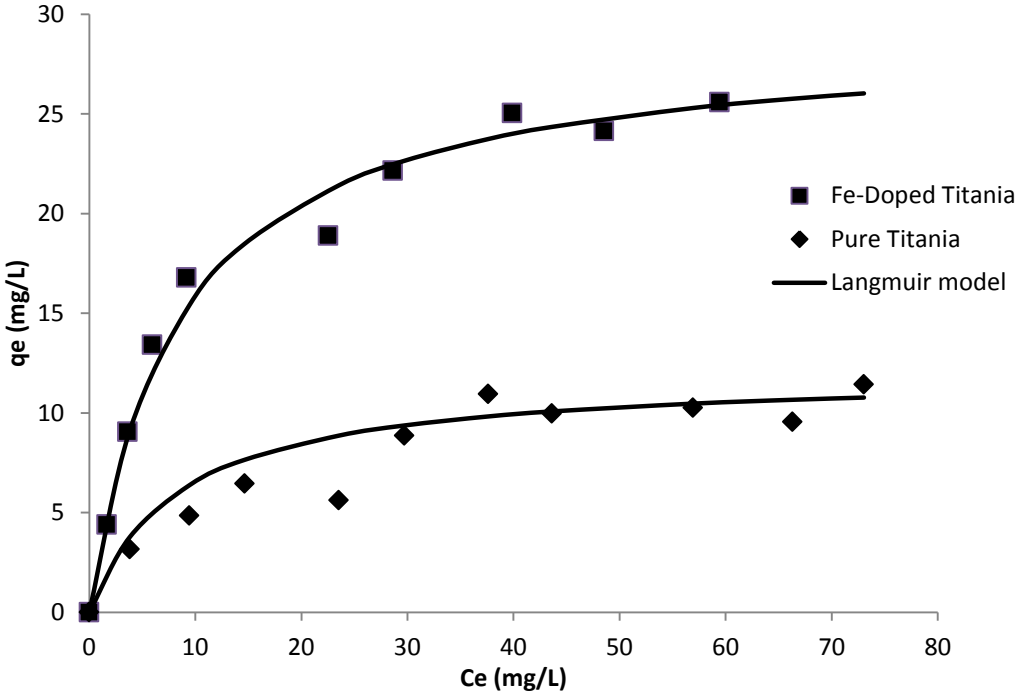

Figure 5-5: Isotherms of photocatalytic degradation of MB using pure and Fe-doped titanium dioxide.

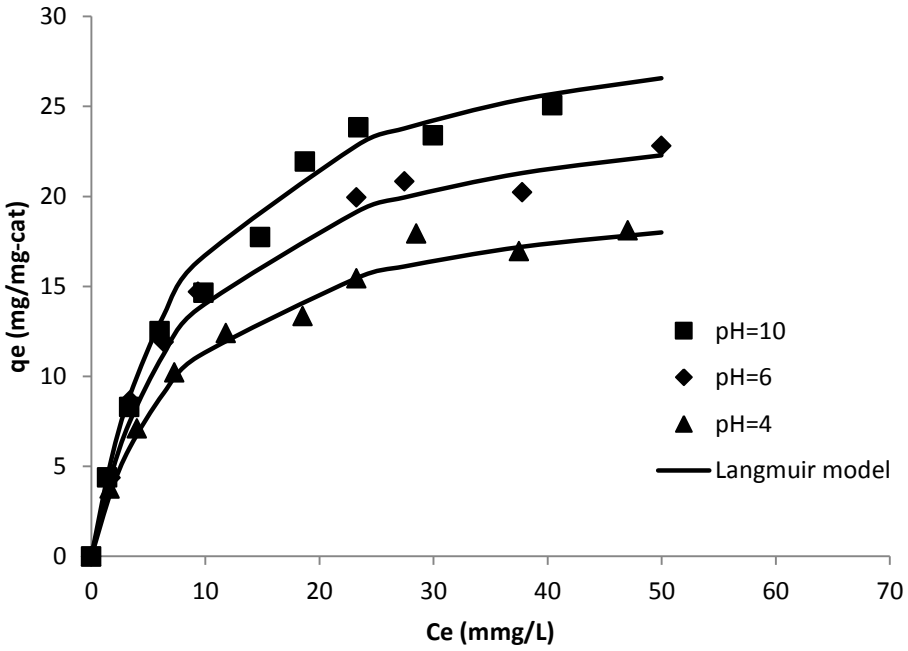

Figure 5-6: Isotherms of photocatalytic degradation of MB at different pH using Fe-doped titanium dioxide.

5.1.2 Reduction isotherms of Zn, Pb and Cd by pure and metal-doped titanium dioxide

The effect of titanium dioxide doping on the removal of Zn and Pb from aqueous solutions was investigated using different doping percentages of 0 % (pure titanium dioxide), 1.4 wt% and 2.7 wt% (maximum doping percentage achieved) where the solution pH was kept constant at 4 for all solutions using a buffer solution (addition of more tungsten decreases pH as tungsten oxide is mildly acidic than pure titanium dioxide) and the results are shown in Figures 5.7 and 5.8 for Zn and Pb respectively. It can be noticed that the catalyst maximum uptake strongly depends on the amount of tungsten present for both Zn and Pb. The maximum uptake of Pb was found to be more than that of Zn. This trend can be explained by the physical and chemical properties of metal ions, mainly the oxidation state which can be higher for Pb (+4, +2) than Zn (+2) which is resulting in the ratio of charge to volume. In addition to that, the atomic radius of Zn and Pb which are 175 pm and 134 pm respectively may have a direct result on the adsorption on the catalyst surface.

The adsorption of zinc and lead was studied using pure and vanadium doped titanium dioxide at the same conditions in order to verify the metal uptake using both catalysts. The results of isotherms of Zn and Pb are shown if Figures 5.9 and 5.10 respectively. It is noticed that, pure titanium dioxide adsorbs lead more efficiently than zinc. For pure titanium dioxide, a maximum uptake of 7 mg Zn^{+2}/g of solid was obtained, whereas the uptake of Pb increased to 17 mg Pb^{+2}/g of solid for. In the case of vanadium doped titanium dioxide, the maximum uptake of Zn was increased from 7 mg Zn^{+2}/g of solid to 11 mg Zn^{+2}/g of solid, and for Pb, the maximum uptake was increased from 17 mg Pb^{+2}/g of solid to 26 mg Pb^{+2}/g of solid.

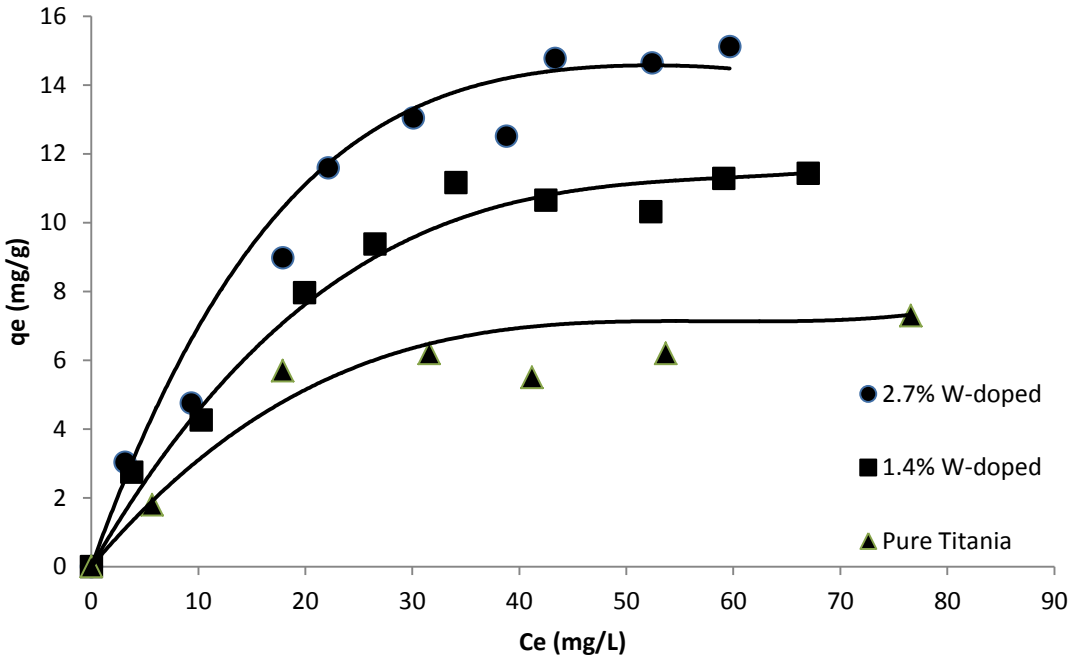

Figure 5-7: Adsorption of Zn using pure and W-doped Titanium dioxide.

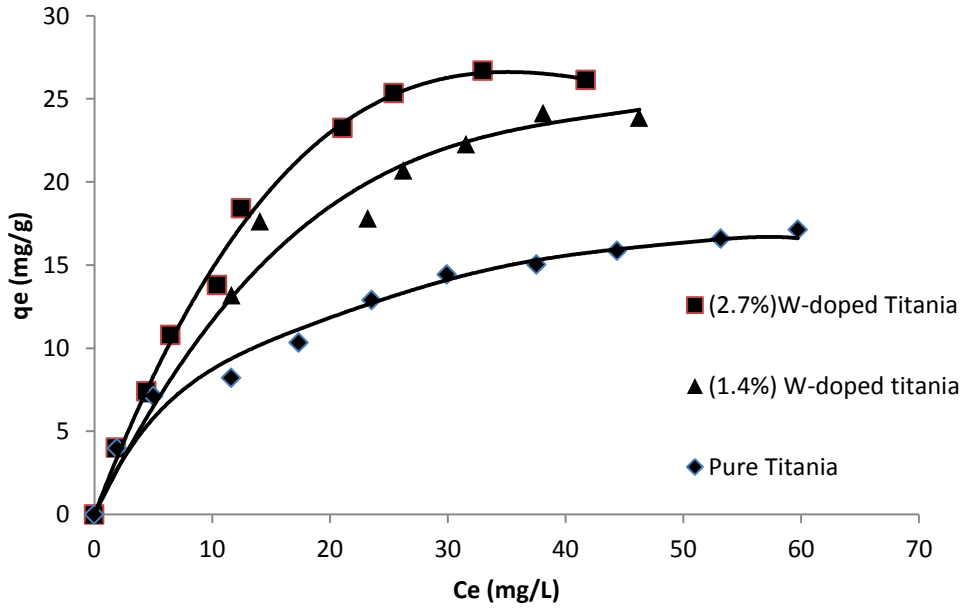

Figure 5-8: Adsorption of Pb using pure and W-doped Titanium dioxide.

There are many factors that can justify the trend of specific adsorbents toward some adsorbates more than another. The trend of titanium dioxide to uptake more Pb than Zn can be explained by the ratio of charge to volume, where both, Pb and Zn, are amphoteric oxides, Pb has oxidation states of +4 and +2, while Zn has oxidation states of +2 and +1. The atomic radius of Pb and Zn are 175 pm and 134 pm respectively, so, the higher oxidation state of Pb makes the surface of titanium dioxide more attractive for Pb than Zn in this case. On the other side, the electronegativity of Pb, which is 2.33 (Pauling scale) is higher than that of Zn (1.65 on Pauling scale), this makes the negatively charged surface of titanium dioxide more attractive to Zn than Pb, however, the sum of these two factors (charge to volume ratio and electronegativity) indicates that, titanium dioxide is more attractive for Pb than Zn as indicated by the adsorption isotherms[33, 37, 44, 46-48].

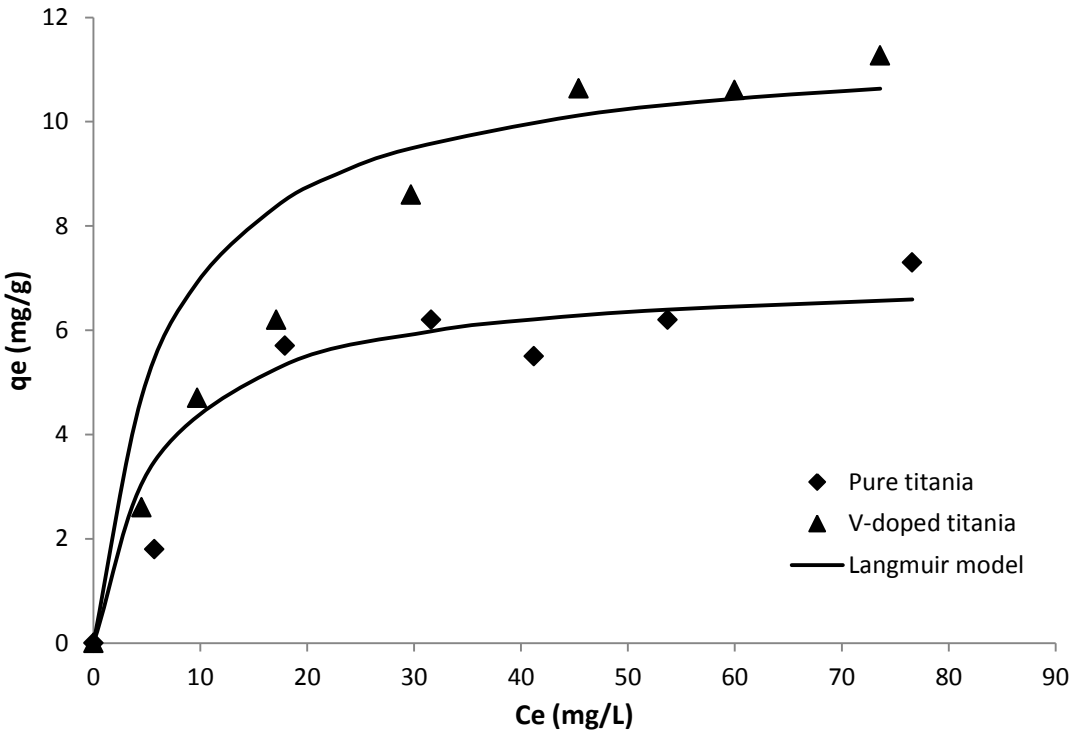

Figure 5-9: Adsorption isotherm of Zinc on Pure and V-doped titanium dioxide.

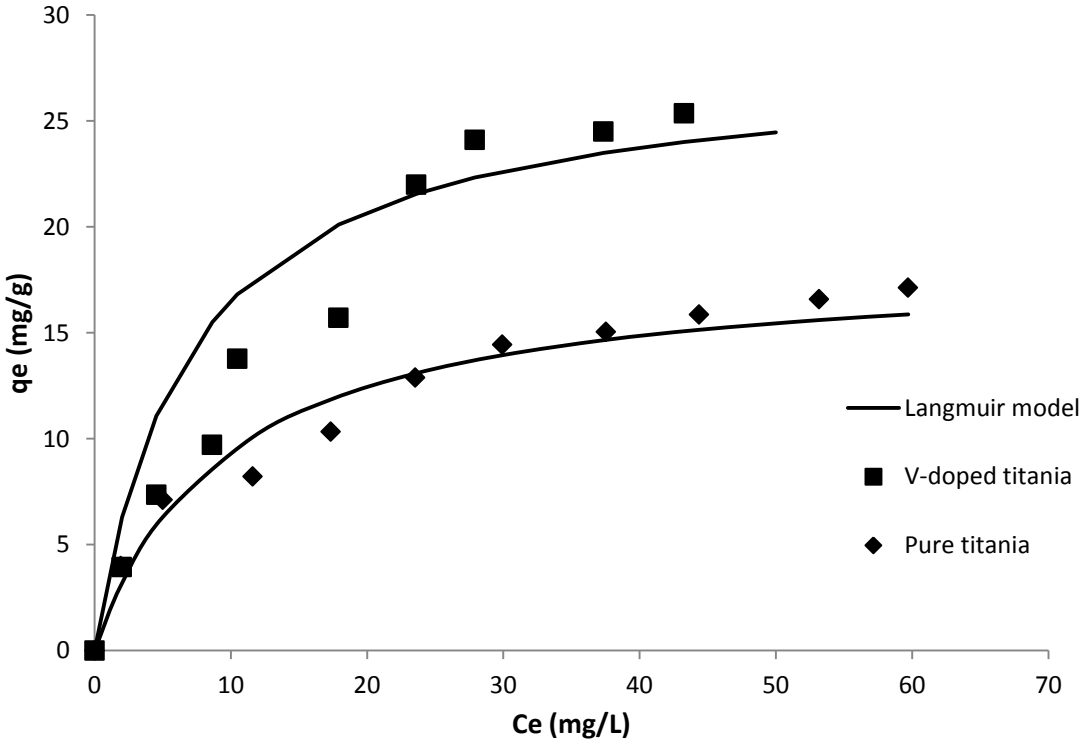

Figure 5-10: Adsorption isotherm of Lead on Pure and V-doped titanium dioxide.

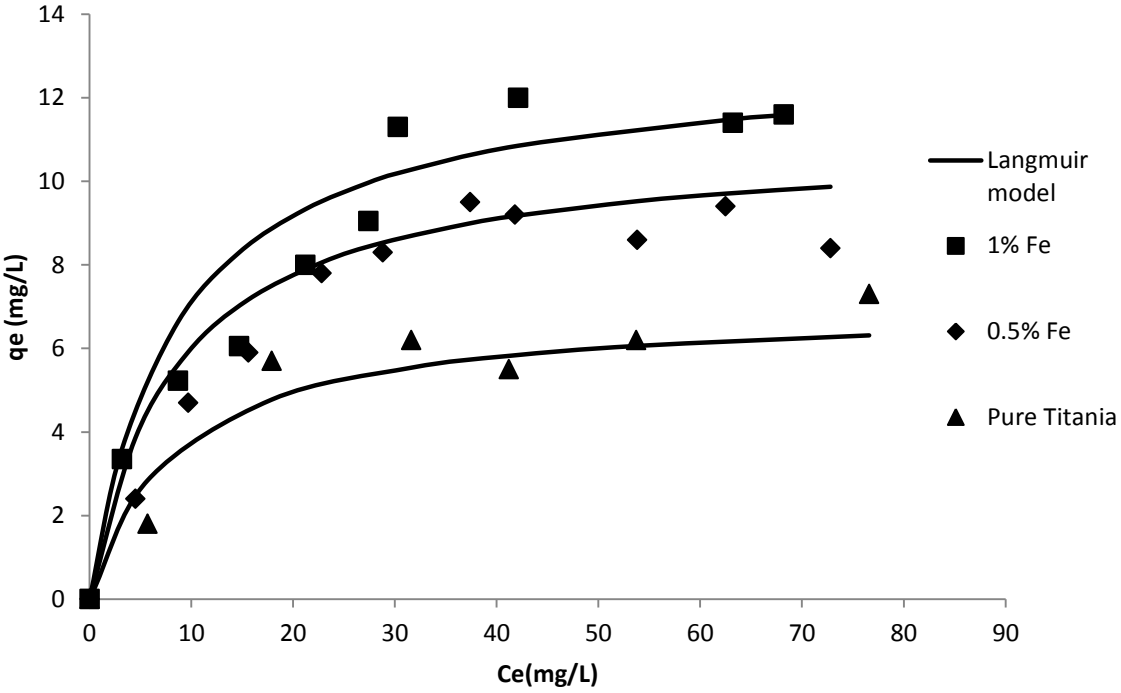

Figure 5-11: Adsorption isotherm of Zinc on Pure and Fe-doped titanium dioxide.

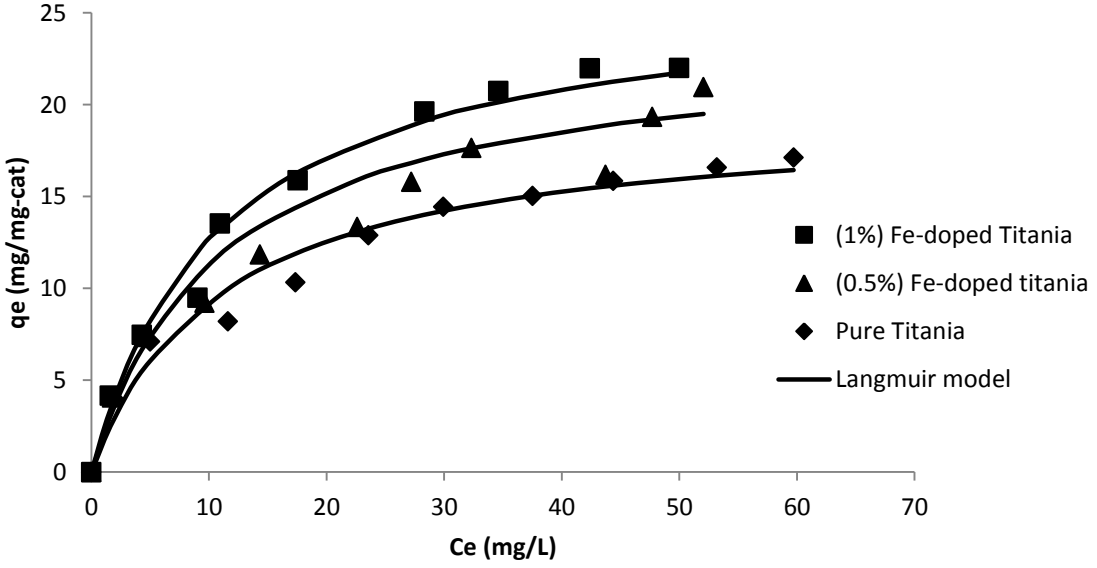

Figure 5-12: Adsorption isotherm of Lead on Pure and Fe-doped titanium dioxide.

5.1.3 Experimental isotherm data fitting

In order to fully describe the kinetics of heavy metals, it is crucial to fit the experimental data of adsorption isotherms -as describes in the kinetics modeling part- by one of isotherms models. In this section, the experimental data fitting is shown for the three types of metal doped titanium dioxide. Tables of the isotherms models parameters are provided for each type of catalyst.

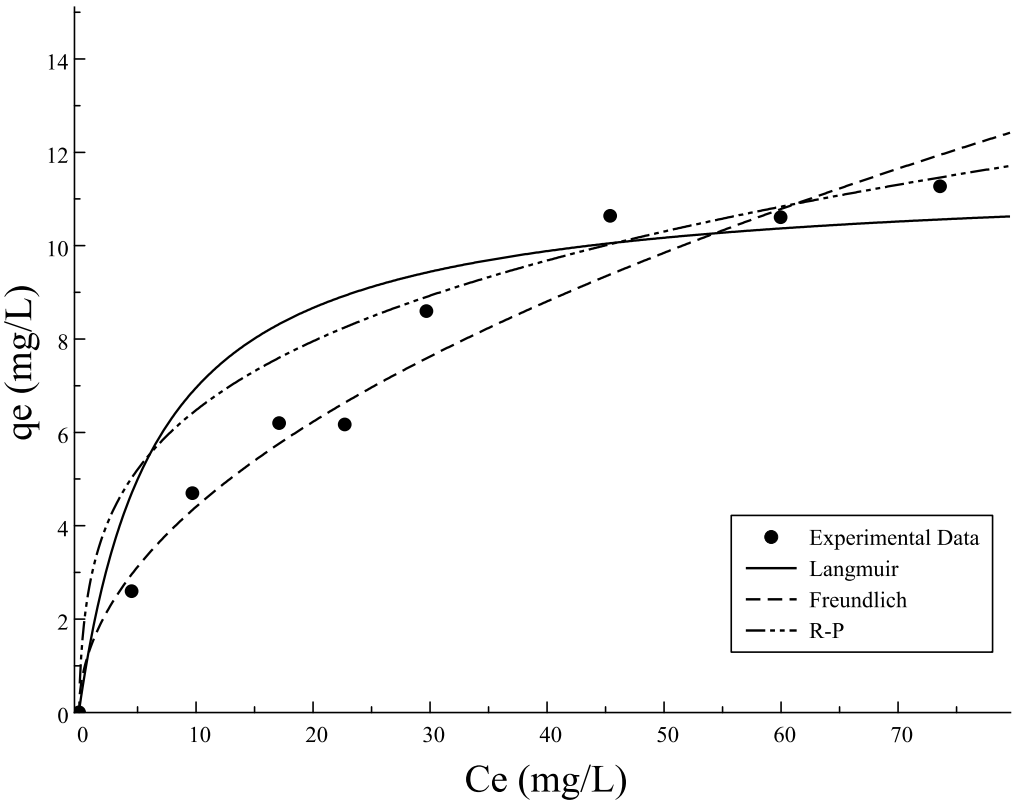

Figure 5-13: Isotherms fitting of Zn removal by V-doped titanium dioxide.

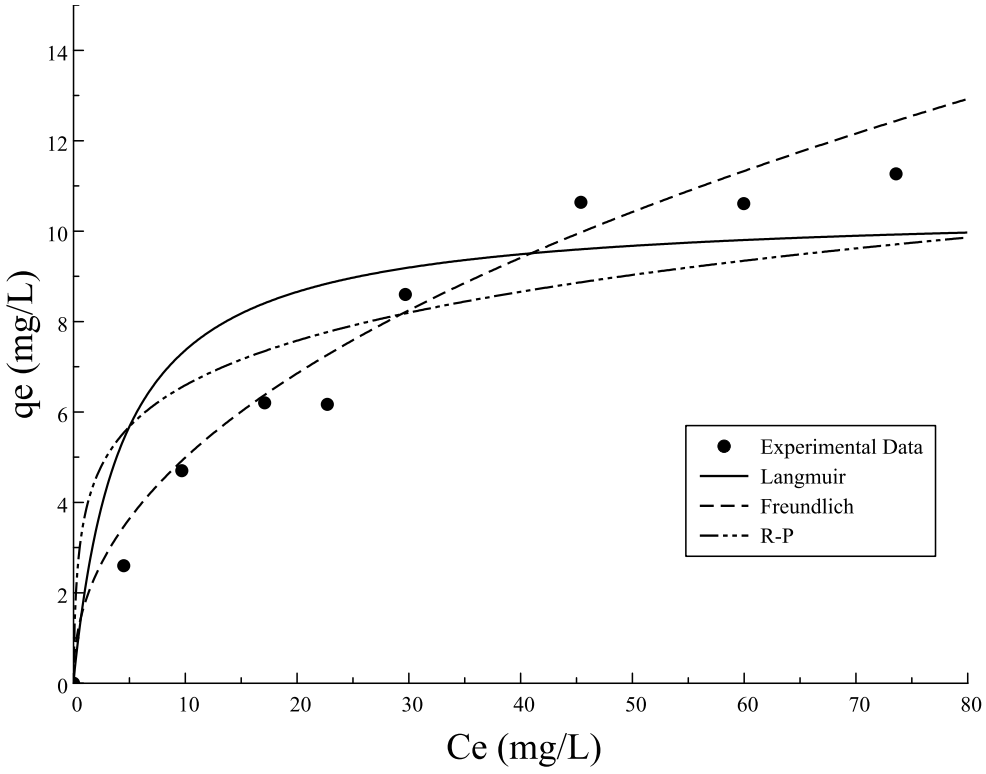

Figure 5-14: Isotherms fitting of Pb removal by V-doped titanium dioxide.

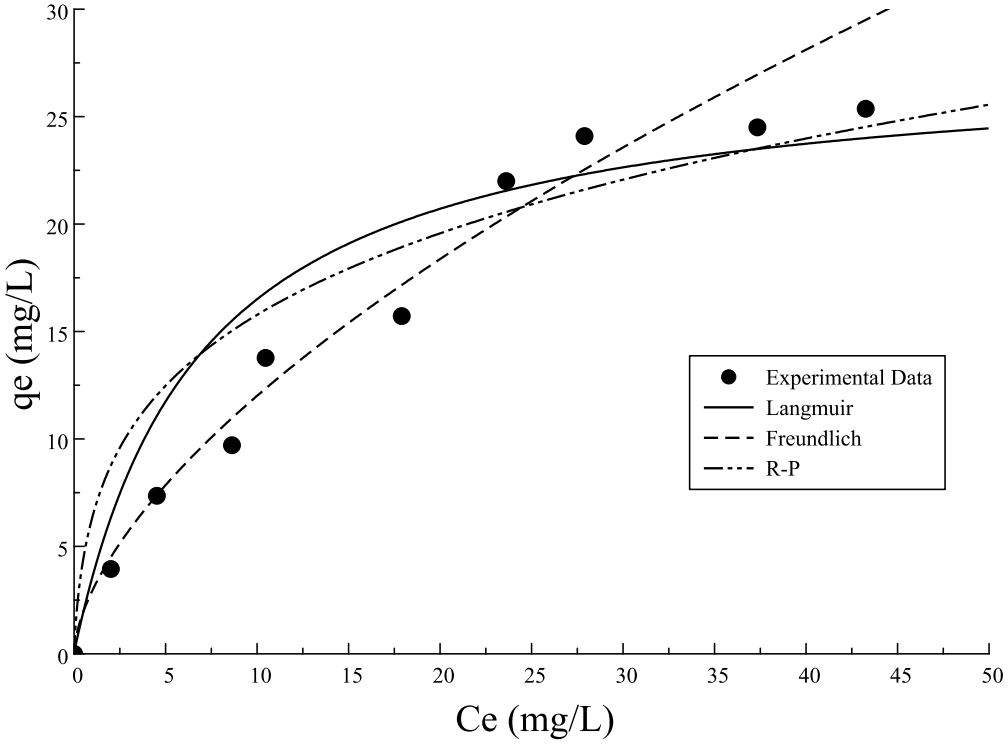

Figure 5-15: Isotherms fitting of Cd removal by V-doped titanium dioxide.

Table 5-1: Isotherms models parameters of V-doped titanium dioxide

Model	Parameters	V-doped titanium dioxide		
		Zn	Pb	Cd
Langmuir	b	0.1528	0.1459	0.1315
	q_{max}	11.5	27.8	16.9
	R^2	0.9521	0.9422	0.9834
Freundlich	K	1.3919	1.7377	2.9167
	n	0.5001	0.4579	0.6142
	R^2	0.9815	0.9756	0.9612
Redlich-Peterson	g	0.7355	0.8192	0.7356
	B	3.1469	4.4916	2.113
	A	11.74	20.19	19.72
	R^2	0.9714	0.9447	0.9781

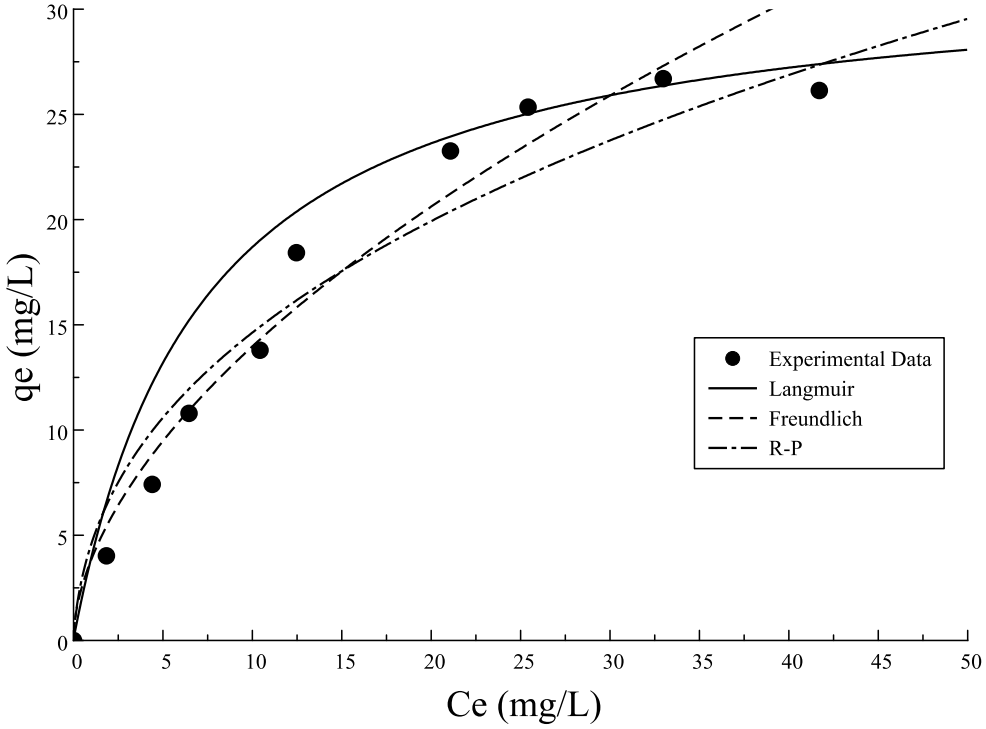

Figure 5-16: Isotherms fitting of Zn removal by W-doped titanium dioxide.

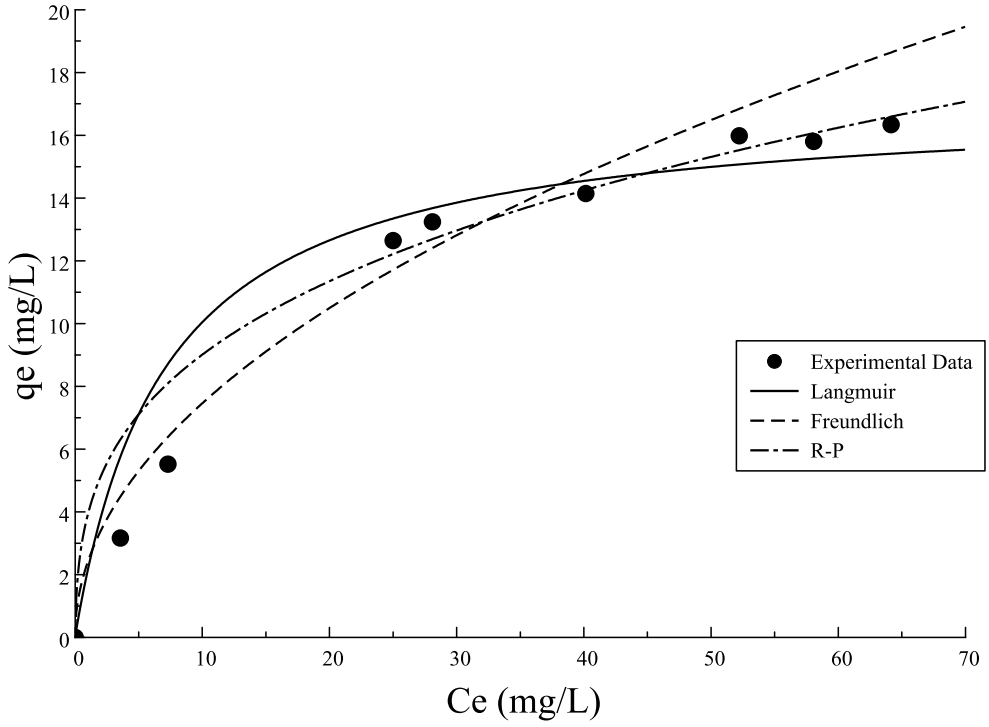

Figure 5-17: Isotherms fitting of Pb removal by W-doped titanium dioxide.

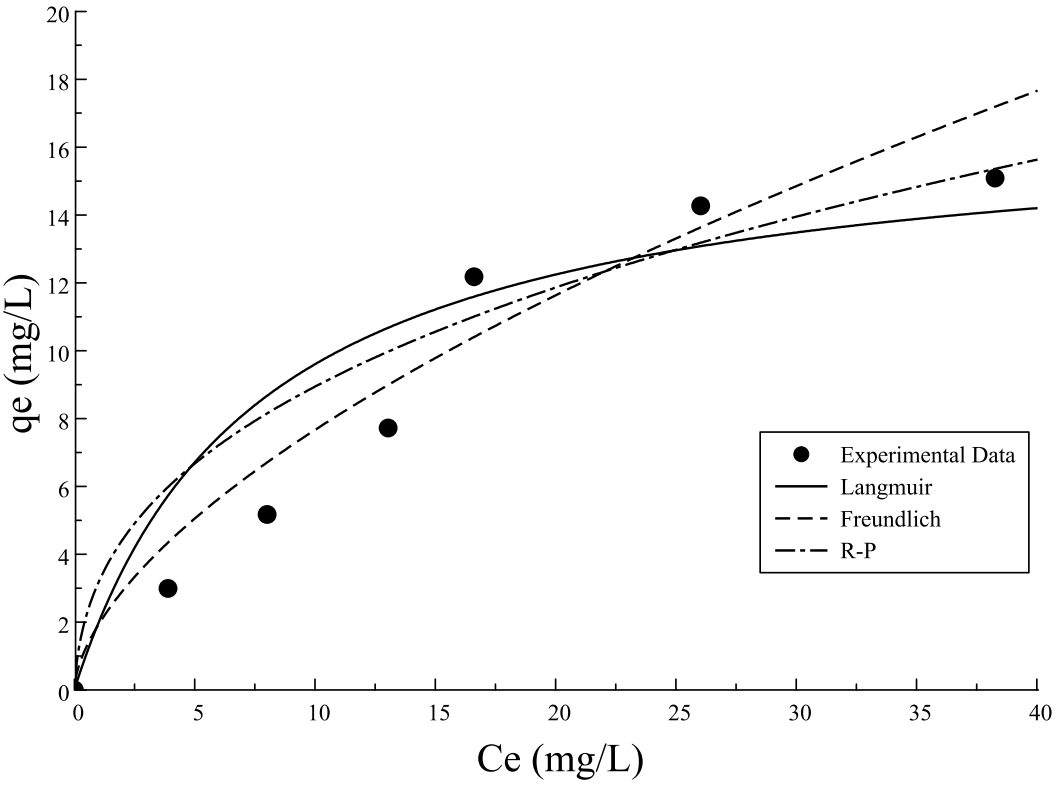

Figure 5-18: Isotherms fitting of Cd removal by W-doped titanium dioxide.

Table 5-2: Isotherms models parameters of W-doped titanium dioxide

Model	Parameters	W-doped titanium dioxide		
		Zn	Pb	Cd
Langmuir	b	0.1921	0.139	0.1421
	q_{max}	16.3	32.1	17.1
	R^2	0.9741	0.9823	0.9253
Freundlich	K	3.8299	2.3958	1.9149
	n	0.5618	0.493	0.6022
	R^2	0.9632	0.9851	0.9311
Redlich-Peterson	G	0.5993	0.6828	0.6251
	B	2.4913	6.7995	3.8813
	A	15.93	30.39	15.41
	R^2	0.9552	0.9621	0.9055

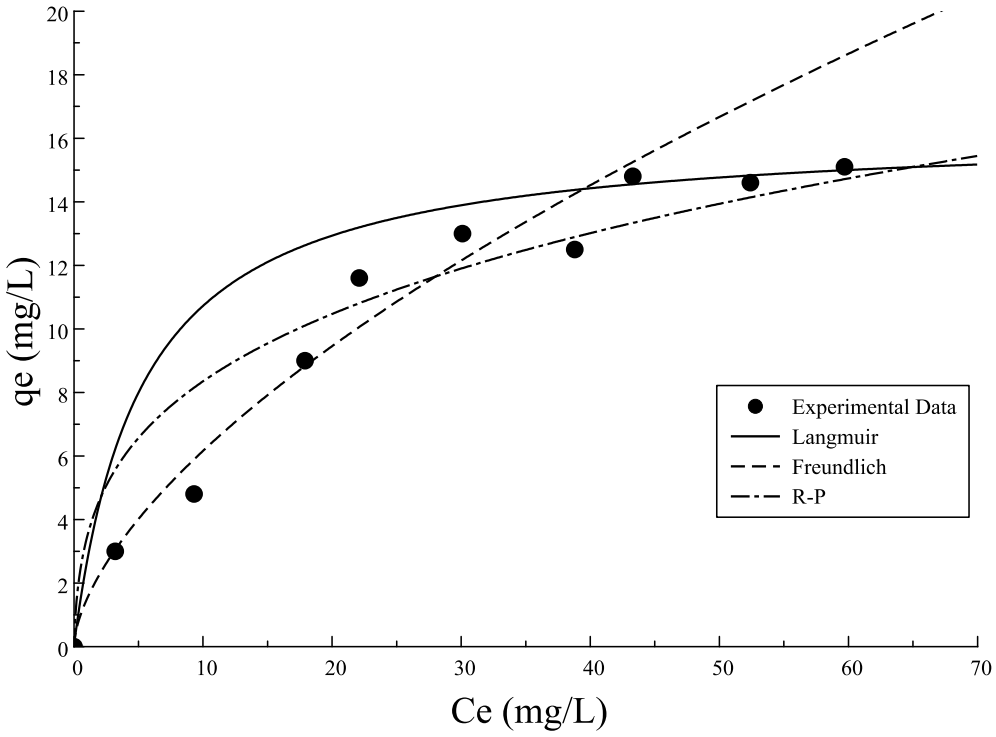

Figure 5-19: Isotherms fitting of Zn removal by Fe-doped titanium dioxide.

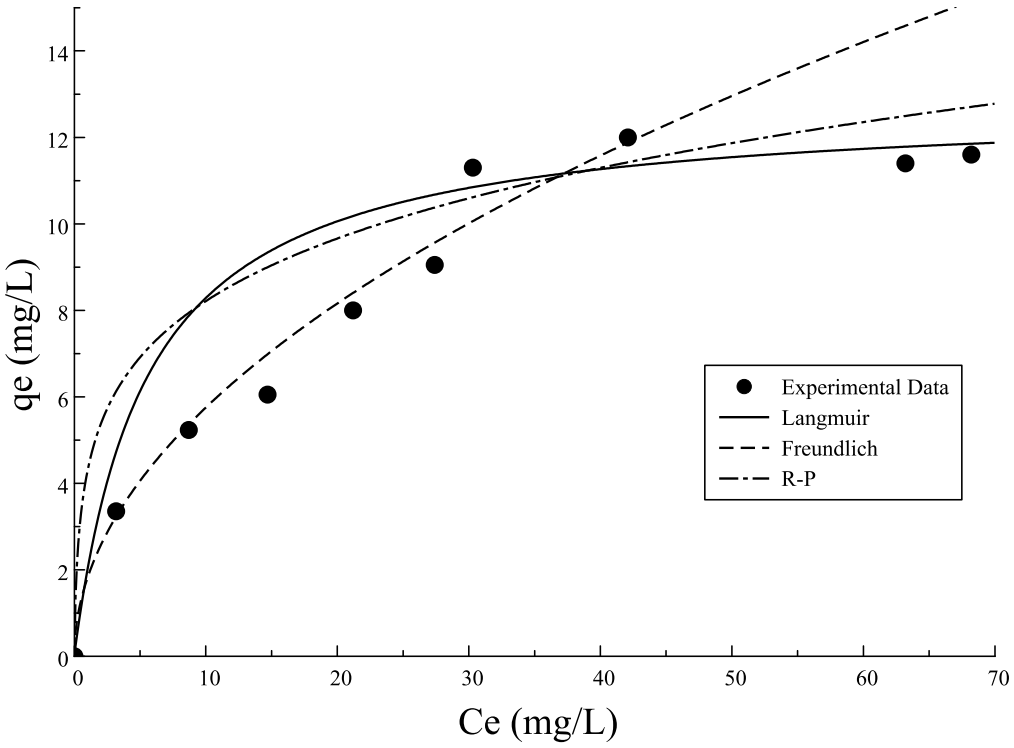

Figure 5-20: Isotherms fitting of Pb removal by Fe-doped titanium dioxide.

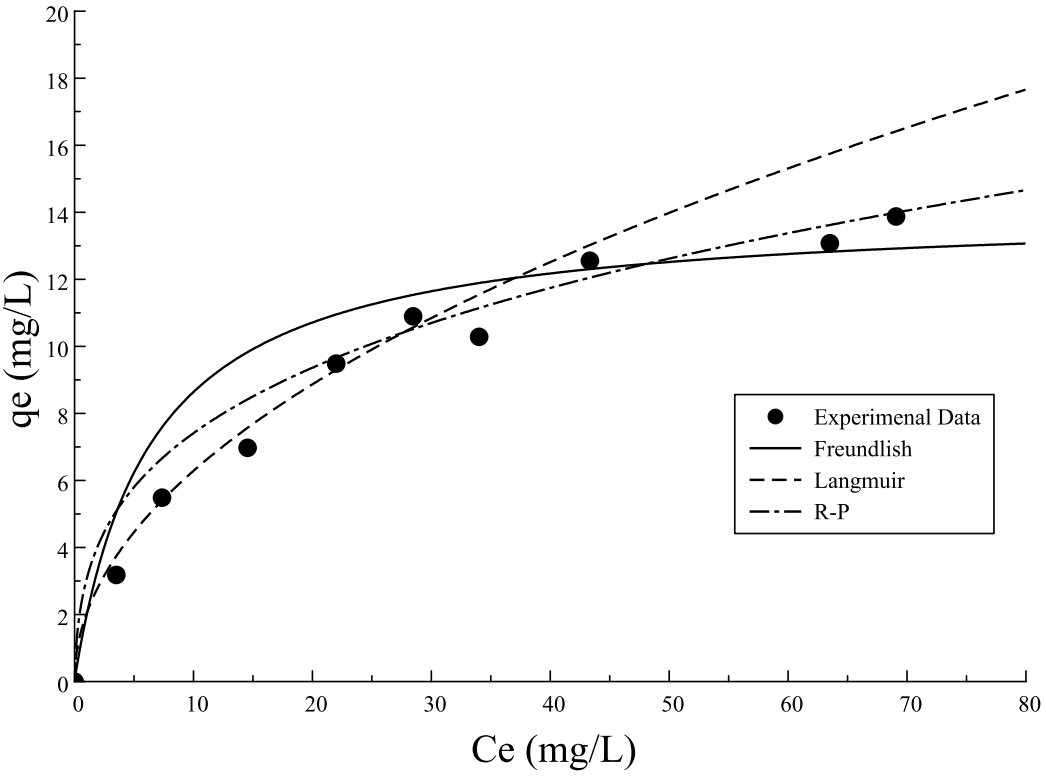

Figure 5-21: Isotherms fitting of Cd removal by Fe-doped titanium dioxide.

Table 5-3: Isotherms models parameters of Fe-doped titanium dioxide

Model	Parameters	Fe-doped titanium dioxide		
		Zn	Pb	Cd
Langmuir	b	0.1834	0.1658	0.1578
	q_{max}	12.8	24.6	14.1
	R^2	0.9041	0.9331	0.9512
Freundlich	K	1.4811	1.7989	1.9974
	n	0.6188	0.5048	0.4973
	R^2	0.9263	0.9732	0.9518
Redlich-Peterson	g	0.7079	0.7871	0.6915
	B	3.0106	4.495	3.6178
	A	13.66	23.42	13.91
	R^2	0.9167	0.9215	0.9831

5.2 Kinetics modeling

Analysis of Variance was done in order to investigate the effects of experimental parameter on reduction of heavy metals from aqueous solutions. The parameters under study are temperature, initial metal concentration, mass of catalyst and stirring speed, which are denoted as A, B, C and D, respectively. For each parameter, two different values corresponding the lower level and higher level were selected.

Table 5-4: ANONA parameters and levels for the kinetics of heavy metals reduction.

Factors	**Name**	**Level 1**	**Level 2**
A	Temperature	4	25
B	Initial concentration	10	25
C	Catalyst mass	0.5	1
D	Stirring speed	100	600

For the removal of heavy metals in general by either W-doped, Fe-doped or V-doped TiO_2 nanoparticles, it is clear that, as the temperature decreased the degradation percentage increased accordingly as shown in Figure (22-a). This trend revealed that, the adsorption on the surface is endothermic as a result of the higher affinity of active sites. Similar trend was observed by Zinab Ghasemi, et al, [2011] on adsorption of Hg (II) by nanocrystalline titanium dioxide.

The effect of initial metal concentration on the adsorption behavior of TiO_2 was investigated by increasing the concentration from 10 to 25 while fixing the same amount of the catalyst. The results indicate that, negligible difference on the degradation percentage was noticed as shown in Figure (22-b), which indicates that, the limiting step in the adsorption process is the availability

of active sites and the surface has not reached the saturation level in both cases. The same trend was reported in the work of Fatemeh Rashidi, et al, [2010].

Dosages of 0.1 g and 1 g of TiO_2 were used to verify the extent of adsorption of heavy metals on the surface of the catalyst. It is found that, as the catalyst dosage was increased, accordingly as shown in Figure (22-c). This is due to the more active site available on the surface. These findings are in agreement with the observations of Mustafa Karatas, [2011] on removal of Pb (II) using natural zeolite tuff and Erling Du, et al, [2011] on the adsorption of Pb (II) on montmorillonite.

In addition, the effect of stirring speed was studied as well and the results are shown in Figure (22-d). It was noticed that, as the stirring speed was increased from 100 rpm to 600 rpm, the degradation percentage was increased. This trend can be explained by the decrement of mass transfer resistance at higher speed, which leads to increase the diffusivity from the external surface into the pores, and hence, more active sites will be available at the surface. The trends of interactions between these parameters were in agreement with the observations of the main effect. It was noticed that, at low temperature and higher concentration, the degradation was significantly higher compared to the other combination of high temperature and low concentration. The same trend was noticed for the combination of temperature and stirring speed. In addition to that, interactions between the initial species concentration and stirring speed were controlled by the relation between the mass transfer resistance and the film resistance, where it was noticed that, at low concentration and low stirring speed, the degradation percentage was the lowest due to the controlling of film resistance and the lower driving force, while the highest degradation was achieved when the speed and concentration were increased accordingly. All graphs showing the combinations for all types of heavy metals are shown in Appendix C.

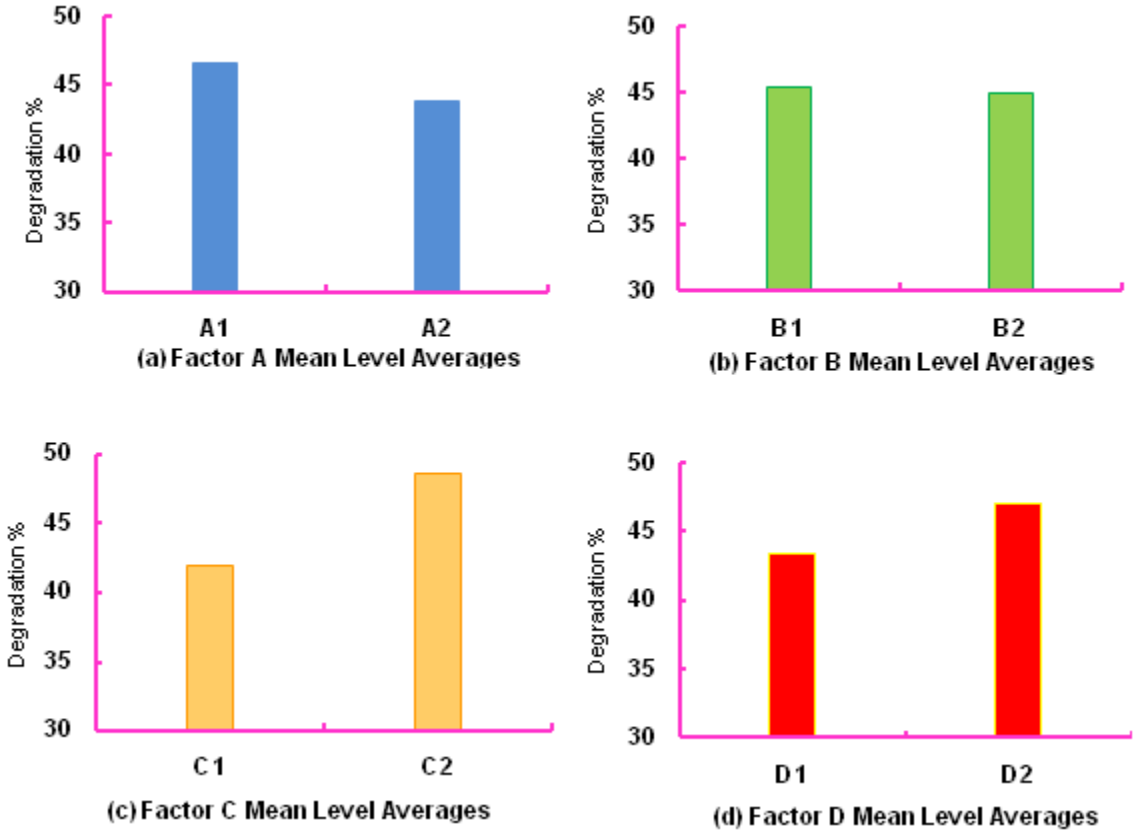

Figure 5-22: Level average of main effects for reduction of Pb (II) by W-doped titanium dioxide.

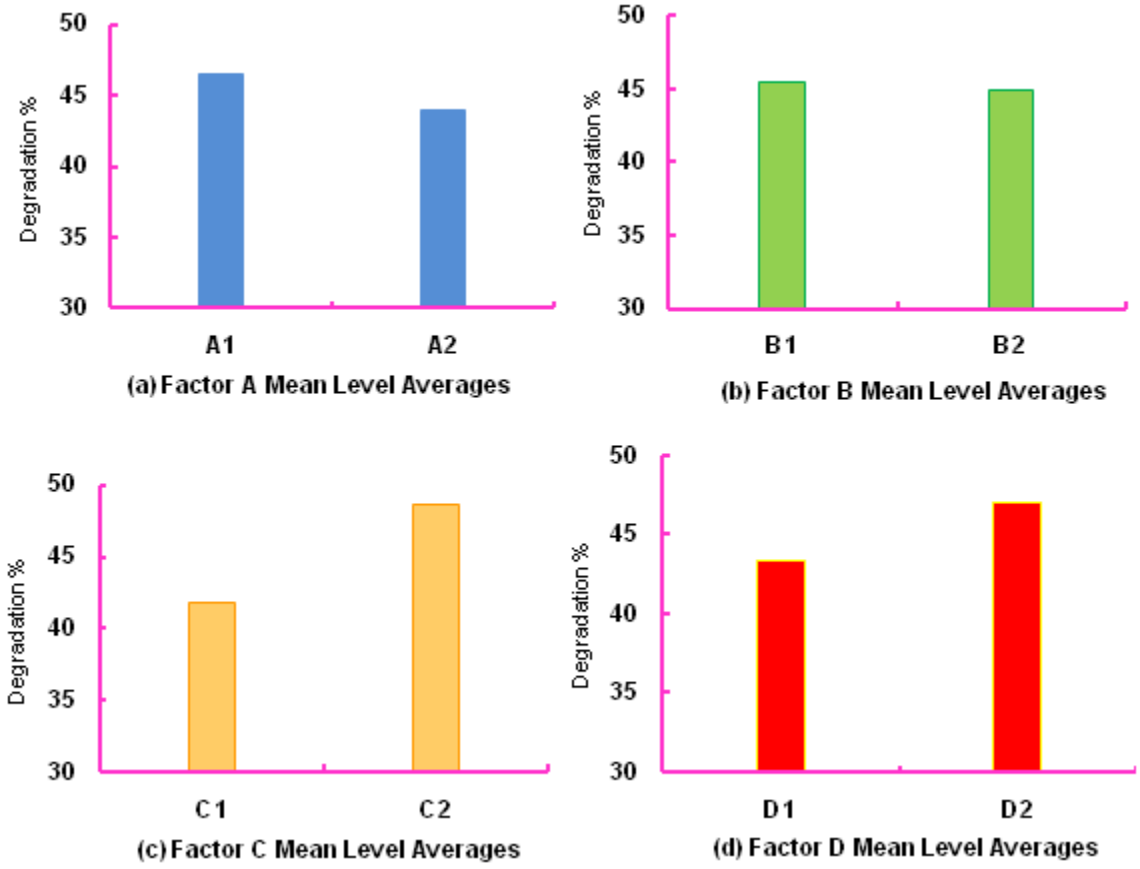

Figure 5-23: Level average of main effects for reduction of Zn (II) by Fe-doped titanium dioxide.

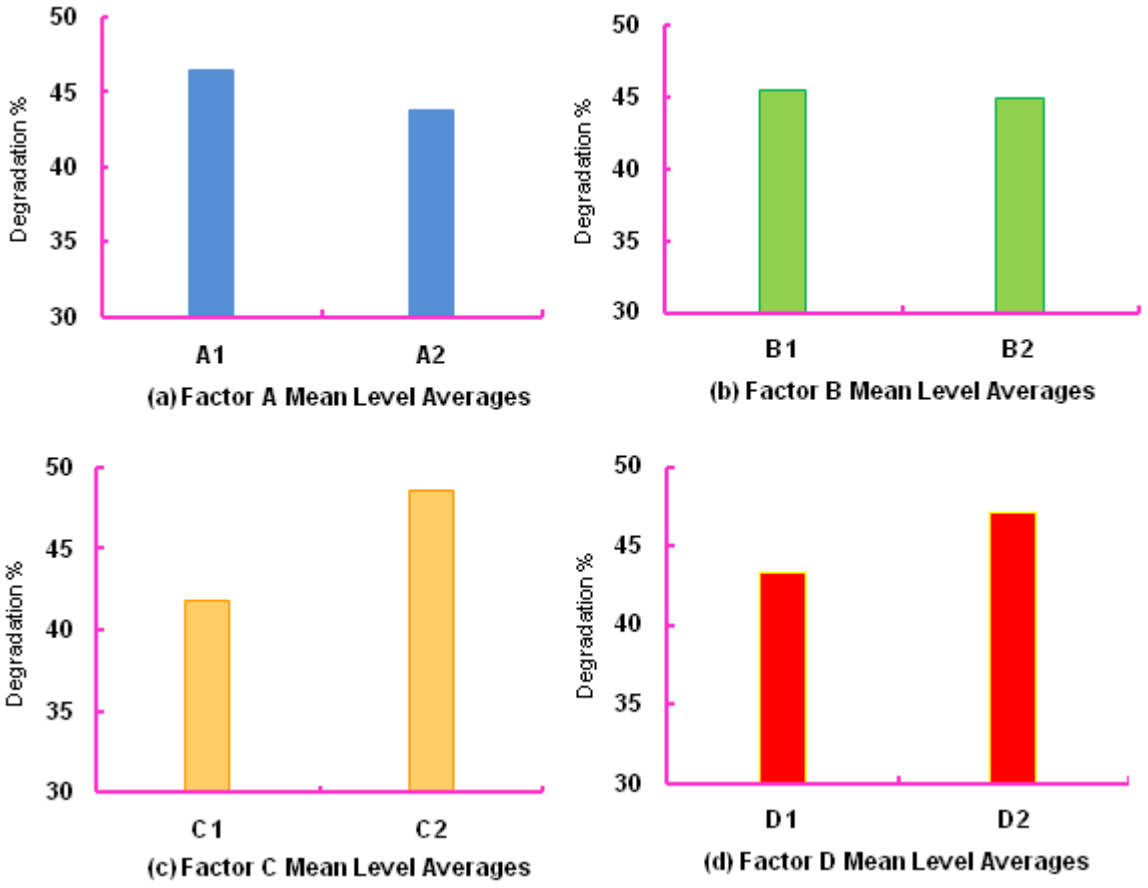

Figure 5-24: Level average of main effects for reduction of Cd (II) by V-doped titanium dioxide.

5.2.1 Kinetics of Pb removal by W-doped titanium dioxide

Effect of temperature on the removal of Pb(II) was investigated at different stirring speeds as shown in Table 3.6, experiments E1, E2 and E3, E4, and the results are shown in Figures 5.25 and 5.26 for 100 rpm and 600 rpm, respectively. It can be seen that, as the solution temperature was increased from 4^{o}C to 25^{o}C, the percentage of removal was increased accordingly. This trend can be explained by the enhancement of adsorption rate between the metal ions and active sites on the surface of the catalyst[45]. It was also noticed that, at a lower stirring speed (100 rpm), the enhancement of Pb(II) was approximately 10% at equilibrium, while at higher stirring speed (600 rpm), it was reduced to approximately 5%. This trend indicates that, at these conditions, the mass transfer between the bulk and catalyst surface is the dominant step.

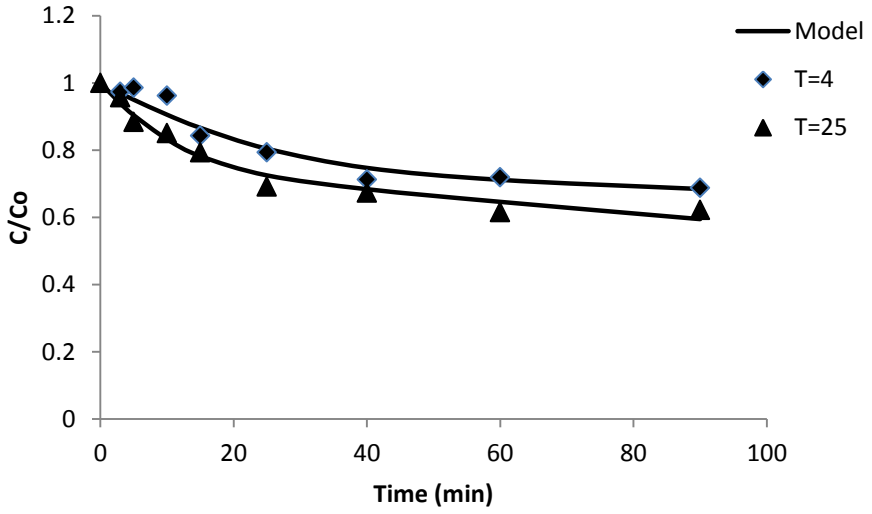

Figure 5-25: Effect of temperature on Pb removal at a relatively low stirring speed (100 rpm).

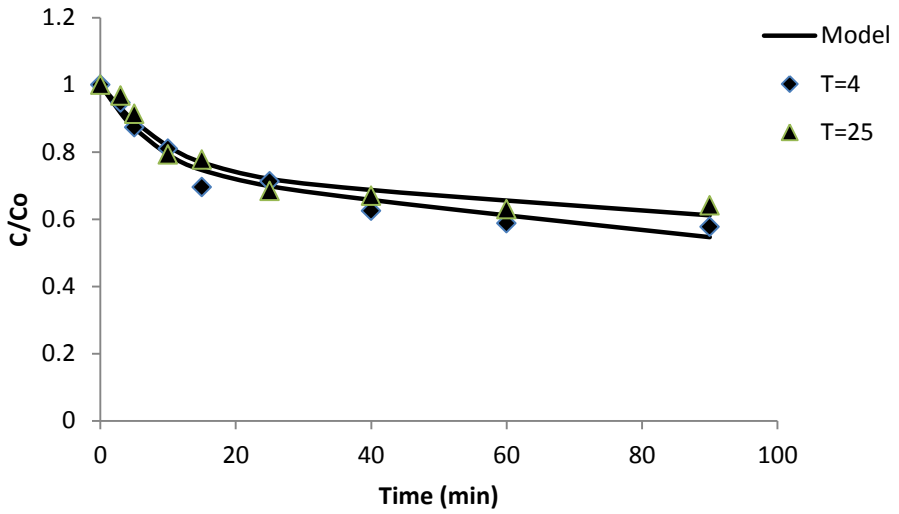

Figure 5-26: Effect of temperature on Pb removal at a relatively high stirring speed (600 rpm).

The effect of initial concentration was studied at different temperatures as indicated in experiment E5 and E6 as well as E7 and E8. As shown in Figures 5.27 and 5.28, the removal of Pb(II) was increased when the initial concentration of metal was decreased from 25 ppm to 10 ppm at both 4^{o}C and 25^{o}C. This trend is due to the fact that, at higher initial concentration, the formation of more layers at the catalyst surface reduces the physical interaction between metal ions in the bulk liquid and the active sites on the catalyst surface. In addition to that, at higher initial concentration of Pb (II), the absorption of illuminated light by the metal ions may reduce the photocatalytic activity of the catalyst, hence, less metal ions will be absorbed on the surface[45].

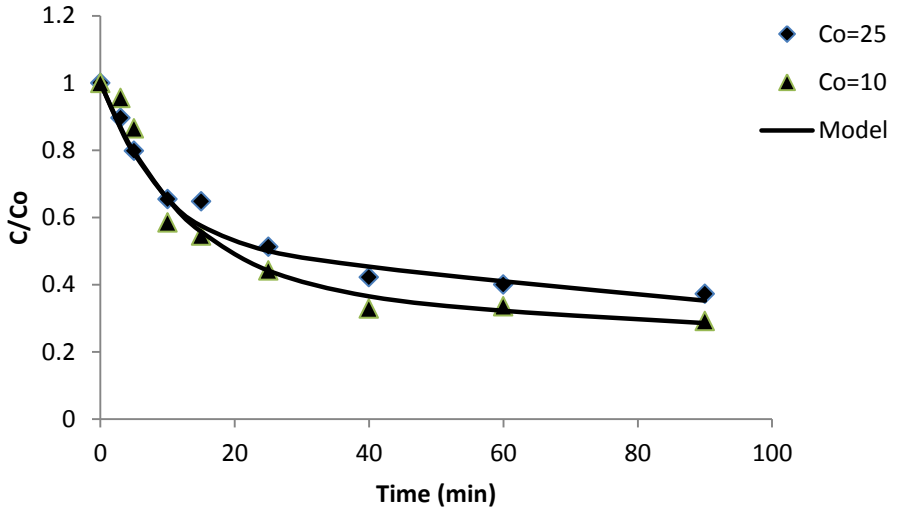

Figure 5-27: Effect of initial concentration on Pb removal at a relatively lower temperature (4^{o}C).

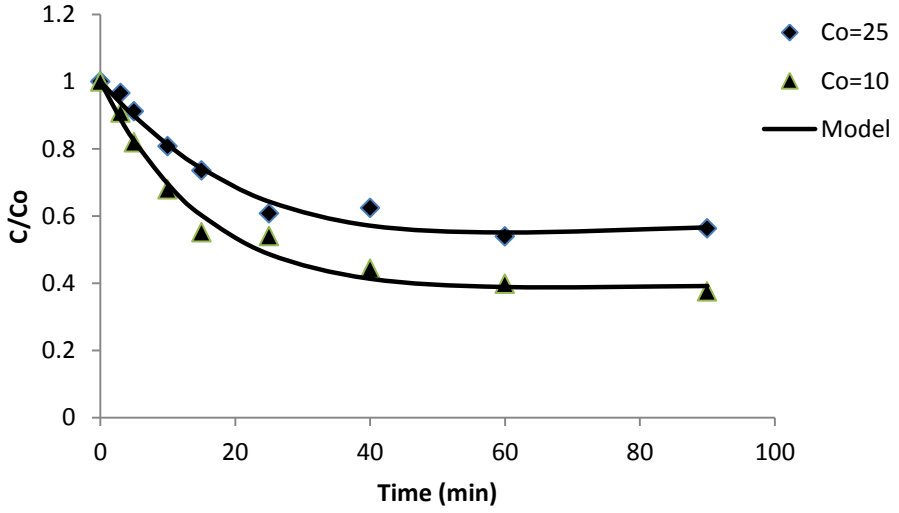

Figure 5-28: Effect of initial concentration on Pb removal at a relatively higher temperature (25^{o}C).

The effect of catalyst dosage on Pb(II) removal was carried out as shown in experiments E9 and E10 when the initial concentration was adjusted at 10 ppm as well as E11 and E12 where the initial concentration was 25 ppm. As shown in Figures 5.29 and 5.30 that the uptake of Pb(II) was increased by approximately 16 % when the dosage of W-doped titanium dioxide was increased from 0.5 g to 1 g. this enhancement is due to the more adsorption sites provided by W-doped titanium dioxide when the dosage was increased[33, 37, 44, 46-48].

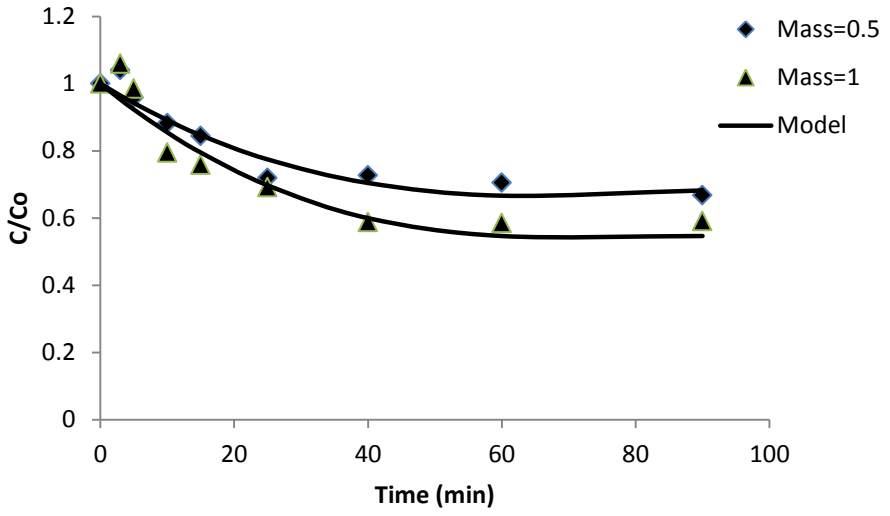

Figure 5-29: Effect of catalyst mass on Pb removal at a relatively low initial concentration (10 ppm).

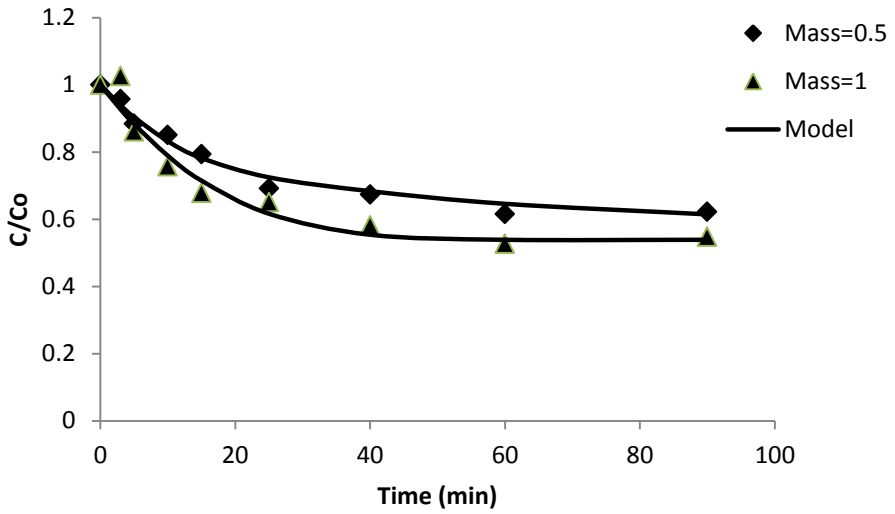

Figure 5-30: Effect of catalyst mass on Pb removal at a relatively high initial concentration (25 ppm).

The effect of stirring speed on Pb(II) removal was conducted at different dosages of catalyst as indicated in experiments E13 and E14 for 0.5 g of catalyst, as well as E15 and E16 for 1 g of catalyst. It was noticed as shown in Figures 5.31 and 5.32 that, the catalyst uptake was increased by approximately 10 wt% in both cases. This increment is attributed to the enhancement of mass transfer that is associated with higher stirring speed[46, 48]. Moreover, it is noticed that, the increment percentage is the same for both dosages of W-doped titanium dioxide, which may indicate that, the mass transfer step is more dominant in Pb(II) removal using W-doped titanium dioxide[33, 37, 44, 46-48].

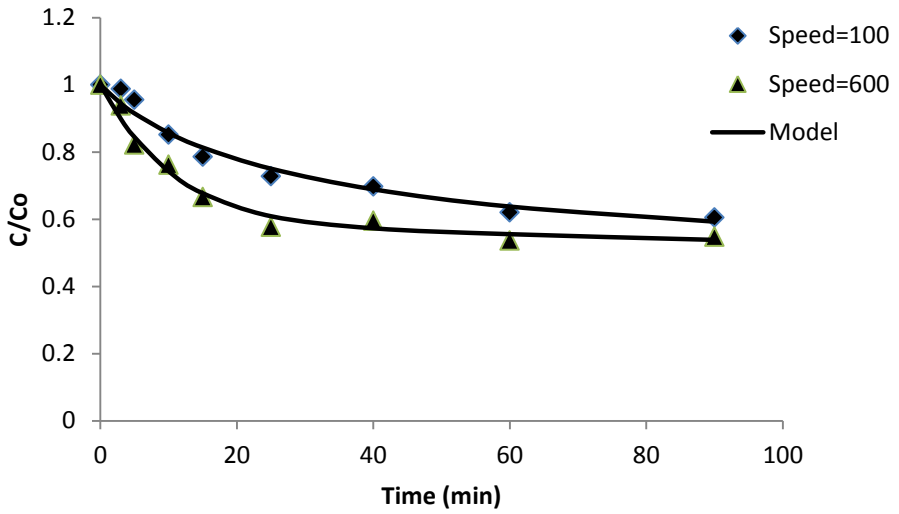

Figure 5-31: Effect of stirring speed on Pb removal when a relatively lower amount of catalyst was added (0.5 g).

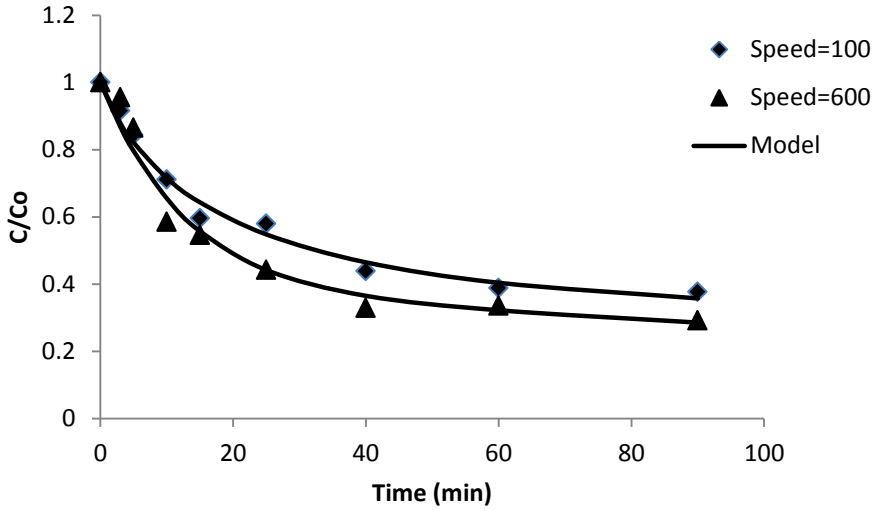

Figure 5-32: Effect of stirring speed on Pb removal when a relatively higher amount of catalyst was added (1 g).

Table 5-5: Reaction and adsorption constants values of Pb removal by W-doped titanium dioxide.

					Constants values obtained by the model			
EXP	**SPEED**	**MASS**	**Co**	**T**	**Krxn (10^{-4})**	**95% conf (10^{-4})**	**Kf (10^{-4})**	**95% conf (10^{-4})**
E1	100	0.5	25	4	1.21	0.2095	7.81	0.3044
E2	100	0.5	25	25	3.02	0.1357	5.59	0.2816
E3	600	0.5	25	4	3.95	0.1863	2.38	0.1217
E4	600	0.5	25	25	2.52	0.1924	8.17	0.4688
E5	600	1	25	4	2.67	0.1448	5.17	0.2904
E6	600	1	10	4	2.99	0.1671	6.15	0.3416
E7	600	1	25	25	0.95	0.1036	1.81	0.1549
E8	600	1	10	25	1.35	0.1752	3.21	0.2523
E9	100	0.5	10	25	2.09	0.3069	3.54	0.4125
E10	100	1	10	25	2.13	0.2814	2.36	0.3227
E11	100	0.5	25	25	3.02	0.2653	5.59	0.5012
E12	100	1	25	25	1.54	0.1418	3.52	0.3356
E13	100	0.5	10	4	1.47	0.0947	8.24	0.6738
E14	600	0.5	10	4	1.04	0.2041	7.71	0.8469
E15	100	1	10	4	1.23	0.1252	6.86	0.5463
E16	600	1	10	4	2.99	0.2146	6.15	0.7181

5.2.2 Kinetics of Zn removal by Fe-doped titanium dioxide

The trends of Zn removal by Fe-doped titanium dioxide are shown in Figure 5.33 throughout 5.40. it was noticed that, the temperature has less effect on the overall performance of the catalyst compared to that of W-doped titanium dioxide, which is due to the higher activity of tungsten (high band gab energy) compared to iron (lower band gab energy). The other effects of initial concentration, catalyst mass and stirring speed were noticed to be similar to that of W-doped titanium dioxide.

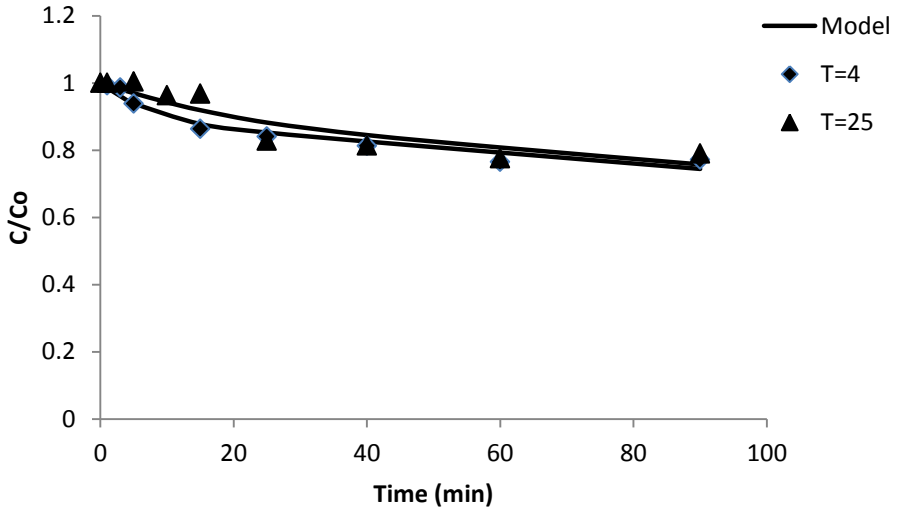

Figure 5-33: Effect of temperature on Zn removal at a relatively low stirring speed (100 rpm).

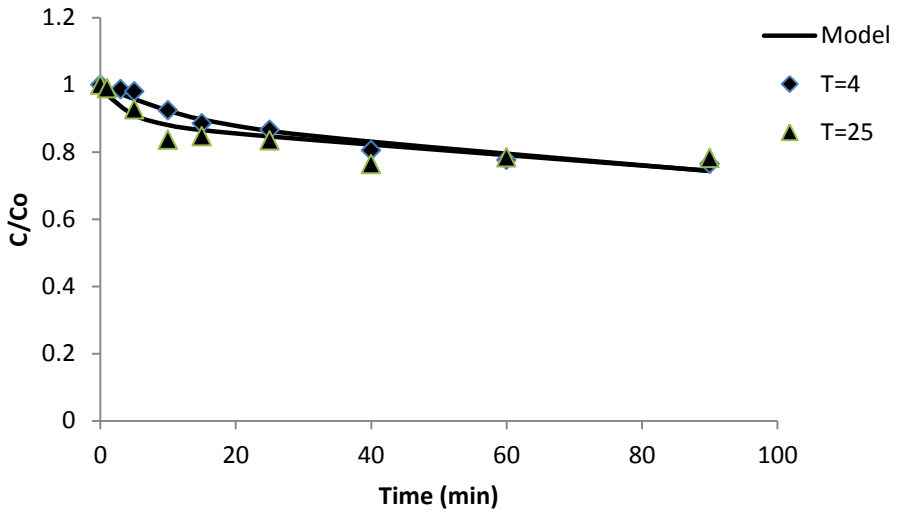

Figure 5-34: Effect of temperature on Zn removal at a relatively high stirring speed (600 rpm).

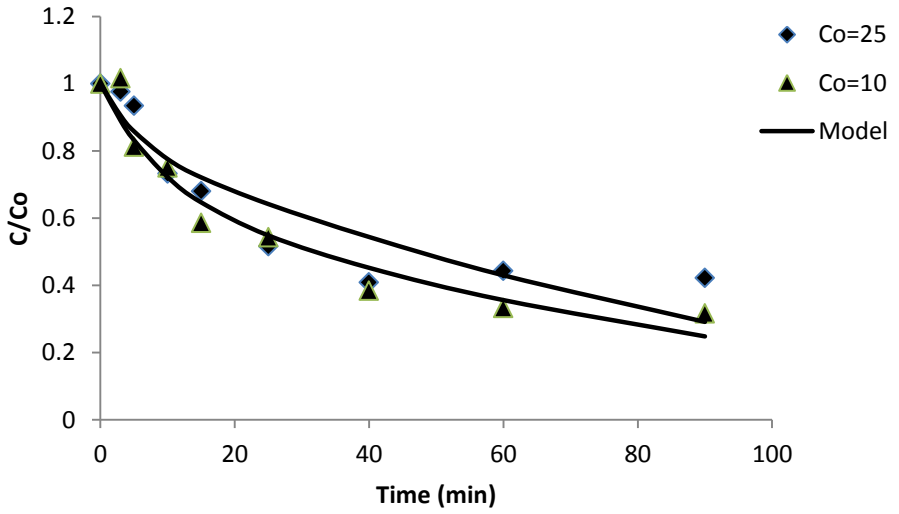

Figure 5-35: Effect of initial concentration on Zn removal at a relatively lower temperature (4^{o}C).

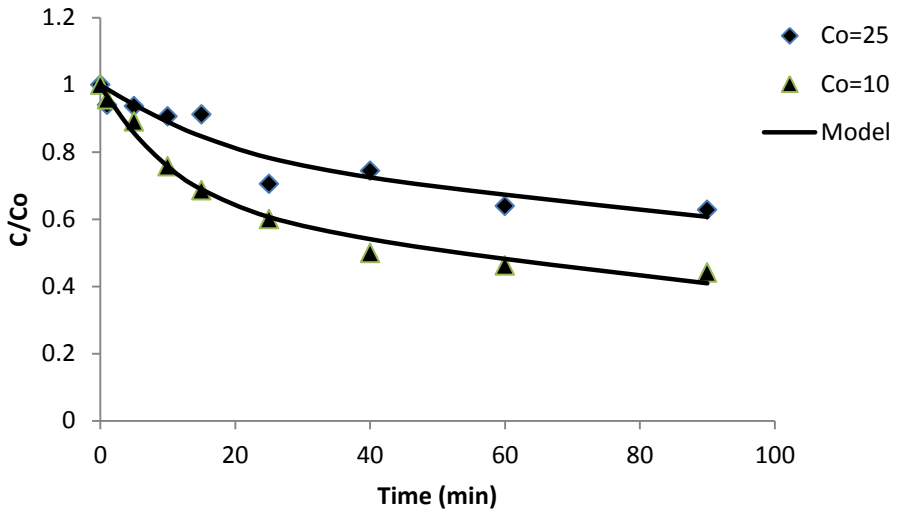

Figure 5-36: Effect of initial concentration on Zn removal at a relatively higher temperature (25^{o}C).

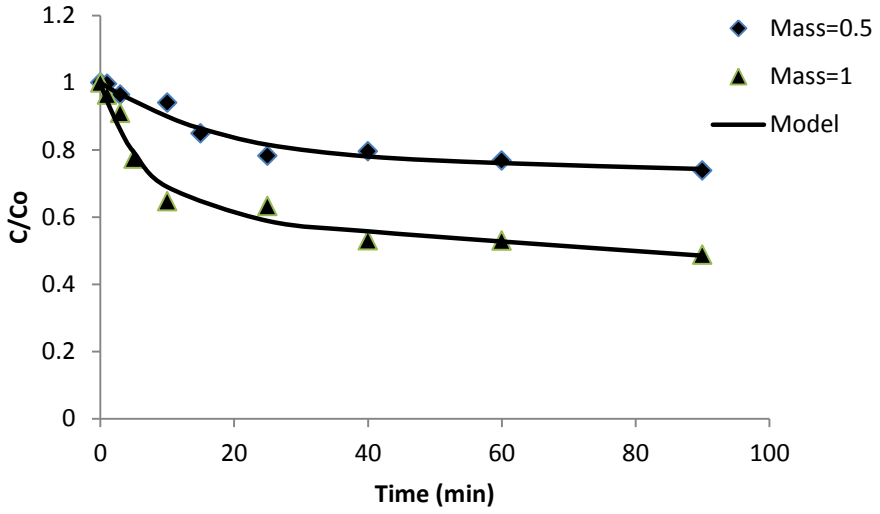

Figure 5-37: Effect of catalyst mass on Zn removal at a relatively low initial concentration (10 ppm).

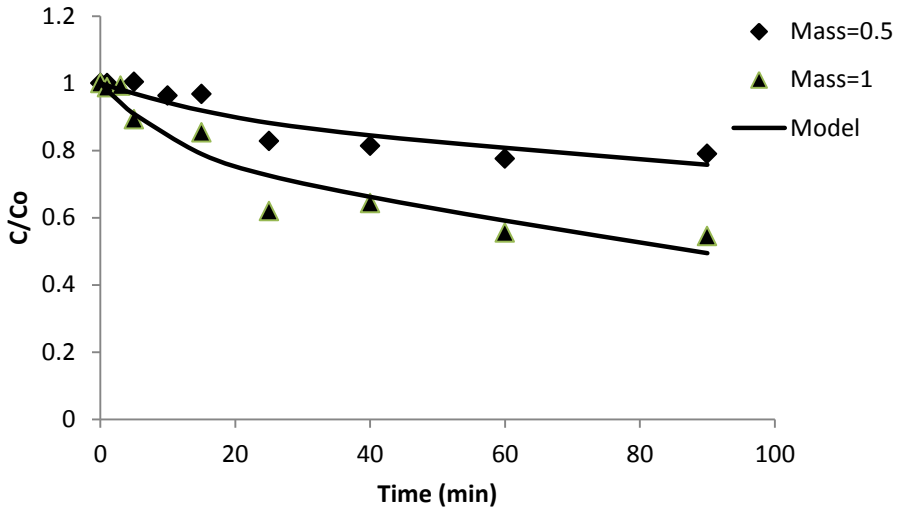

Figure 5-38: Effect of catalyst mass on Zn removal at a relatively high initial concentration (25 ppm).

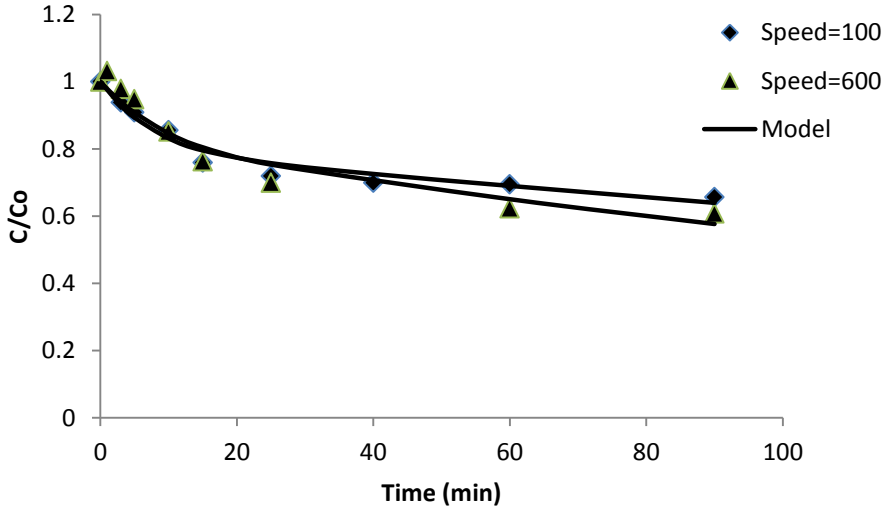

Figure 5-39: Effect of stirring speed on Zn removal when a relatively lower amount of catalyst was added (0.5 g).

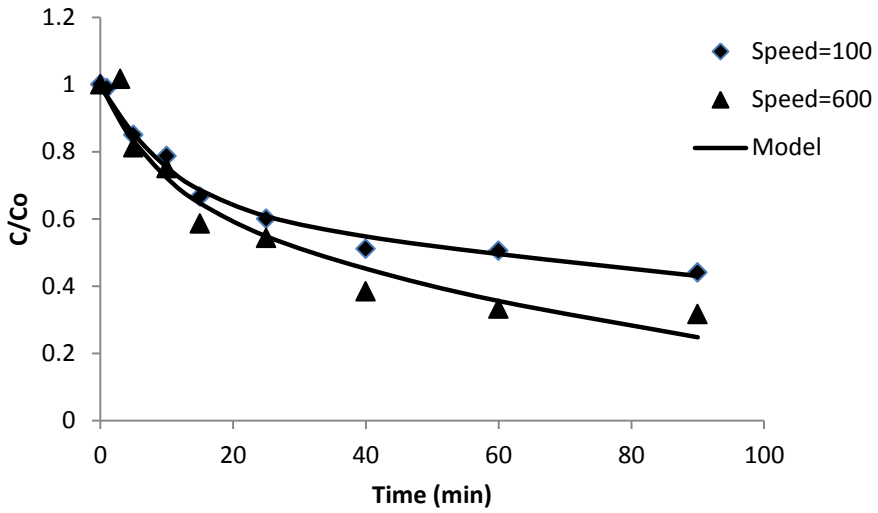

Figure 5-40: Effect of stirring speed on Zn removal when a relatively higher amount of catalyst was added (1 g).

Table 5-6: Reaction and adsorption constants values of Zn removal by Fe-doped titanium dioxide.

					Constants values obtained by the model			
EXP	**SPEED**	**MASS**	**Co**	**T**	**Krxn (10^{-4})**	**95% conf (10^{-4})**	**Kf (10^{-4})**	**95% conf (10^{-4})**
E1	100	0.5	25	4	2.08	0.1046	8.65	0.178
E2	100	0.5	25	25	6.78	0.259	4.45	0.866
E3	600	0.5	25	4	4.65	0.0994	3.43	0.468
E4	600	0.5	25	25	2.98	0.371	6.79	0.853
E5	600	1	25	4	12.67	2.167	24.15	4.825
E6	600	1	10	4	7.64	1.021	10.68	0.971
E7	600	1	25	25	4.07	0.325	2.98	0.282
E8	600	1	10	25	1.61	0.084	3.49	0.311
E9	100	0.5	10	25	1.58	0.066	3.66	0.279
E10	100	1	10	25	1.35	0.047	10.06	0.438
E11	100	0.5	25	25	6.78	0.550	4.45	0.265
E12	100	1	25	25	5.33	1.231	7.78	2.053
E13	100	0.5	10	4	1.68	0.104	11.8	0.949
E14	600	0.5	10	4	3.78	0.355	13.05	1.064
E15	100	1	10	4	3.61	0.308	1.34	0.046
E16	600	1	10	4	7.64	1.314	10.68	2.328

5.2.3 Kinetics of Cd removal by V-doped titanium dioxide

Removal of Cd by V-doped titanium dioxide has been studied as well, and the effects of experimental conditions are shown in Figures 5.41 throughout 5.48. it was also noticed that – as for Fe-doped titanium dioxide- temperature has less effect of the removal of Cd. The other under study experimental conditions were found to be less effective as well, due to the fact that, among the studied transition metals, vanadium has the least band gab energy, which makes it less active when used as a photocatalyst compared to tungsten and vanadium.

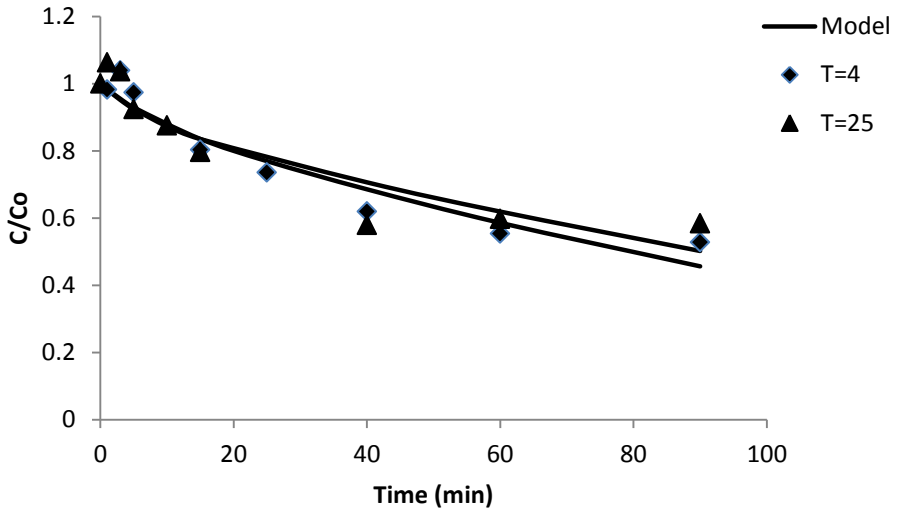

Figure 5-41: Effect of temperature on Cd removal at a relatively low stirring speed (100 rpm).

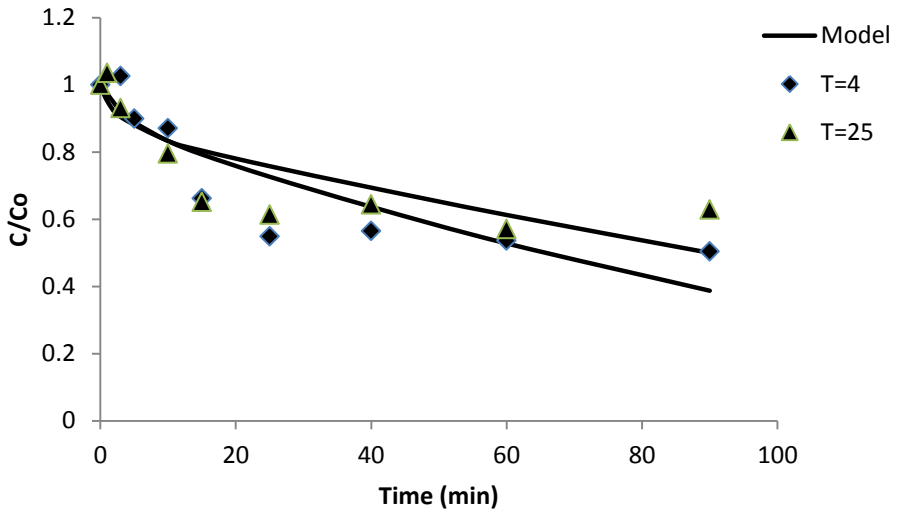

Figure 5-42: Effect of temperature on Cd removal at a relatively high stirring speed (600 rpm).

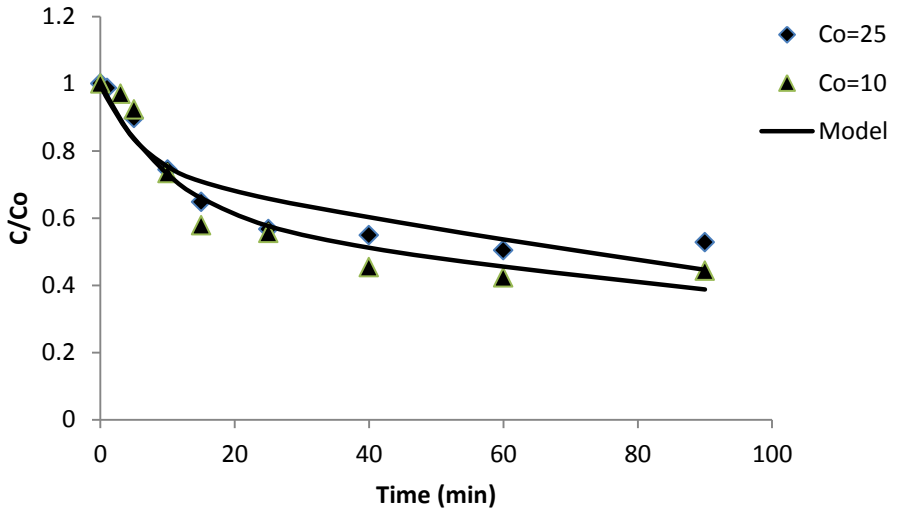

Figure 5-43: Effect of initial concentration on Cd removal at a relatively lower temperature (4^{o}C).

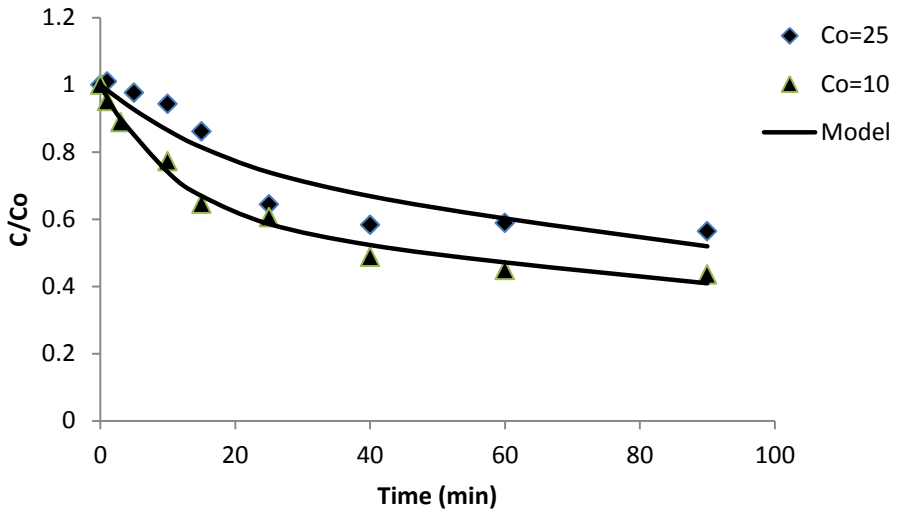

Figure 5-44: Effect of initial concentration on Cd removal at a relatively higher temperature (25^{o}C).

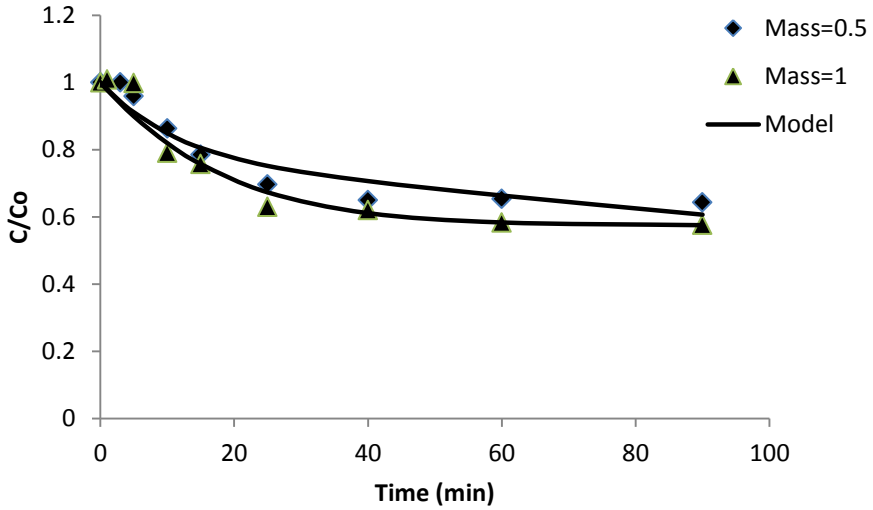

Figure 5-45: Effect of catalyst mass on Cd removal at a relatively low initial concentration (10 ppm).

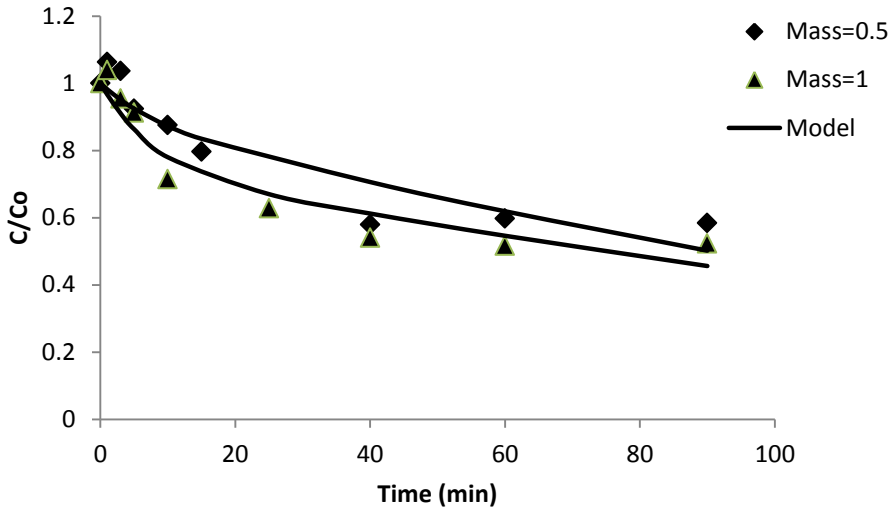

Figure 5-46: Effect of catalyst mass on Cd removal at a relatively high initial concentration (25 ppm).

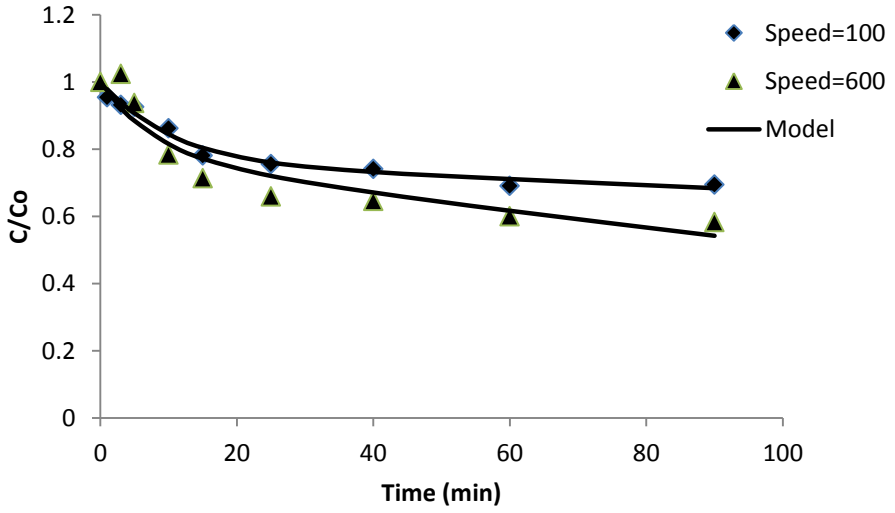

Figure 5-47: Effect of stirring speed on Cd removal when a relatively lower amount of catalyst was added (0.5 g).

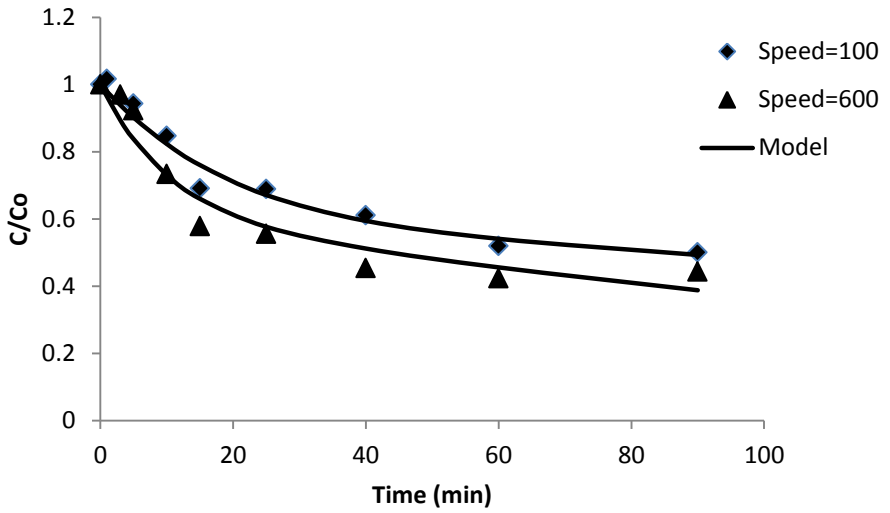

Figure 5-48: Effect of stirring speed on Cd removal when a relatively higher amount of catalyst was added (1 g).

Table 5-7: Reaction and adsorption constants values of Cd removal by V-doped titanium dioxide.

					Constants values obtained by the model			
EXP	**SPEED**	**MASS**	**Co**	**T**	**Krxn (10^{-4})**	**95% conf (10^{-4})**	**Kf (10^{-4})**	**95% conf (10^{-4})**
E1	100	0.5	25	4	20.11	1.689	18.32	1.664
E2	100	0.5	25	25	23.21	1.877	10.34	1.041
E3	600	0.5	25	4	8.14	2.041	29.12	7.429
E4	600	0.5	25	25	12.79	3.184	4.96	1.028
E5	600	1	25	4	5.97	0.616	17.53	1.152
E6	600	1	10	4	4.02	0.343	15.34	0.784
E7	600	1	25	25	5.52	0.391	4.77	0.346
E8	600	1	10	25	3.49	0.246	4.01	0.188
E9	100	0.5	10	25	3.52	0.221	11.88	0.594
E10	100	1	10	25	2.11	0.137	3.57	0.372
E11	100	0.5	25	25	23.21	1.946	10.34	0.895
E12	100	1	25	25	6.01	0.428	12.87	0.951
E13	100	0.5	10	4	1.75	0.085	5.08	0.433
E14	600	0.5	10	4	5.88	0.423	23.63	1.015
E15	100	1	10	4	1.95	0.072	8.21	0.416
E16	600	1	10	4	4.02	0.208	15.34	0.894

The values of reaction constants for Pb (II) removal by W-doped titanium dioxide are given in Table 5.5. It is noticed that, the mass transfer coefficients are higher than the rate constants of photocatalytic degradation. This trend indicates that the dominant step is the reaction on the catalyst surface. In addition to that, when the catalyst mass and temperature were low (0.5 g and 4^{o}C, respectively), the difference between the reaction constant and mass transfer coefficient was the highest (Tables 5.5, E13 and E14). This is cause by the enhanced diffusivity due to the lower bulk density when less amount of catalyst was added. In addition to that, as the temperature increases from 4^{o}C to 25^{o}C, at fixed dosage of 1 g of catalyst (E7 and E8), the values of mass transfer coefficients were significantly decreased accordingly. This is because of the lower diffusivity from bulk liquid to the internal pores, as it is inversely proportional to temperature which indicates the domination of surface reaction as well [39,40].

Similar trends were observed for the degradation of Zn(II) and Cd(II) by Fe-doped and V-doped titanium dioxide, respectively, where the values of reaction constants were lower compared to those achieved for W-doped titanium dioxide as shown in Tables 5.6 and 5.7. This is caused by the higher band gap energy of tungsten oxide compared to the oxides of iron and vanadium.

The highest reported value of reaction constant for Pb(II) removal by W-doped titanium dioxide is 3.95 cm.g/W.s. This value corresponds stirring speed of 600 rpm and initial concentration of 25 ppm, in which, the higher speed increases the rate of species migration from the bulk liquid to the catalyst surface[41], while the high initial concentration increases the number of species on the surface and hence increases the reaction rate[42].

In contrast, the lower stirring speed of 100 rpm and lower initial concentration of 10 ppm resulted in the highest mass transfer coefficient of 8.24 cm/s. This is caused by the lower number

of species available in the bulk at low concentration, and the lower rate of migration at low stirring speed [43, 44]. The same observations were reported for Zn(II) removal by Fe-doped titanium dioxide, where the highest values of reaction constant and mass transfer coefficient were 12.68 cm.g/W.s and 13.05 cm/s, respectively.

In addition to that, the lowest value of reaction constant for removal of Cd(II) by V-doped titanium dioxide was found to be 1.75. This due to the low dosage of catalyst (0.5 g), which results in decreasing the number of active sites available on the catalyst surface, and the low initial concentration of 10 ppm reduces the number of species that migrate from the bulk liquid into surface [4, 43, 46].

The general trend observed for mass transfer coefficient, which were higher at low temperatures, can be explained by the fact that, increasing the temperature will result in desorption of species back to the bulk solution. This trend is governed by the product of Schmidt and Reynold's numbers (ScRe), and the desorption at high temperatures is responsible for the less values of mass transfer coefficients. Furthermore, since both heat and mass transfer were occurring simultaneously, the mass transfer in this case is governed by the energy flux (Diffusion-thermo effect or Dufour effect), in which, the mass transfer coefficient is more affected by temperature than stirring speed. These trends are supported by the work of Jeffery. S. and Kfoussias in modeling of heat and mass transfer through CSTRs[49].

In general, it is noticed that, the degradation percentages of Pb(II), Zn(II) and Cd(II) by metal-doped titanium dioxide were higher at low temperature, which indicates that the adsorption is endothermic. These degradation percentages were also higher at high dosages of catalyst as a result of the more active sites available on the surface. Moreover, decreasing the stirring speed

and initial concentration of heavy metals led to lower degradation percentages because of the less driving force for species migration [33, 50].

CHAPTER 6

CONCLUDING REMARKS AND RECOMMENDATIONS

6.1 Concluding remarks

Sol-gel process with continuous ultrasonication was used to produce pure and metal-doped titanium dioxide. Different experimental parameters were investigated in order to achieve the best conditions of synthesis, these parameters include the type of solvent, type of acid, concentration of acid, amount of water and ultrasonication period. It is found that, based on the shape and size of the final catalyst, methanol is the suitable solvent to use at these experimental conditions, along with acetic acid (HAc) (1-2 M) at ultrasonication period of 30 minutes. Though HAc (organic acid) is a milder acid that HCl, it is still preferred to use HCl in this process because of the fact that, the carbon residuals from HAc after calcination may block the active sites on the catalyst surface. These carbon residuals can be burned and removed from the surface by increasing the calcination temperature, but the phase of titanium dioxide will be transformed to the less preferable rutile.

Metal-doped titanium dioxide was synthesis at these optimum condition at which, water was replaced by a solution of salt of the target metal. Iron (III) nonahydrate, vanadium metavanadate, and tungsten oxide were used as a source for iron, vanadium and tungsten respectively. In the case of synthesis of W-doped titanium dioxide, few drops of sulfuric acid was added to prevent any sedimentation during preparation process.

The characterization of synthesized pure and metal-doped titanium dioxide for shape and morphology was done by SEM, which has shown spherical particles at the optimum conditions. The shape of catalyst was clusters and agglomerates when the acid concentration was higher than 2 M or when the amount of water added was higher than 5 ml.

All catalyst phases of pure and metal-doped titanium dioxide were found to be mainly anatase as shown by XRD patterns. The surface area measured using BET was found to be increased when a transition metal was incorporated into titanium dioxide matrix (i.e. 62.9 m^2/g for pure titanium dioxide to 152.3 m^2/g for W-doped titanium dioxide). Further investigations of the particle size were done by PSA, which revealed a range of 6-14 nm of average particle size distribution.

The photocatalytic activity was tested for pure and metal-doped catalysts by the measurement of MB degradation from aqueous solutions. It is found that, the incorporation of transition metals into titanium dioxide matrix has enhanced the photocatalytic activity. This trend was noticed in the increment of catalyst maximum uptake from 11.5 mg/g for pure titanium dioxide to 17.4 mg/g for V-doped titanium dioxide, 25.6 mg/g for Fe-doped titanium dioxide and 20.8 mg/g for W-doped titanium dioxide. Furthermore, the impact of solution pH was investigated by measuring the catalyst uptake at pH 4, 6 and 10, and the catalyst was found to be more active at higher pH using all types of titanium dioxide.

Removal of toxic heavy metal including Pb(II), Zn(II) and Cd(II) was studied intensively by applying all types of metal-doped titanium dioxide to measure the isotherms and kinetics. The isotherms studies showed that, the highest removal percentage of Pb(II) was achived by W-doped titanium dioxide, while Fe-doped titanium dioxide and V-doped titanium dioxide performed better for removal of Zn(II) and Cd(II) respectively. Detailed kinetics studies of these

metals were carried out to investigate the effect of temperature, initial concentration, catalyst mass and stirring speed on the removal of each metal from aqueous solutions.

The kinetics study of heavy metals degradation by metal-doped titanium dioxide indicated that, the adsorption process in endothermic. This was concluded by the higher degradation percentages achieved at lower temperature of 4^{o}C. In addition to that, the higher stirring speed and catalyst dosage led to higher degradation percentage as well, due to the increasing of the driving force for movement of species from the bulk liquid to the catalyst surface and the more active sites available.

6.2 Recommendations and future work

This work will be further extended in both, synthesis and applications as can be described by the following:

Synthesis of other metal-doped titanium dioxide

In this field, more transition metals will be investigated as doping materials such as cerium and lanthanide, and more synthesis techniques to be applied to study the quality of each process, these processes include:

- Sputtering.
- Chemical vapor deposition (CVD).
- Flame synthesis.
- Metal precipitation.
-

Application

- Removal of more hydrocarbons toxics (i.e. phenol).
- Removal of arsenic and mercury from wastewater.

REFERENCES

1. Andronic, L. and A. Duta, *The influence of TiO2 powder and film on the photodegradation of methyl orange.* Materials Chemistry and Physics, 2008. **112**(3): p. 1078-1082.
2. Chang, H.T., N.M. Wu, and F. Zhu, *A kinetic model for photocatalytic degradation of organic contaminants in a thin-film TiO2 catalyst.* Water Research, 2000. **34**(2): p. 407-416.
3. Einaga, H., S. Futamura, and T. Ibusuki, *Photocatalytic decomposition of benzene over TiO2 in a humidified airstream.* Physical Chemistry Chemical Physics, 1999. **1**(20): p. 4903-4908.
4. Engates, K.E. and H.J. Shipley, *Adsorption of Pb, Cd, Cu, Zn, and Ni to titanium dioxide nanoparticles: Effect of particle size, solid concentration, and exhaustion.* Environmental Science and Pollution Research. **18**(3): p. 386-395.
5. Tao, Y., et al., *Removal of Pb(II) from aqueous solution on chitosan/TiO2 hybrid film.* Journal of Hazardous Materials, 2009. **161**(2-3): p. 718-722.
6. Xiao, X., C. Tang, and Q. Chen, *Preparation of Nanocrystalline TiO2 thin films and its photocatalytic activity.* Huazhong Keji Daxue Xuebao (Ziran Kexue Ban)/Journal of Huazhong University of Science and Technology (Natural Science Edition), 2004. **32**(8): p. 22-24.
7. Trung, T., W.J. Cho, and C.S. Ha, *Preparation of TiO2 nanoparticles in glycerol-containing solutions.* Materials Letters, 2003. **57**(18): p. 2746-2750.

8. Wei, G., Y. Zhang, and R. Xiong, *Photocatalytic degradation kinetics of Rhodamine B catalyzed by nanosized TiO2 film.* Chinese Science Bulletin, 2003. **48**(1): p. 49-52.

9. Serpone, et al., eds. *Photochemical Conversion and storage of Solar Energy*. 1991, Kluwer Academic Publishers: Dordrecht. 451-475.

10. Li, Y., et al., *Preparation of cerium-doped titania macroporous films by a sol-gel spin coating using polypropylene glycol (PPG) as pore-creating agent: Effects of Ce ions, PPG and calcination on photocatalytic activity.* Surface and Coatings Technology. **204**(9-10): p. 1353-1358.

11. Yu, Y., J. Wang, and J.F. Parr, *Preparation and properties of TiO2/fumed silica composite photocatalytic materials.* Procedia Engineering. **27**(0): p. 448-456.

12. Popovici, E., et al., *Development of systems for the laser synthesis of nanoparticles starting from liquid precursors.* Applied Surface Science, (0).

13. Chen, Z., et al., *Preparation of porous TiO2 using eggshell membrane as template and its photocatalytic activity.* Procedia Engineering. **27**(0): p. 512-518.

14. Shi, X., et al., *Enhanced photocatalytic activity of titanium dioxide by nut shell carbon.* Journal of Hazardous Materials, 2009. **167**(1-3): p. 692-695.

15. Takeuchi, M., et al., *Enhancement of the photocatalytic reactivity of TiO2 nano-particles by a simple mechanical blending with hydrophobic mordenite (MOR) zeolite.* Applied Catalysis B: Environmental, 2009. **89**(3-4): p. 406-410.

16. Tian, G., et al., *Enhanced photocatalytic activity of S-doped TiO2-ZrO2 nanoparticles under visible-light irradiation.* Journal of Hazardous Materials, 2009. **166**(2-3): p. 939-944.

17. Zhang, Z., et al. *Photocatalytic activity of nitrogen doped nano-titanias and titanium nitride towards methylene blue decolouration*. in *Technical Proceedings of the 2008 NSTI Nanotechnology Conference and Trade Show, NSTI-Nanotech, Nanotechnology 2008*. 2008. Quebec City, QC.

18. Saha, S., J.M. Wang, and A. Pal, *Nano silver impregnation on commercial TiO2 and a comparative photocatalytic account to degrade malachite green.* Separation and Purification Technology. **89**(0): p. 147-159.

19. Farnoush, H., et al., *Modification of electrophoretically deposited nanoâ€“hydroxyapatite coatings by wire brushing on Tiâ€“6Alâ€“4 V substrates.* Ceramics International, (0).

20. Bhattacharyya, K., et al., *Microstructural characterization of the V-doped nano-titania.* Journal of Alloys and Compounds, 2009. **482**(1-2): p. 256-260.

21. Hamadanian, M., A. Reisi-Vanani, and A. Majedi, *Preparation and characterization of S-doped TiO2 nanoparticles, effect of calcination temperature and evaluation of photocatalytic activity.* Materials Chemistry and Physics, 2009. **116**(2-3): p. 376-382.

22. Kaczmarek, D., et al., *TiO2 thin films doped with Pd and Eu for optically and electrically active TOS-Si heterojunction.* Optical Materials, 2009. **31**(9): p. 1337-1339.

23. Kalfa, O.M., O. Yalʲ§inkaya, and A.R. Tʲ¼rker, *Synthesis of nano B2O3/TiO2 composite material as a new solid phase extractor and its application to preconcentration and separation of cadmium.* Journal of Hazardous Materials, 2009. **166**(1): p. 455-461.

24. Shankar, M.V., et al., *One-pot synthesis of peroxo-titania nanopowder and dual photochemical oxidation in aqueous methanol solution.* Journal of Colloid and Interface Science, 2009. **331**(1): p. 132-137.

25. Hu, M.Z., et al. *Synthesis and characterization of anodized titanium oxide nanotubes arrays*. in *Nanotechnology 2009: Fabrication, Particles, Characterization, MEMS, Electronics and Photonics - Technical Proceedings of the 2009 NSTI Nanotechnology Conference and Expo, NSTI-Nanotech 2009*. 2009. Houston, TX.

26. Ray, S., J.A. Lalman, and N. Biswas, *Using the Box-Benkhen technique to statistically model phenol photocatalytic degradation by titanium dioxide nanoparticles.* Chemical Engineering Journal, 2009. **150**(1): p. 15-24.

27. Jha, A.K., K. Prasad, and A.R. Kulkarni, *Synthesis of TiO2 nanoparticles using microorganisms.* Colloids and Surfaces B: Biointerfaces, 2009. **71**(2): p. 226-229.

28. Rahimpour, A., et al., *Structural and performance properties of UV-assisted TiO2 deposited nano-composite PVDF/SPES membranes.* Desalination. **285**(0): p. 31-38.

29. Chen, L., et al., *Photoreduction of CO2 by TiO2 nanocomposites synthesized through reactive direct current magnetron sputter deposition.* Thin Solid Films, 2009. **517**(19): p. 5641-5645.

30. Canuto, C., Hussaini, M. Y., Quarteroni, A. & Zang, T. A. . , *Spectral Methods in Fluid Dynamics.* Springer, 1988.

31. Sato, K., et al., *Ultrasonic dispersion of TiO2 nanoparticles in aqueous suspension.* Journal of the American Ceramic Society, 2008. **91**(8): p. 2481.

32. Termnak, S., W. Triampo, and D. Triampo, *Effect of acid during synthesis on the agglomerated strength of TiO 2 nanoparticles.* Journal of Ceramic Processing Research, 2009. **10**(4): p. 491.

33. Rashidi, F., et al., *Kinetic, equilibrium and thermodynamic studies for the removal of lead (II) and copper (II) ions from aqueous solutions by nanocrystalline TiO2.* Superlattices and Microstructures. **48**(6): p. 577-591.

34. Rengifo-Herrera, J.A., et al., *Photocatalytic discoloration of aqueous malachite green solutions by UV-illuminated TiO2 nanoparticles under air and nitrogen atmospheres: effects of counter-ions and pH.* Photochemical & Photobiological Sciences. **10**(1): p. 29-34.

35. Shah, S.I., et al. *Colloquium Paper: Study of Nd3+, Pd2+, Pt4+, and Fe3+ dopant effect on photoreactivity of TiO2 nanoparticles* 2002: Proceeding of the National Academy of Sciences of the United States of America.

36. Kim, S.B. and S.C. Hong, *Kinetic study for photocatalytic degradation of volatile organic compounds in air using thin film TiO2 photocatalyst.* Applied Catalysis B: Environmental, 2002. **35**(4): p. 305-315.

37. Lorret, O., et al., *W-doped titania nanoparticles for UV and visible-light photocatalytic reactions.* Applied Catalysis B: Environmental, 2009. **91**(1-2): p. 39-46.

38. Madden, T.H., et al., *Oxidation of metal - EDTA complexes by TiO2 photocatalysis.* Environmental Science and Technology, 1997. **31**(12): p. 3475-3481.

39. Mohseni Meybodi, S., et al., *Synthesis of wide band gap nanocrystalline NiO powder via a sonochemical method.* Ultrasonics Sonochemistry. **19**(4): p. 841-845.

40. Hameed, B.H., D.K. Mahmoud, and A.L. Ahmad, *Equilibrium modeling and kinetic studies on the adsorption of basic dye by a low-cost adsorbent: Coconut (Cocos nucifera) bunch waste.* Journal of Hazardous Materials, 2008. **158**(1): p. 65-72.

41. Shawabkeh, R.A., *Hydrometallurgical extraction of zinc from Jordanian electric arc furnace dust.* Hydrometallurgy. **104**(1): p. 61-65.

42. Dutta, S., et al., *Kinetic study of adsorption and photo-decolorization of Reactive Red 198 on TiO2 surface.* Chemical Engineering Journal, 2009. **155**(3): p. 674-679.

43. Choi, J.H., et al., *Adsorption behaviors of nano-sized ETS-10 and Al-substituted-ETAS-10 in removing heavy metal ions, Pb2+ and Cd2+*. Microporous and Mesoporous Materials, 2006. **87**(3): p. 163-169.

44. Kabra, K., R. Chaudhary, and R.L. Sawhney, *Effect of pH on solar photocatalytic reduction and deposition of Cu(II), Ni(II), Pb(II) and Zn(II): Speciation modeling and reaction kinetics.* Journal of Hazardous Materials, 2007. **149**(3): p. 680-685.

45. Shawabkeh, R.A. and E.S.M. Abu-Nameh, *Absorption of phenol and methylene blue by activated carbon from pecan shells.* Colloid Journal, 2007. **69**(3): p. 355-359.

46. Kabbashi, N.A., et al., *Kinetic adsorption of application of carbon nanotubes for Pb(II) removal from aqueous solution.* Journal of Environmental Sciences, 2009. **21**(4): p. 539-544.

47. Luo, T., et al., *Arsenic removal and recovery from copper smelting wastewater using TiO 2*. Environmental Science and Technology. **44**(23): p. 9094-9098.

48. Mustafa, K., *Removal of Pb(II) from water by natural zeolitic tuff: Kinetics and thermodynamics.* Journal of Hazardous Materials. **199â€“200**(0): p. 383-389.

49. Kafoussias, N.G. and E.W. Williams, *Thermal-diffusion and diffusion-thermo effects on mixed free-forced convective and mass transfer boundary layer flow with temperature dependent viscosity.* International Journal of Engineering Science, 1995. **33**(9): p. 1369-1384.

50. Shawabkeh, R., et al., *Conversion of oil shale ash into zeolite for cadmium and lead removal from wastewater.* Fuel, 2004. **83**(7-8): p. 981-985.

APPENDICES

Appendix A:

Detailed BET analysis of pure and metal-doped titanium dioxide

Pure titanium dioxide

Surface Area

Single point surface area at p/p° = 0.199883521:	59.6524 m^2/g
BET Surface Area:	62.9336 m^2/g
Langmuir Surface Area:	88.1457 m^2/g
t-Plot External Surface Area:	67.5459 m^2/g
BJH Adsorption cumulative surface area of pores between 17.000 Å and 3000.000 Å width:	75.361 m^2/g
BJH Desorption cumulative surface area of pores between 17.000 Å and 3000.000 Å width:	91.2494 m^2/g

Pore Volume

Single point adsorption total pore volume of pores less than 707.582 Å width at p/p° = 0.971871537:	0.096891 cm^3/g
Single point desorption total pore volume of pores less than 19.377 Å width at p/p° = 0.140464200:	0.023739 cm^3/g
t-Plot micropore volume:	-0.003023

	cm^3/g
BJH Adsorption cumulative volume of pores between 17.000 Å and 3000.000 Å width:	0.109355 cm^3/g
BJH Desorption cumulative volume of pores between 17.000 Å and 3000.000 Å width:	0.108742 cm^3/g

Pore Size

Adsorption average pore width (4V/A by BET):	61.5828 Å
Desorption average pore width (4V/A by BET):	15.0881 Å
BJH Adsorption average pore width (4V/A):	58.043 Å
BJH Desorption average pore width (4V/A):	47.668 Å

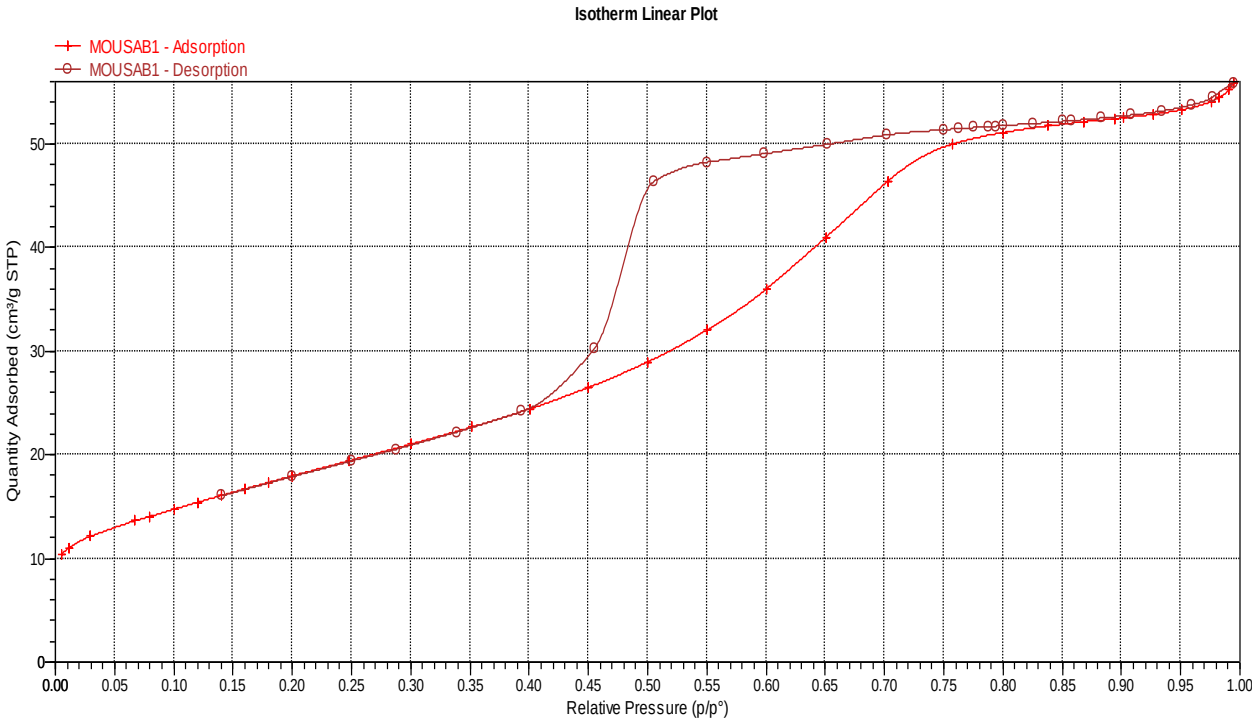

Figure A-1: Adsorption-desorption isotherm of titanium dioxide.

W-doped titanium dioxide

Surface Area

Single point surface area at p/p° = 0.199726388:	144.5454 m^2/g
BET Surface Area:	152.2656 m^2/g
Langmuir Surface Area:	213.2914 m^2/g
t-Plot External Surface Area:	160.0743 m^2/g
BJH Adsorption cumulative surface area of pores between 17.000 Å and 3000.000 Å width:	180.329 m^2/g
BJH Desorption cumulative surface area of pores between 17.000 Å and 3000.000 Å width:	196.6889 m^2/g

Pore Volume

Single point adsorption total pore volume of pores less than 748.912 Å width at p/p° = 0.973459547:	0.233147 cm^3/g
Single point desorption total pore volume of pores less than 19.385 Å width at p/p° = 0.140627080:	0.057736 cm^3/g
t-Plot micropore volume:	-0.005746 cm^3/g
BJH Adsorption cumulative volume of pores between 17.000 Å and 3000.000 Å width:	0.252959 cm^3/g
BJH Desorption cumulative volume of pores between 17.000 Å and 3000.000 Å width:	0.251907 cm^3/g

Pore Size

Adsorption average pore width (4V/A by BET):	61.2473 Å
Desorption average pore width (4V/A by BET):	15.1673 Å
BJH Adsorption average pore width (4V/A):	56.111 Å
BJH Desorption average pore width (4V/A):	51.229 Å

V-doped titanium dioxide

Surface Area

Single point surface area at p/p° = 0.200107898:	62.5524 m²/g
BET Surface Area:	66.1237 m²/g
Langmuir Surface Area:	93.2200 m²/g
t-Plot Micropore Area:	0.3337 m²/g
t-Plot External Surface Area:	24.5490 m²/g
BJH Adsorption cumulative surface area of pores between 17.000 Å and 3000.000 Å width:	27.859 m²/g
BJH Desorption cumulative surface area of pores between 17.000 Å and 3000.000 Å width:	32.2888 m²/g

Pore Volume

Single point adsorption total pore volume of pores less than 669.545 Å width at p/p° = 0.970233647:	0.043058 cm³/g
Single point desorption total pore volume of pores less than 19.365 Å width at p/p° = 0.140201012:	0.009671 cm³/g
t-Plot micropore volume:	-0.000099 cm³/g
BJH Adsorption cumulative volume of pores between 17.000 Å and 3000.000 Å width:	0.067755 cm³/g
BJH Desorption cumulative volume of pores between 17.000 Å and 3000.000 Å width:	0.067523 cm³/g

Pore Size

Adsorption average pore width (4V/A by BET):	69.2177 Å
Desorption average pore width (4V/A by BET):	15.5463 Å
BJH Adsorption average pore width (4V/A):	97.283 Å

Fe-doped titanium dioxide

Surface Area

Single point surface area at p/p° = 0.224971176: 94.7322 m^2/g

BET Surface Area: 86.4948 m^2/g

Langmuir Surface Area: 112.5958 m^2/g

t-Plot Micropore Area: 209.1197 m^2/g

t-Plot External Surface Area: -122.6249 m^2/g

BJH Adsorption cumulative surface area of pores
between 17.000 Å and 3000.000 Å width: 144.717 m^2/g

BJH Desorption cumulative surface area of pores
between 17.000 Å and 3000.000 Å width: 212.8300 m^2/g

Pore Volume

Single point adsorption total pore volume of pores
less than 1587.727 Å width at P/Po = 0.987664177: 0.088396 cm^3/g

t-Plot micropore volume: -0.000429 cm^3/g

BJH Adsorption cumulative volume of pores
between 17.000 Å and 3000.000 Å width: 0.099873 cm^3/g

BJH Desorption cumulative volume of pores

between 17.000 Å and 3000.000 Å width: 0.099599 cm^3/g

Pore Size

Adsorption average pore width (4V/A by BET): 131.9846 Å

BJH Adsorption average pore width (4V/A): 136.860 Å

BJH Desorption average pore width (4V/A): 126.856 Å

Appendix B:

Calibration curves for measuring concentration of MB, Pb, Zn and Cd.

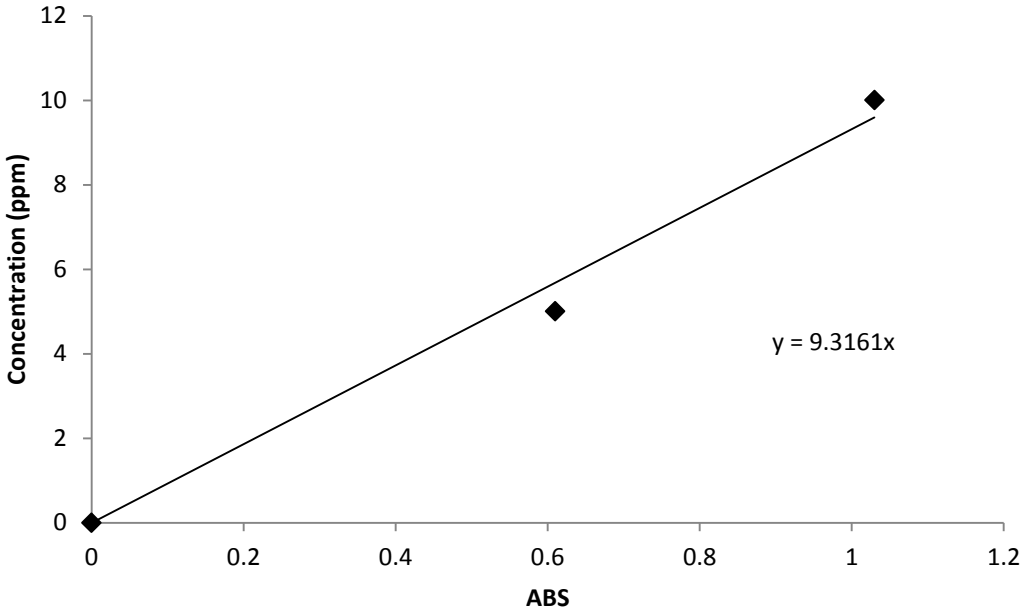

Figure A-2: Calibration curve of MB.

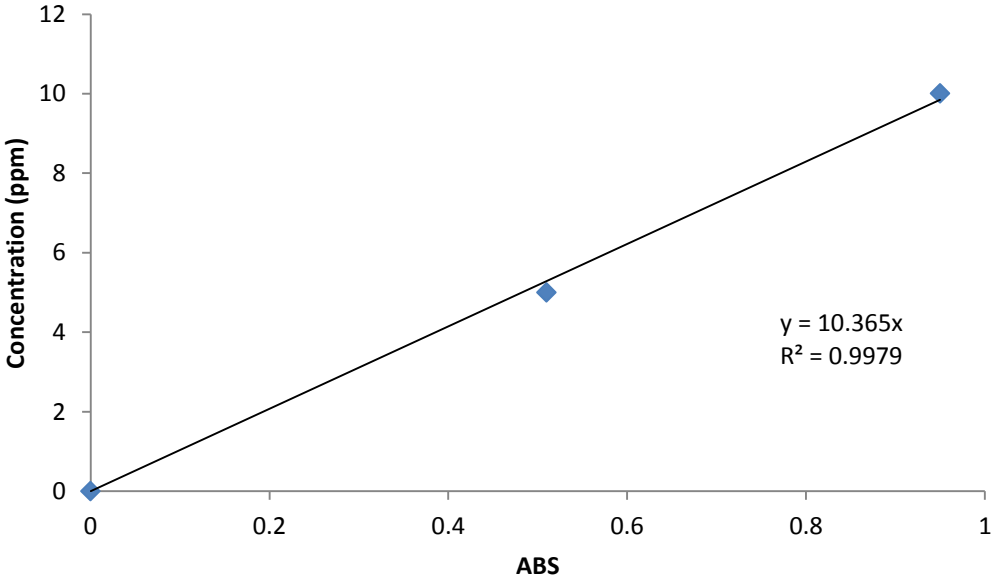

Figure A-3: Calibration curve of Pb

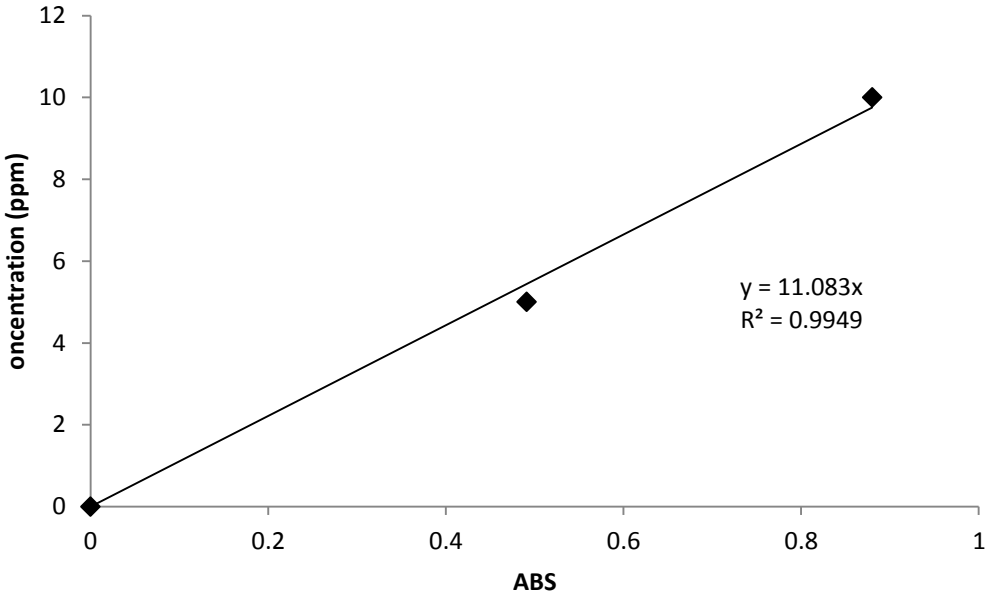

Figure A-4: Calibration curve of Zn.

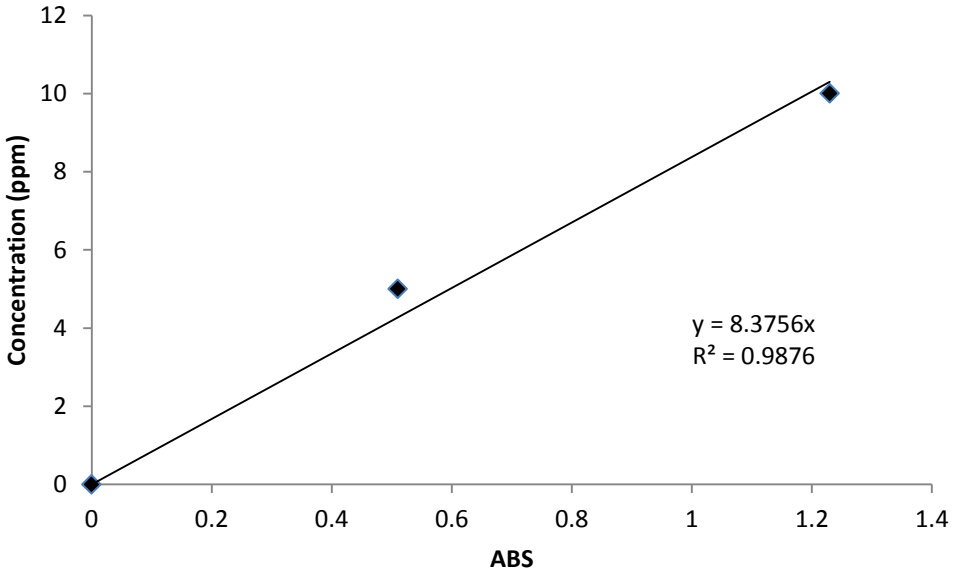

Figure A-5: Calibration curve of Cd

Appendix C:

EDS analysis of all samples of metal-doped titanium dioxide

All percentages representing the elementary analysis of samples are given as weight percent.

W-doped titanium dioxide

Sample 1

Spectrum	C	O	S	Ti	W	Total
Spectrum 1	2.06	53.53	0.86	43.56	0.00	100.00
Spectrum 2	2.56	55.26	0.92	41.26	0.00	100.00
Max.	2.56	55.26	0.92	43.56	0.00	
Min.	2.06	53.53	0.86	41.26	0.00	

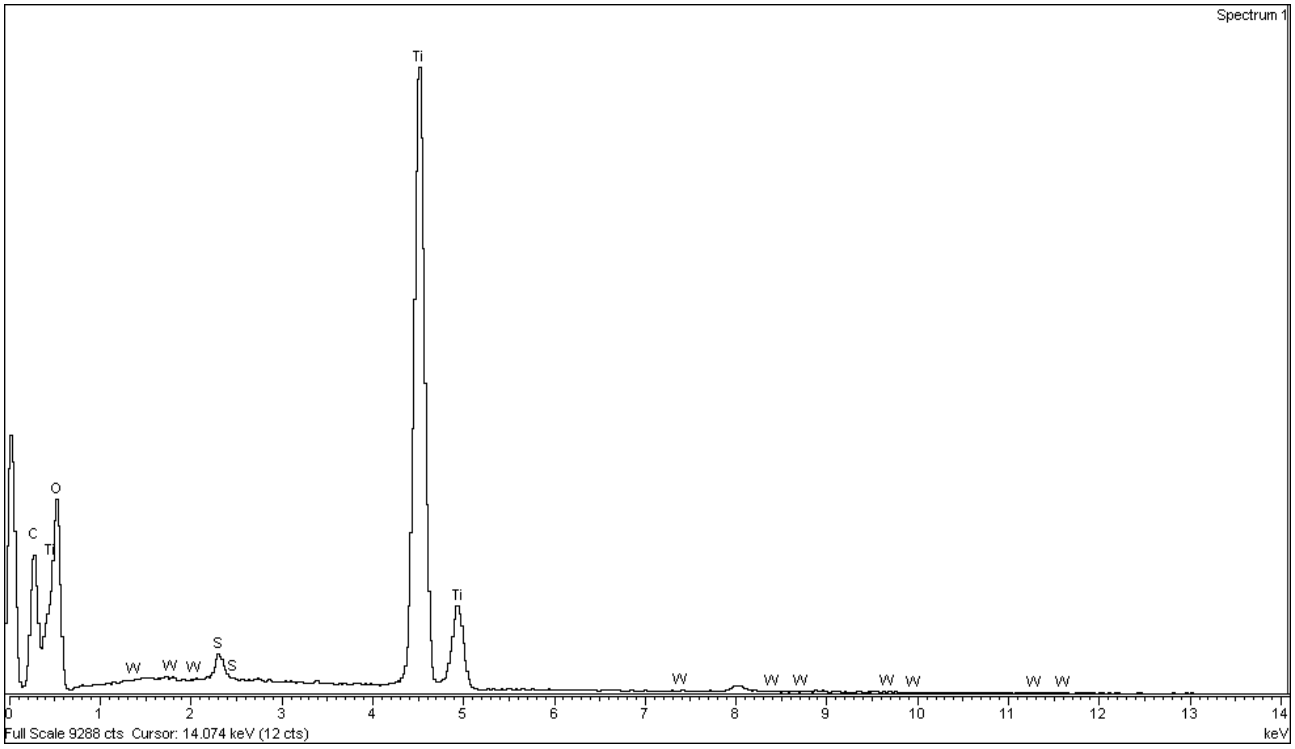

Sample 2

Spectrum	C	O	S	Ti	W	Total
Spectrum 1	2.71	54.32	1.12	41.86	0.00	100.00
Spectrum 2	3.79	55.85	1.09	39.28	0.00	100.00
Max.	3.79	55.85	1.12	41.86	0.00	
Min.	2.71	54.32	1.09	39.28	0.00	

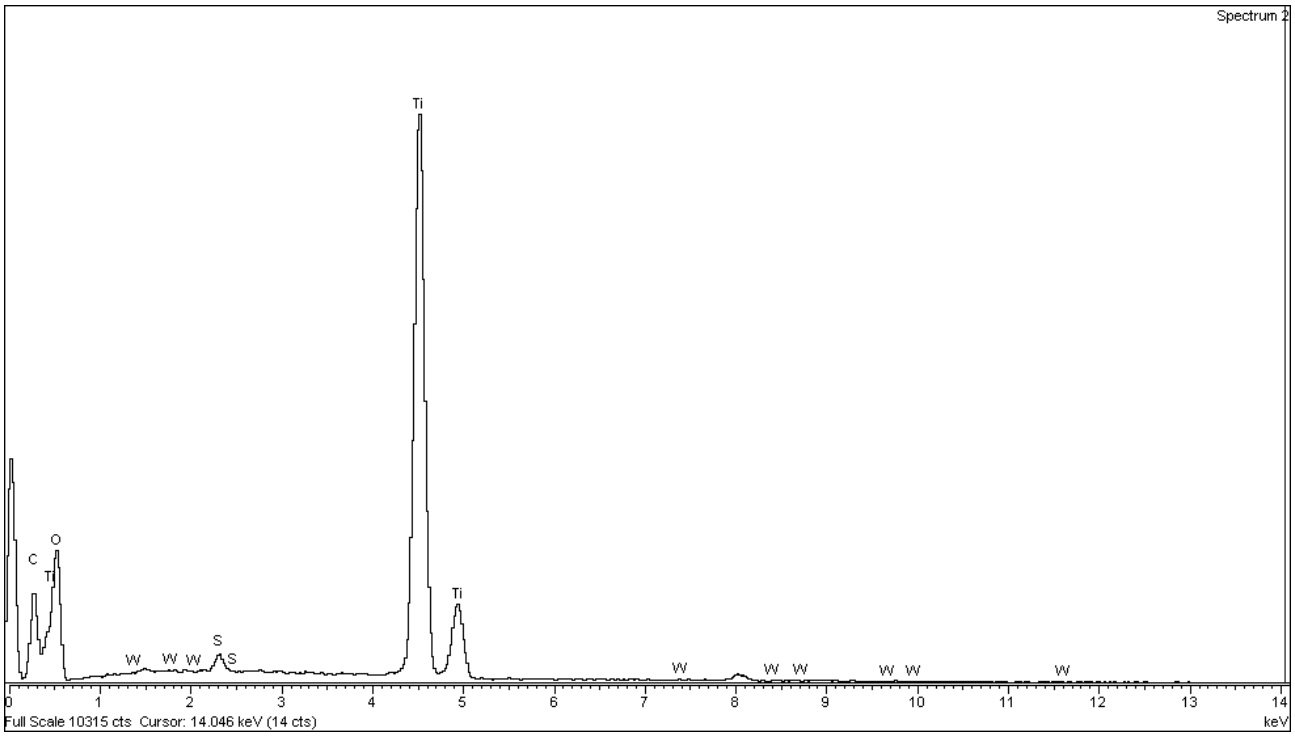

Sample 3

Spectrum	C	O	S	Ti	W	Total
Spectrum 1	3.12	52.52	0.63	43.73	0.00	100.00
Spectrum 2	1.58	50.02	0.67	47.73	0.00	100.00
Max.	3.12	52.52	0.67	47.73	0.00	
Min.	1.58	50.02	0.63	43.73	0.00	

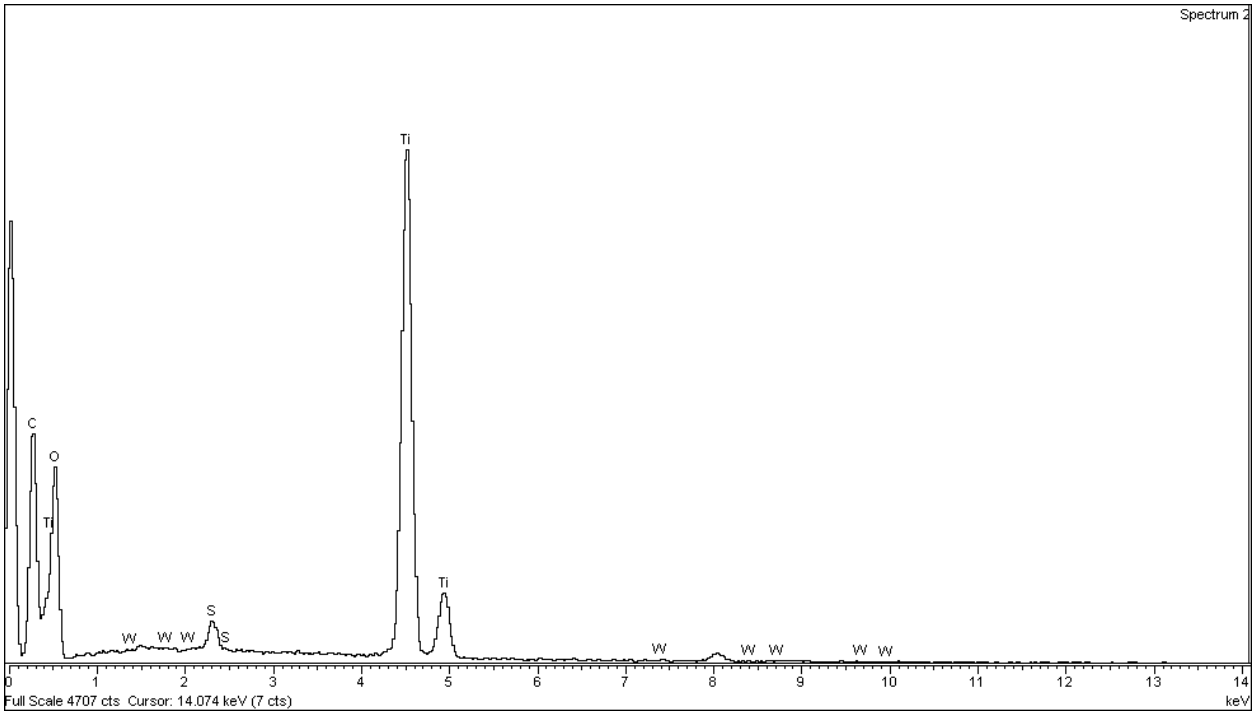

Sample 4

Spectrum	C	O	S	Ti	W	Total
Spectrum 1	13.64	58.06	1.85	26.45	0.00	100.00
Spectrum 2	19.21	60.53	1.39	18.24	0.63	100.00
Max.	19.21	60.53	1.85	26.45	0.63	
Min.	13.64	58.06	1.39	18.24	0.00	

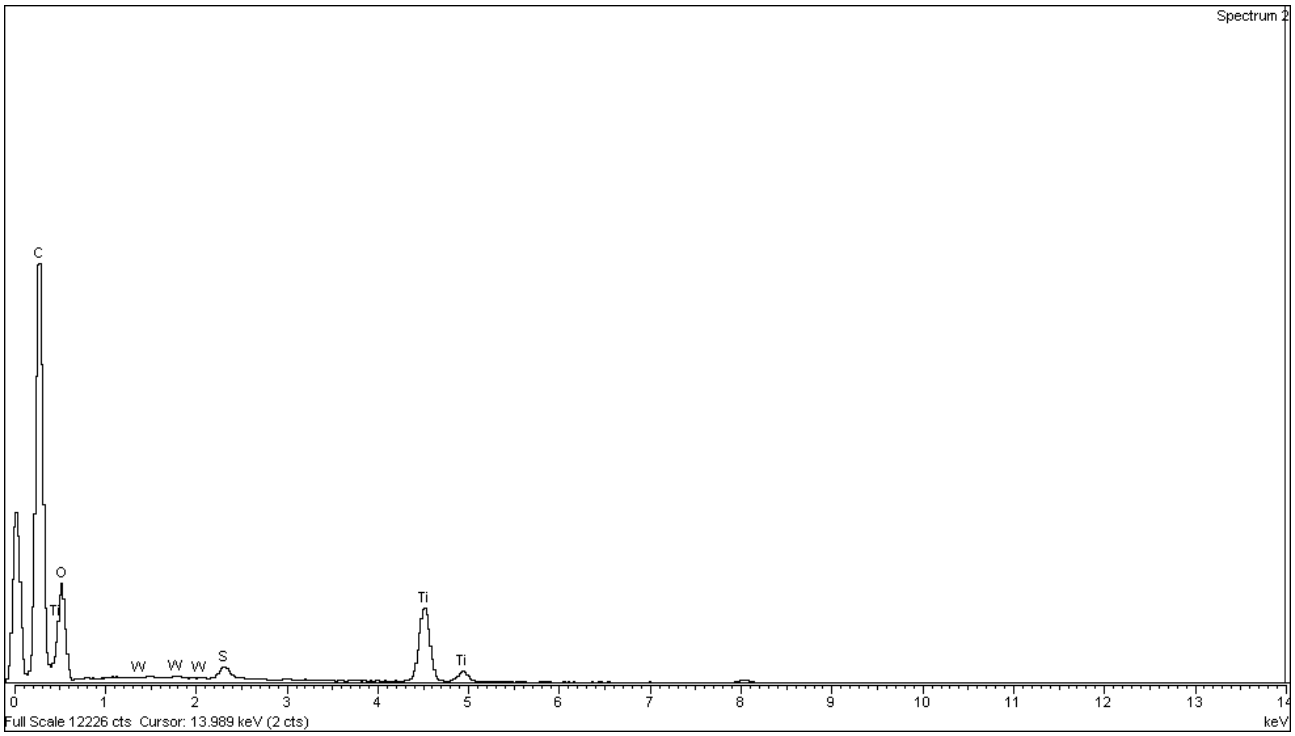

Sample 5

Spectrum	C	O	S	Ti	W	Total
Spectrum 1	3.15	53.78	1.83	40.33	0.92	100.00
Spectrum 2	3.59	53.39	1.91	39.98	1.13	100.00
Max.	3.59	53.78	1.91	40.33	1.13	
Min.	3.15	53.39	1.83	39.98	0.92	

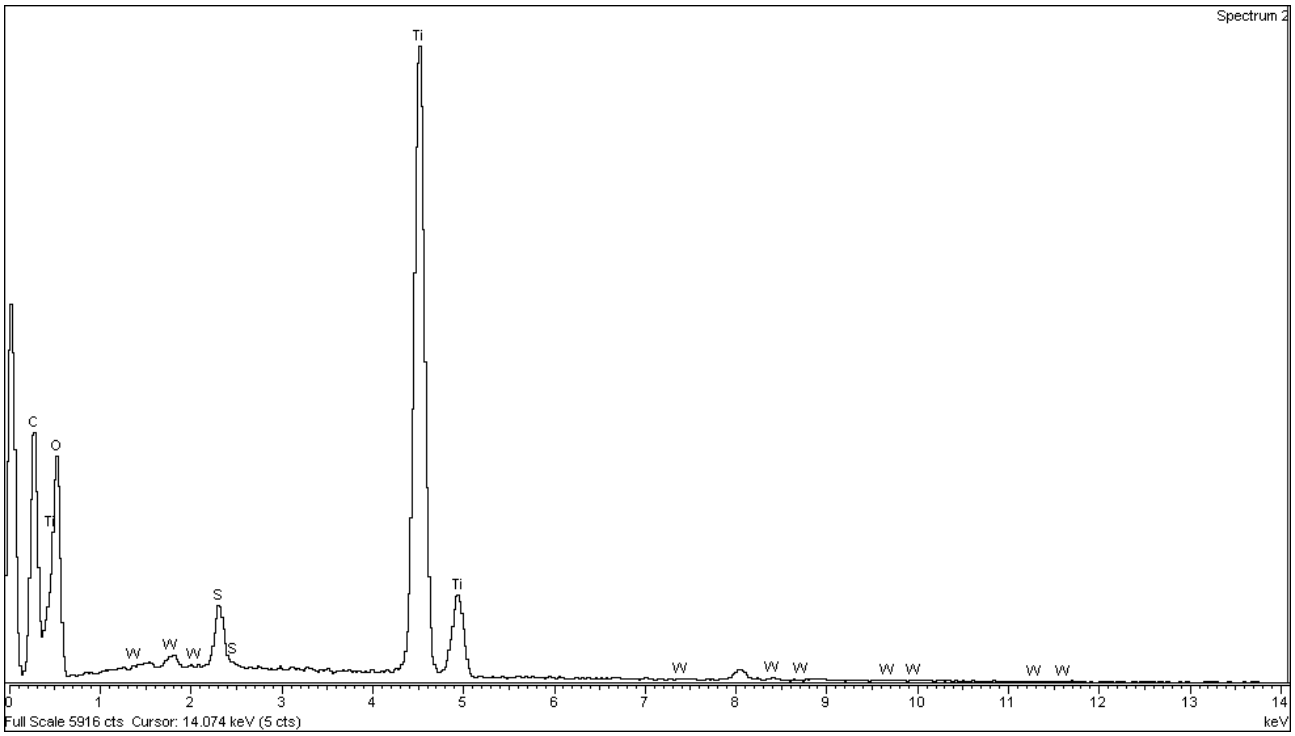

Sample 6

Spectrum	C	O	S	Ti	W	Total
Spectrum 1	3.55	53.71	3.50	36.72	2.52	100.00
Spectrum 2	5.23	56.51	3.44	32.26	2.56	100.00
Max.	5.23	56.51	3.50	36.72	2.56	
Min.	3.55	53.71	3.44	32.26	2.52	

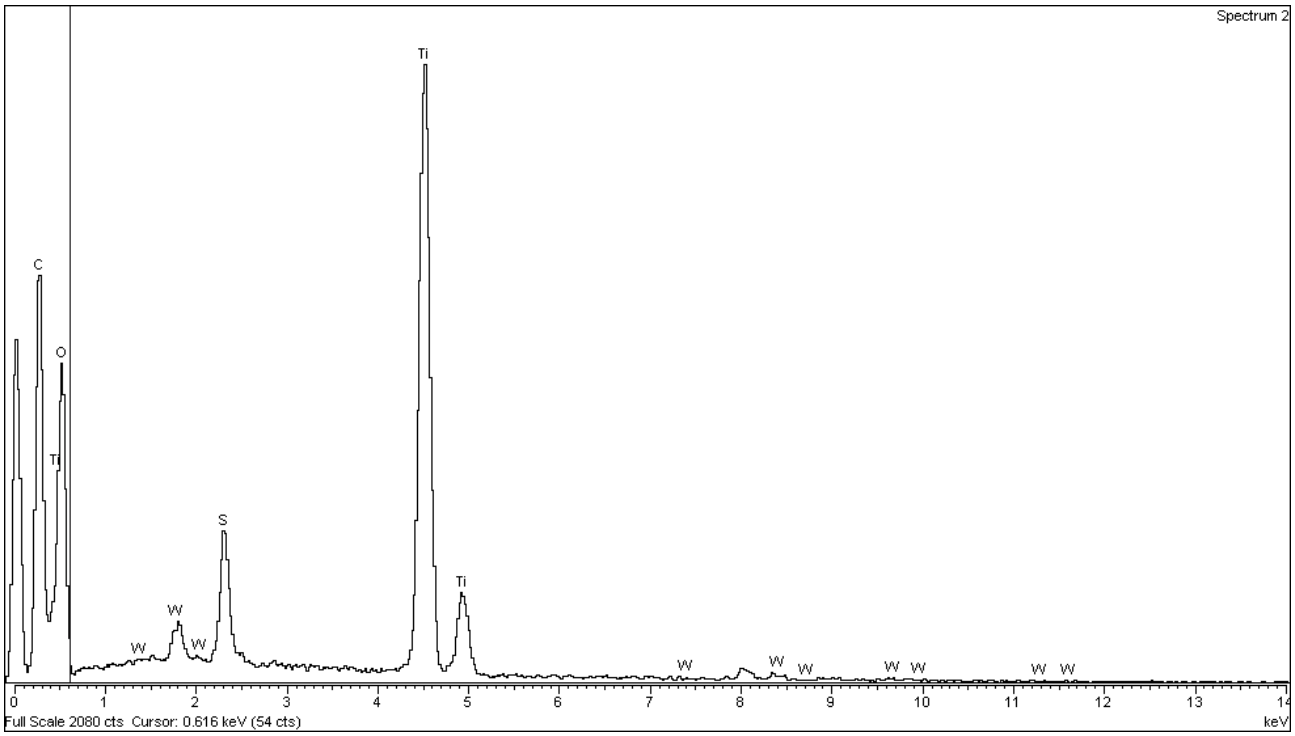

Sample 7

Spectrum	C	O	S	Ti	W	Total
Spectrum 1	2.51	54.36	3.57	36.88	2.68	100.00
Spectrum 2	2.63	53.50	3.52	37.60	2.75	100.00
Max.	2.63	54.36	3.57	37.60	2.75	
Min.	2.51	53.50	3.52	36.88	2.68	

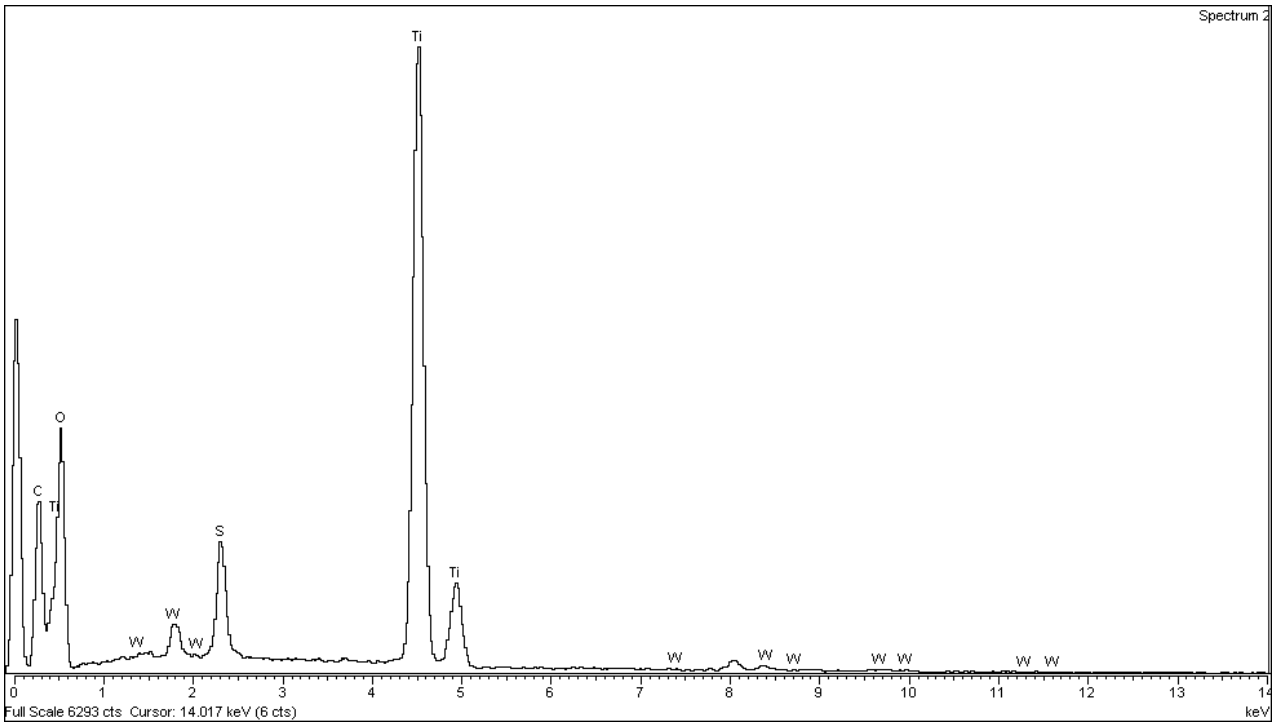
Spectrum 2
Ti
O
C
Ti
S
Ti
W
W
W
W
W
W
W
W
W
W
W
0
1
2
3
4
5
6
7
8
9
10
11
12
13
14
Full Scale 6293 cts Cursor: 14.017 keV (6 cts)
keV

Fe-doped titanium dioxide

Sample 1

Spectrum	O	Cl	Ti	Fe	Total
Spectrum 1	45.60	1.07	52.93	0.40	100.00
Spectrum 2	44.90	1.16	53.94	0.00	100.00
Spectrum 3	41.87	1.16	56.66	0.31	100.00
Max.	45.60	1.16	56.66	0.40	
Min.	41.87	1.07	52.93	0.00	

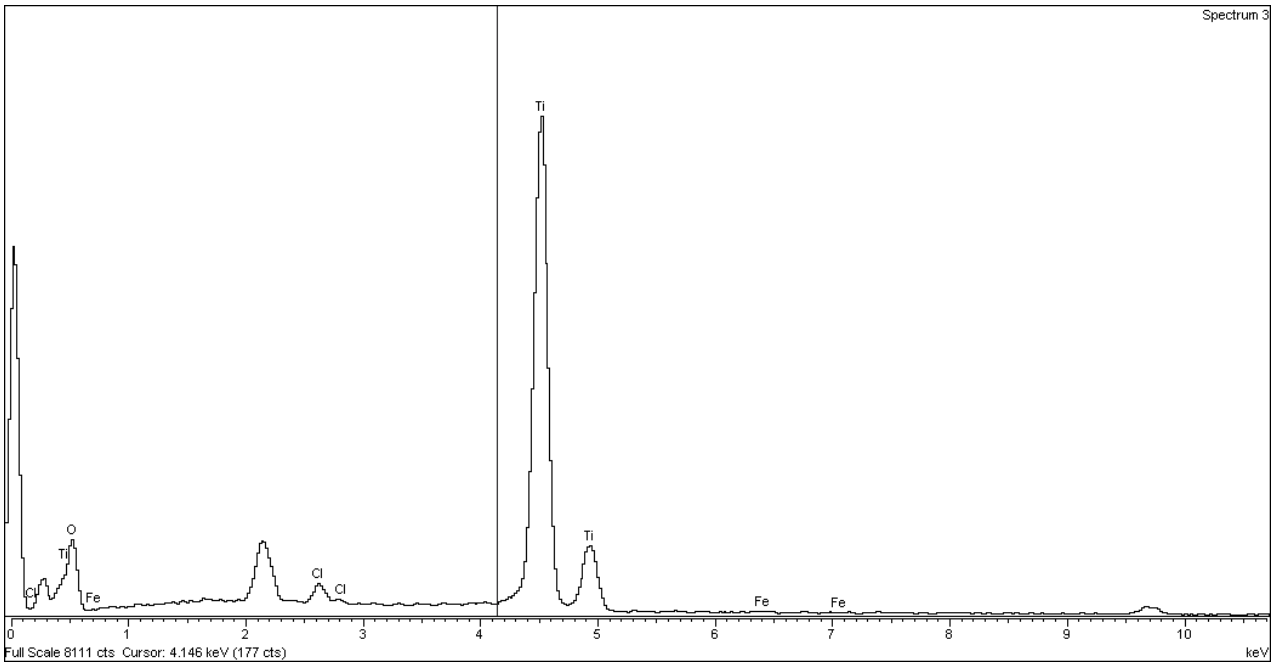

Sample 2

Spectrum	O	Cl	Ti	Fe	Total
Spectrum 1	46.26	1.13	52.26	0.35	100.00
Spectrum 2	44.66	1.13	53.76	0.46	100.00
Spectrum 3	45.25	1.05	53.37	0.33	100.00
Max.	46.26	1.13	53.76	0.46	
Min.	44.66	1.05	52.26	0.33	

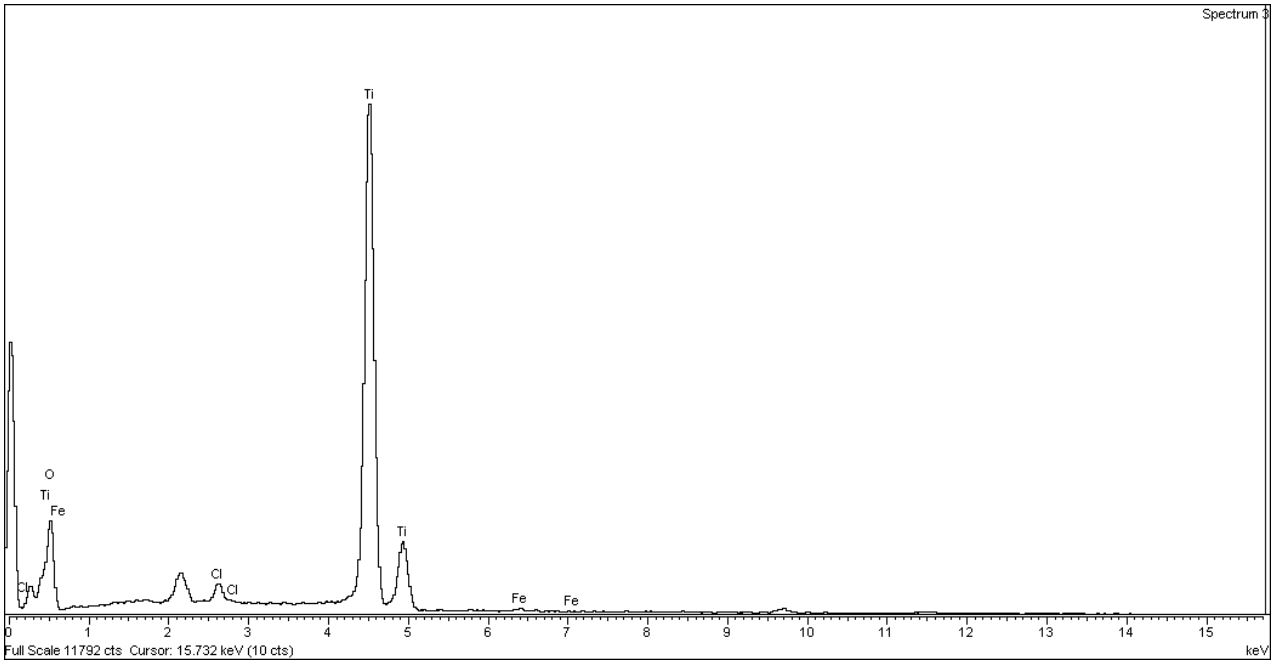

Sample 3

Spectrum	O	Cl	Ti	Fe	Total
Spectrum 1	48.36	0.79	50.37	0.48	100.00
Spectrum 2	43.83	0.75	54.87	0.55	100.00
Spectrum 3	44.69	0.75	54.09	0.47	100.00
Max.	48.36	0.79	54.87	0.55	
Min.	43.83	0.75	50.37	0.47	

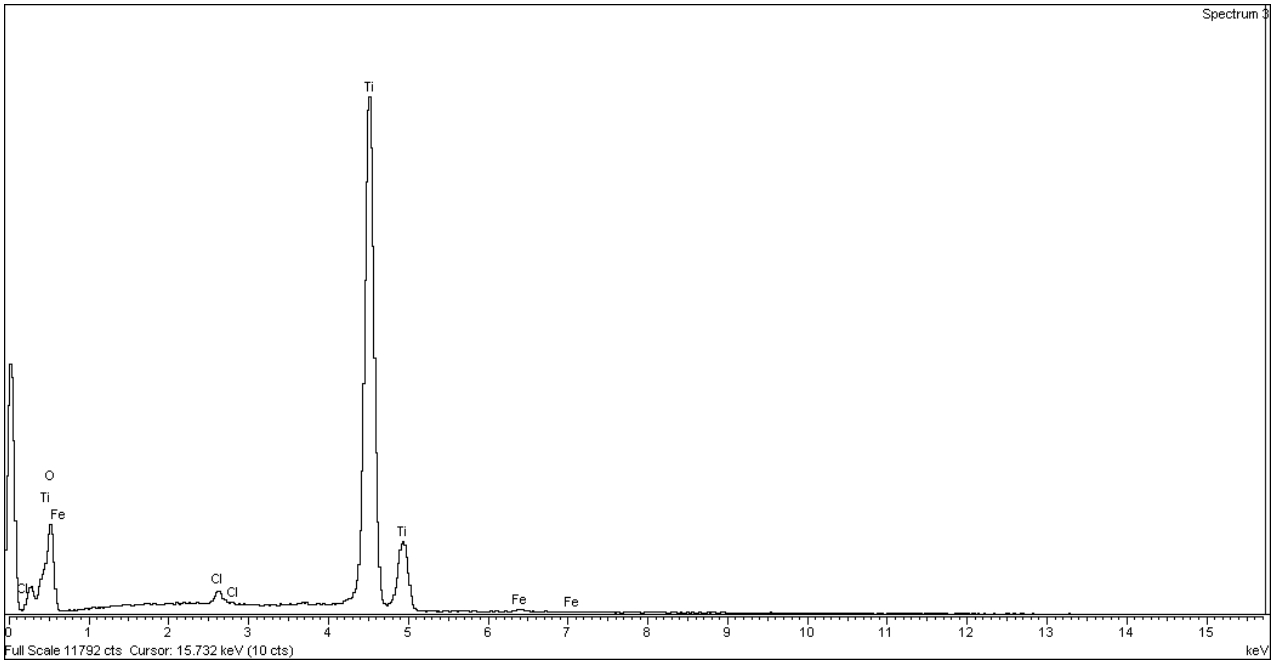

Sample 4

Spectrum	C	O	Cl	Ti	Fe	Total
Spectrum 1	1.47	47.54	2.99	47.43	0.57	100.00
Spectrum 2		50.40	2.94	45.99	0.67	100.00
Spectrum 3	1.08	50.79	2.76	44.75	0.63	100.00
Max.	1.47	50.79	2.99	47.43	0.67	
Min.	1.08	47.54	2.76	44.75	0.57	

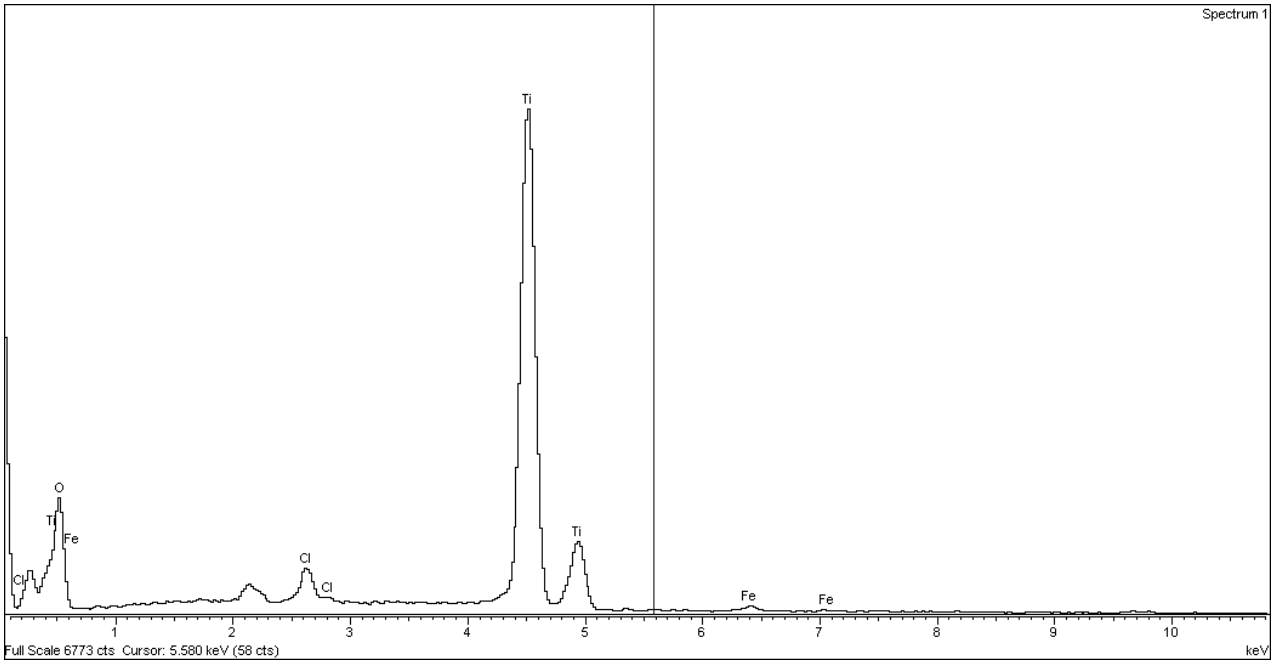

Sample 5

Spectrum	O	Cl	Ti	Fe	Total
Spectrum 1	48.33	1.68	49.06	0.92	100.00
Spectrum 2	47.94	1.65	49.56	0.86	100.00
Spectrum 3	45.05	1.92	52.24	0.78	100.00
Max.	48.33	1.92	52.24	0.92	
Min.	45.05	1.65	49.06	0.78	

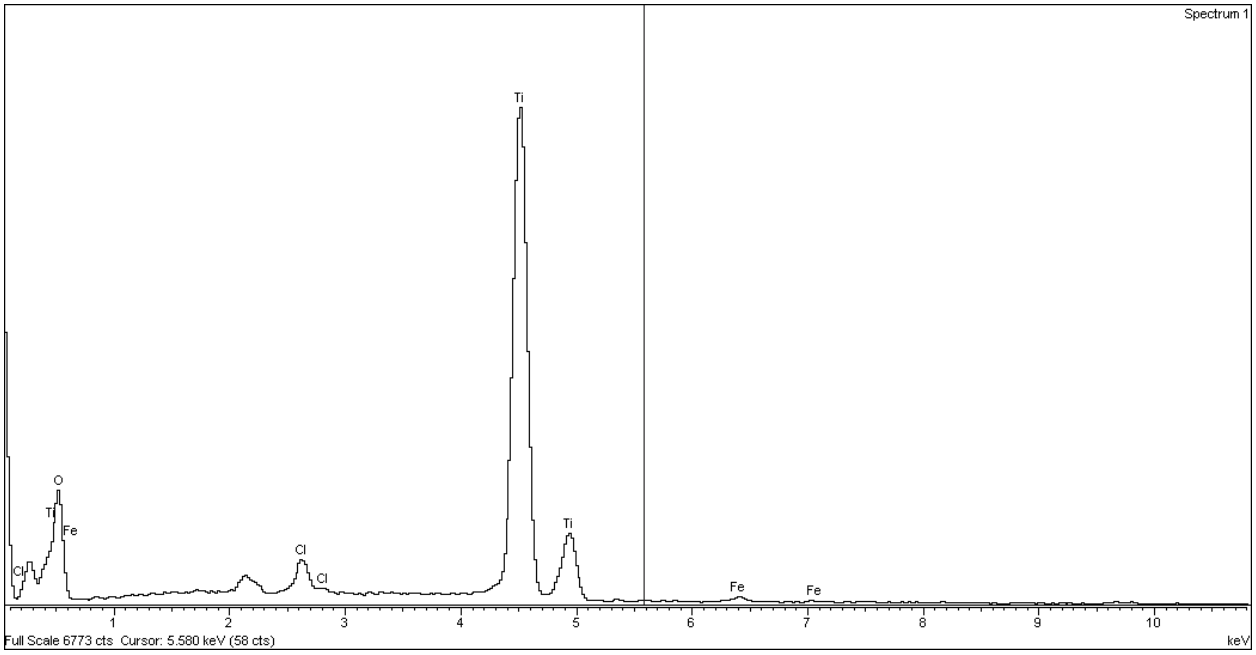

Sample 6

Spectrum	O	Cl	Ti	Fe	Total
Spectrum 1	53.09	0.80	45.34	0.77	100.00
Spectrum 2	47.57	0.86	50.62	0.95	100.00
Spectrum 3	47.84	0.88	50.42	0.86	100.00
Max.	53.09	0.88	50.62	0.95	
Min.	47.57	0.80	45.34	0.77	

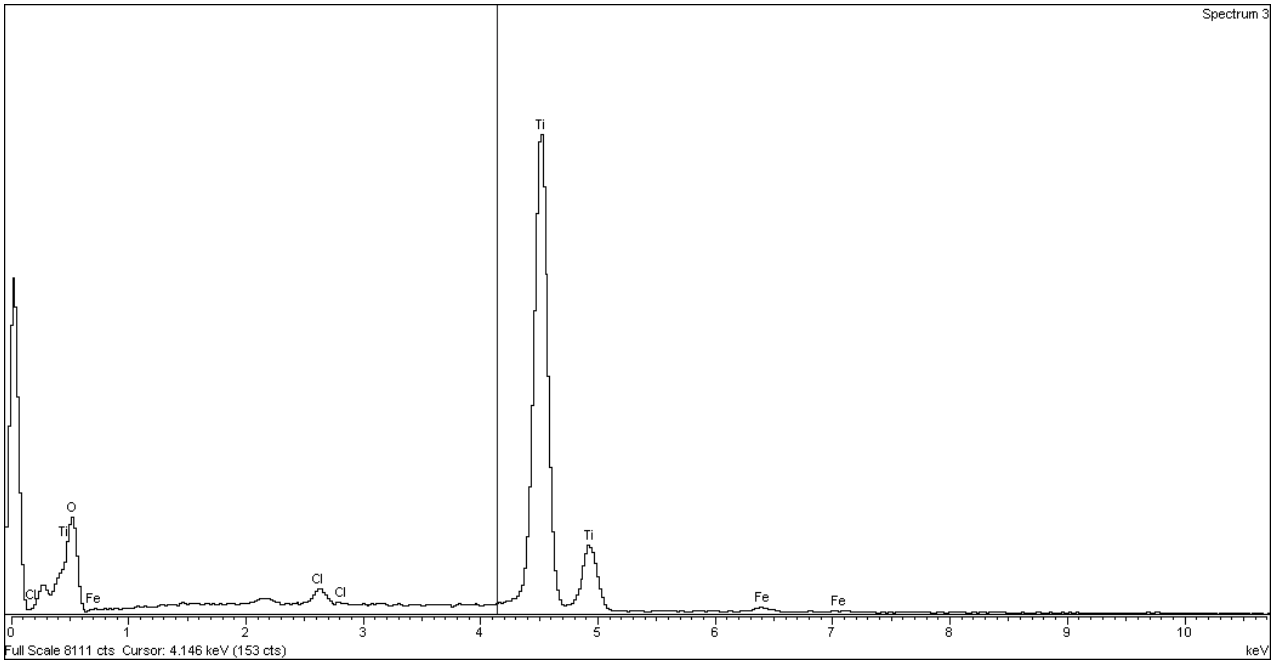

Sample 7

Spectrum	O	Cl	Ti	Fe	Total
Spectrum 1	51.09	1.68	46.43	0.81	100.00
Spectrum 2	50.08	1.75	47.15	1.01	100.00
Spectrum 3	49.65	1.87	47.73	0.75	100.00
Max.	51.09	1.87	47.73	1.01	
Min.	49.65	1.68	46.43	0.75	

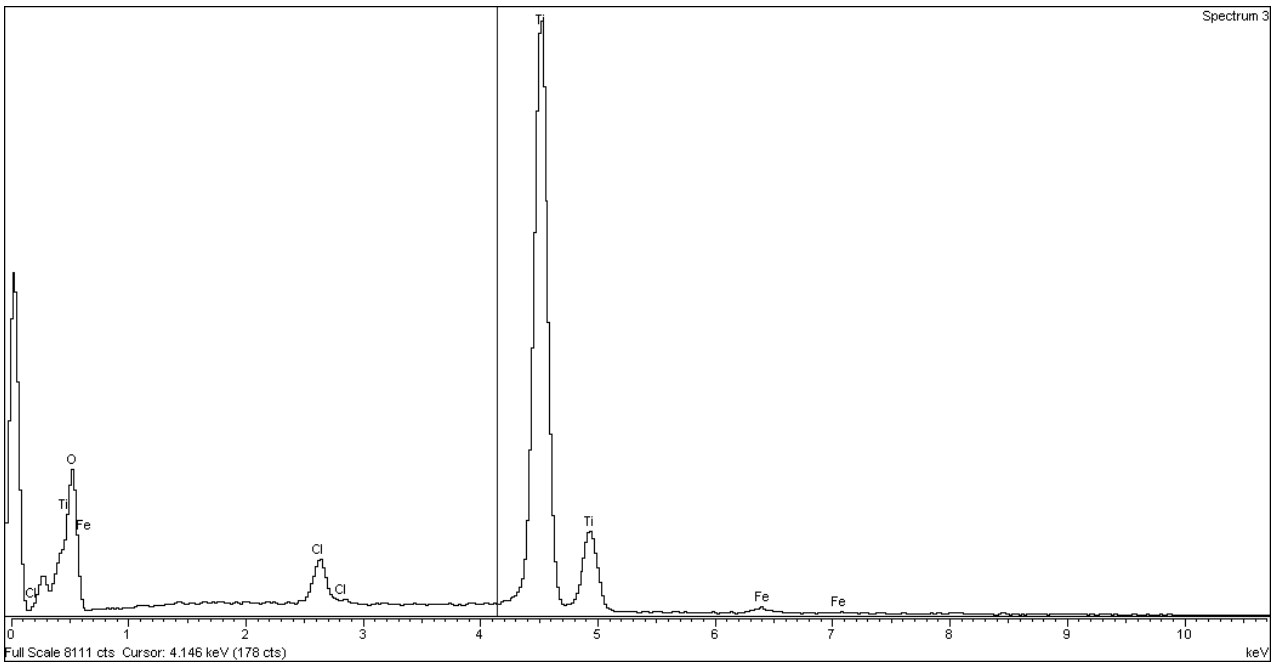

Sample 8

Spectrum	O	Cl	Ti	Fe	Total
Spectrum 1	50.09	1.61	47.49	0.81	100.00
Spectrum 2	49.05	1.74	48.46	0.75	100.00
Spectrum 3	45.98	1.64	51.30	1.08	100.00
Max.	50.08	1.74	51.30	1.08	
Min.	45.98	1.61	47.49	0.75	

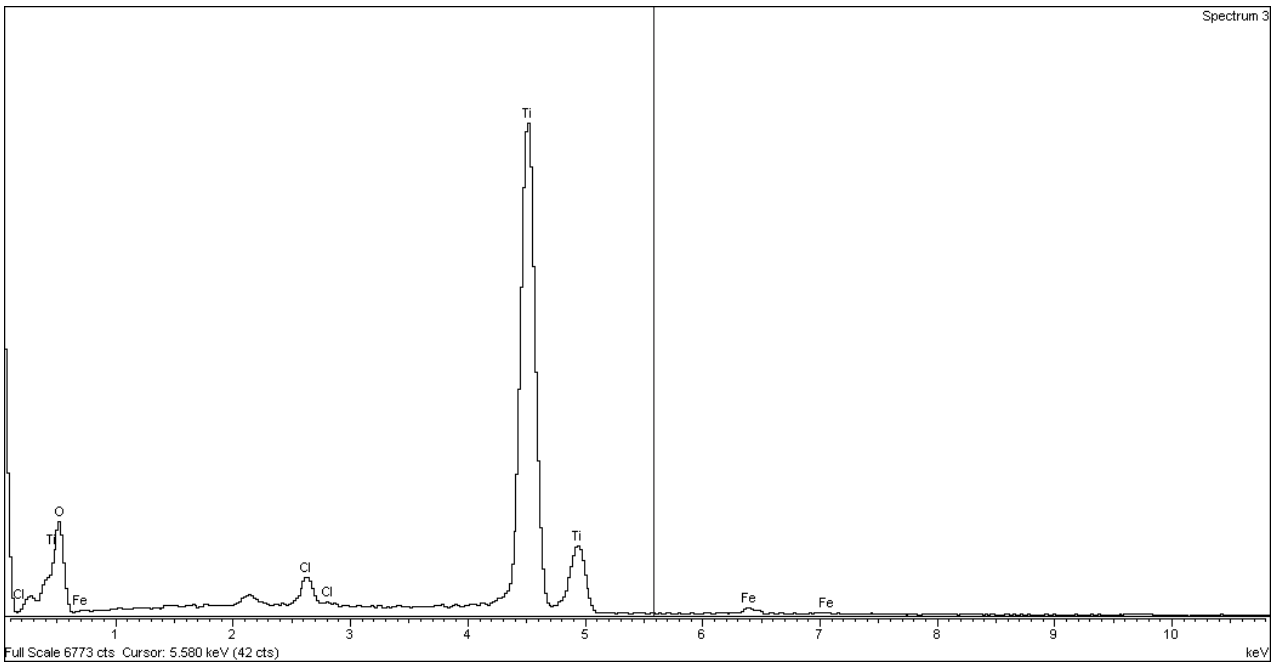

Sample 9

Spectrum	O	Cl	Ti	Fe	Total
Spectrum 1	50.28	0.78	48.20	0.75	100.00
Spectrum 2	48.92	0.82	49.18	1.07	100.00
Spectrum 3	50.37	0.85	47.90	0.89	100.00
Max.	50.37	0.85	49.18	1.07	
Min.	48.92	0.78	47.90	0.75	

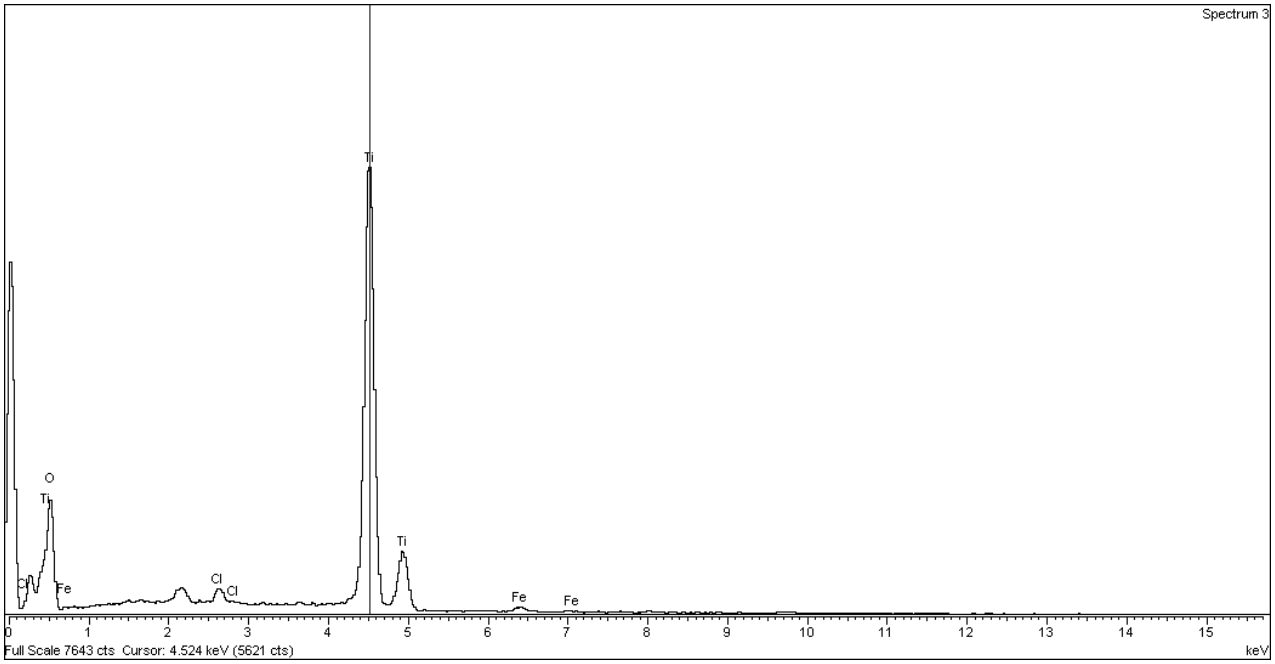

V-doped titanium dioxide

Sample 1

Spectrum	O	Cl	Ti	V	Total
Spectrum 1	42.99	2.69	53.62	0.70	100.00
Spectrum 2	48.22	3.25	47.97	0.56	100.00
Spectrum 3	33.97	2.49	62.61	0.94	100.00
Max.	48.22	3.25	62.61	0.94	
Min.	33.97	2.49	47.97	0.56	

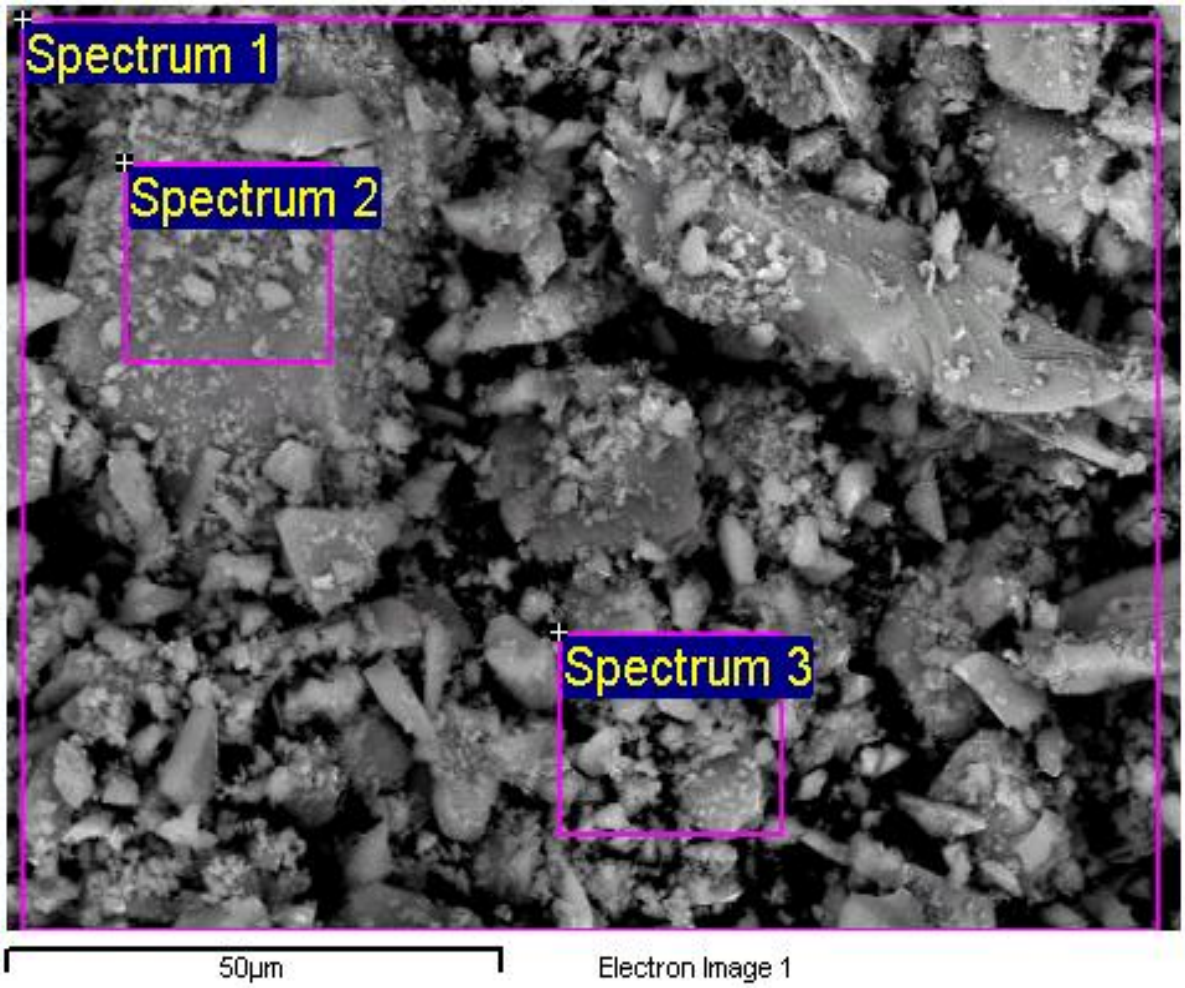
Spectrum 1
Spectrum 2
Spectrum 3
50µm
Electron Image 1

Sample 2

Spectrum	O	Cl	Ti	V	Total
Spectrum 1	40.39	1.62	56.97	1.02	100.00
Spectrum 2	37.50	1.66	60.16	0.68	100.00
Spectrum 3	42.51	1.76	54.87	0.86	100.00
Max.	42.51	1.76	60.16	1.02	
Min.	37.50	1.62	54.87	0.68	

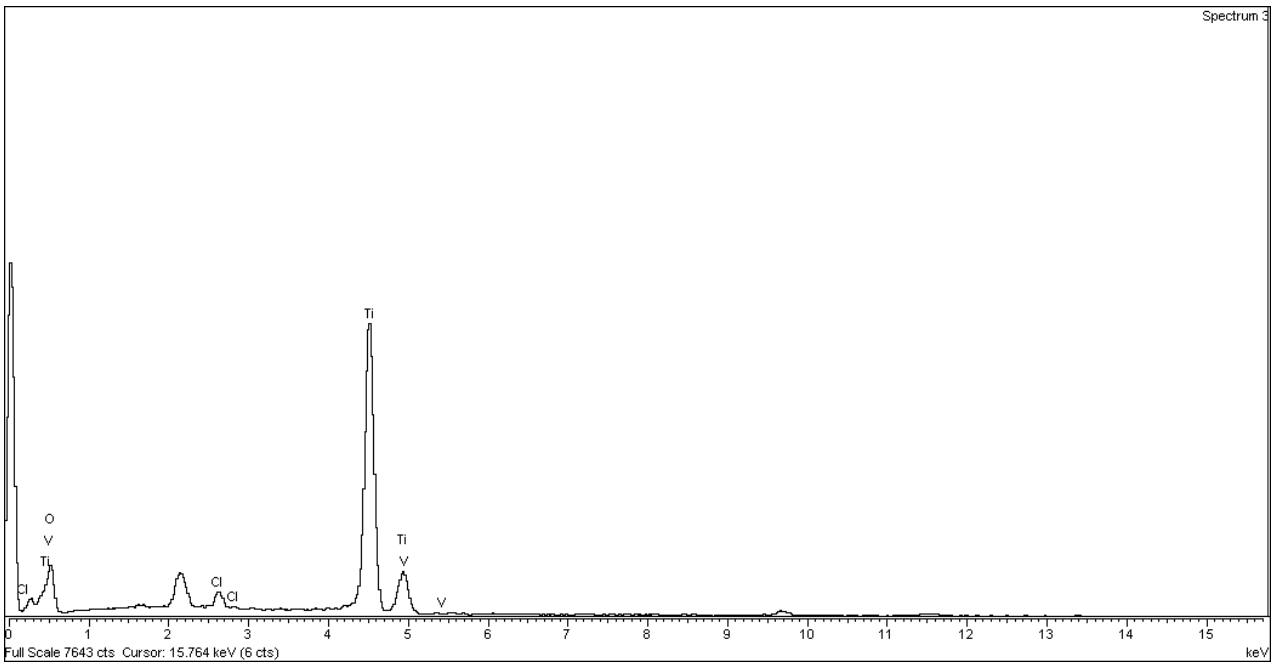

Sample 3

Spectrum	O	Cl	Ti	V	Total
Spectrum 1	40.63	0.85	57.33	1.18	100.00
Spectrum 2	37.10	0.73	61.27	0.90	100.00
Spectrum 3	38.24	0.92	60.29	0.55	100.00
Max.	40.63	0.92	61.27	1.18	
Min.	37.10	0.73	57.33	0.55	

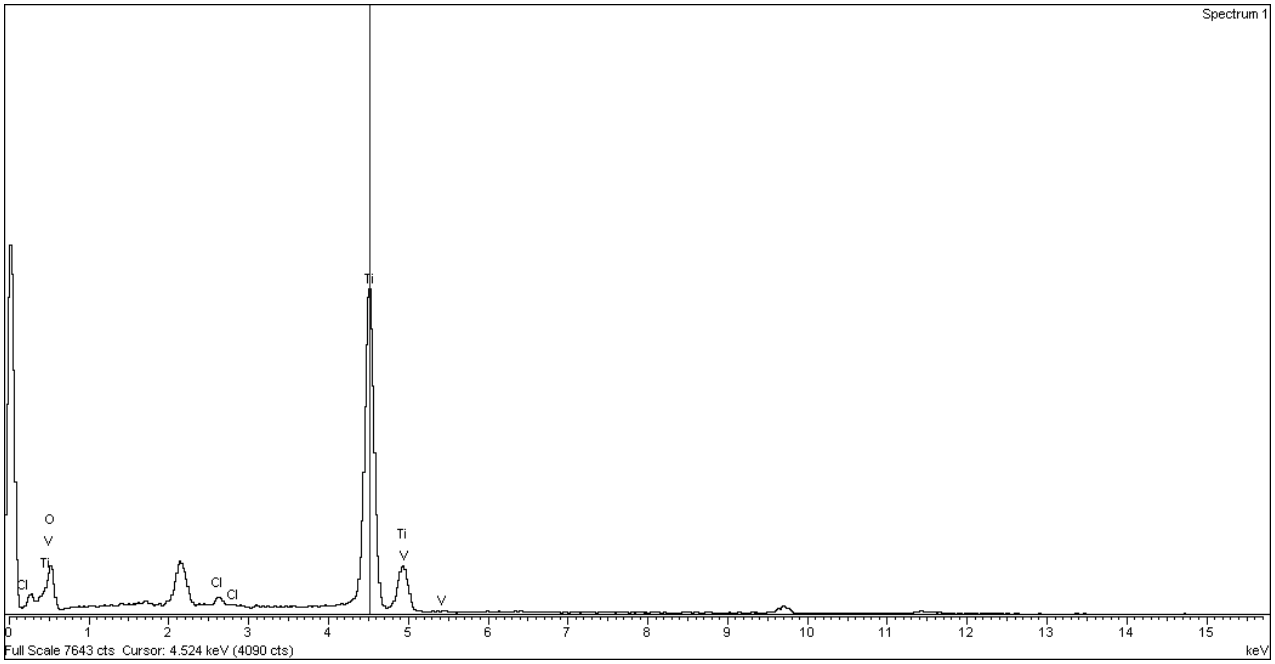

Sample 4

Spectrum	O	Cl	Ti	V	Total
Spectrum 1	41.64	2.57	54.19	1.60	100.00
Spectrum 2	41.03	2.34	55.65	0.98	100.00
Spectrum 3	45.77	2.35	50.59	1.30	100.00
Max.	45.77	2.57	55.65	1.60	
Min.	41.03	2.34	50.59	0.98	

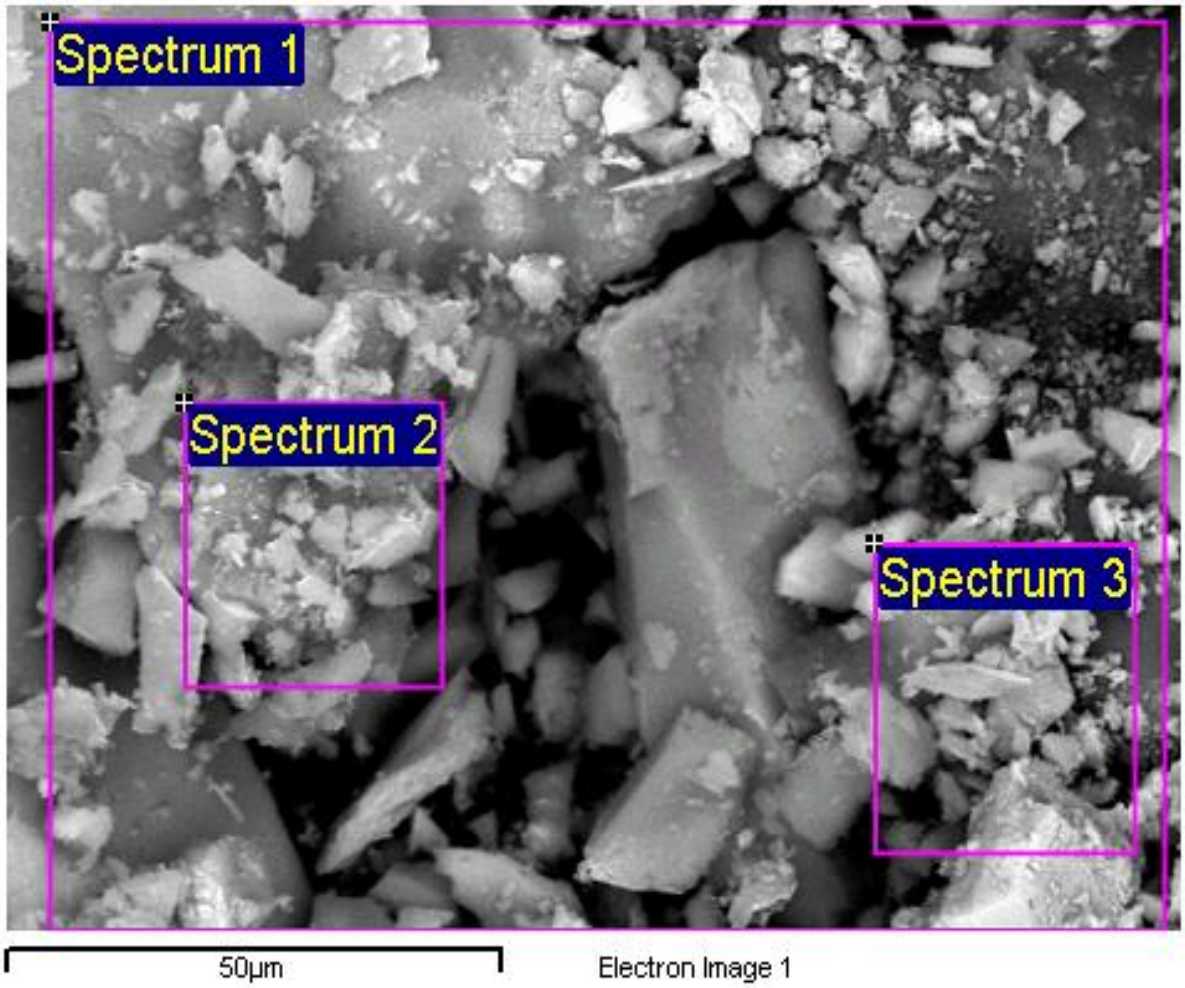
Spectrum 1
Spectrum 2
Spectrum 3
50µm
Electron Image 1

Sample 5

Spectrum	O	Cl	Ti	V	Total
Spectrum 1	41.83	1.88	54.77	1.53	100.00
Spectrum 2	43.96	1.75	52.20	2.09	100.00
Spectrum 3	40.53	2.18	56.04	1.25	100.00
Max.	43.96	2.18	56.04	2.09	
Min.	40.53	1.75	52.20	1.25	

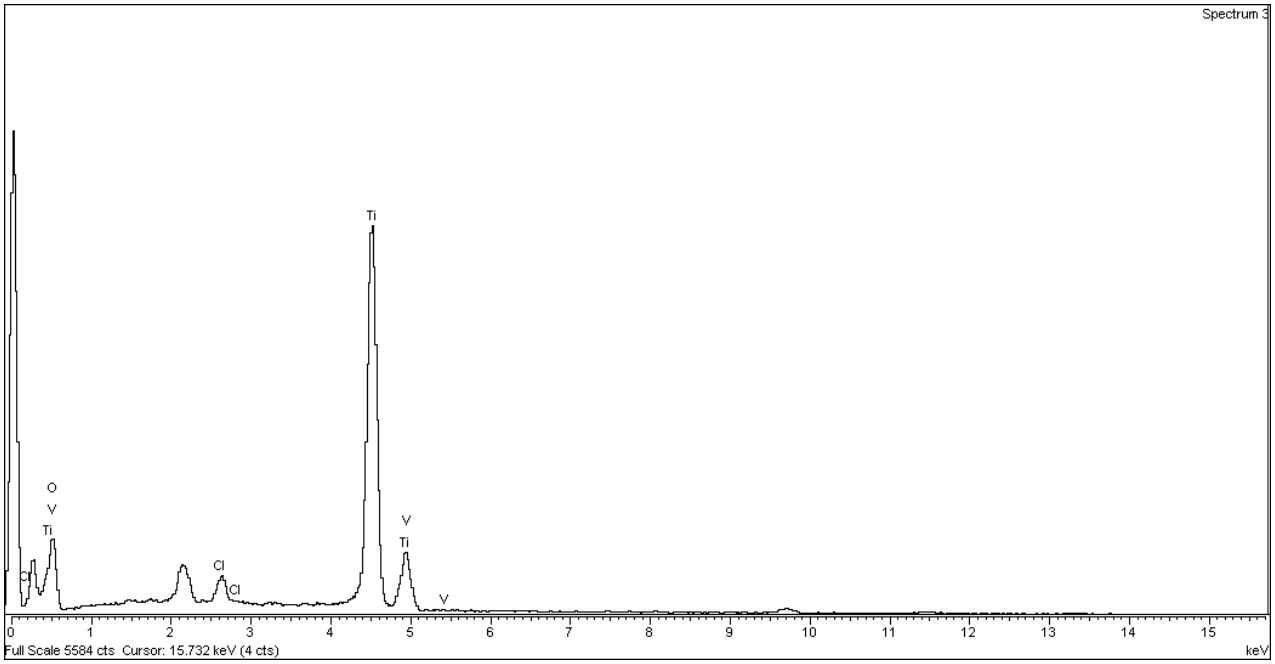

Sample 6

Spectrum	O	Cl	Ti	V	Total
Spectrum 1	42.62	2.16	53.62	1.61	100.00
Spectrum 2	41.43	1.85	55.22	1.49	100.00
Spectrum 3	41.32	1.99	54.76	1.93	100.00
Max.	42.62	2.16	55.22	1.93	
Min.	41.32	1.85	53.62	1.49	

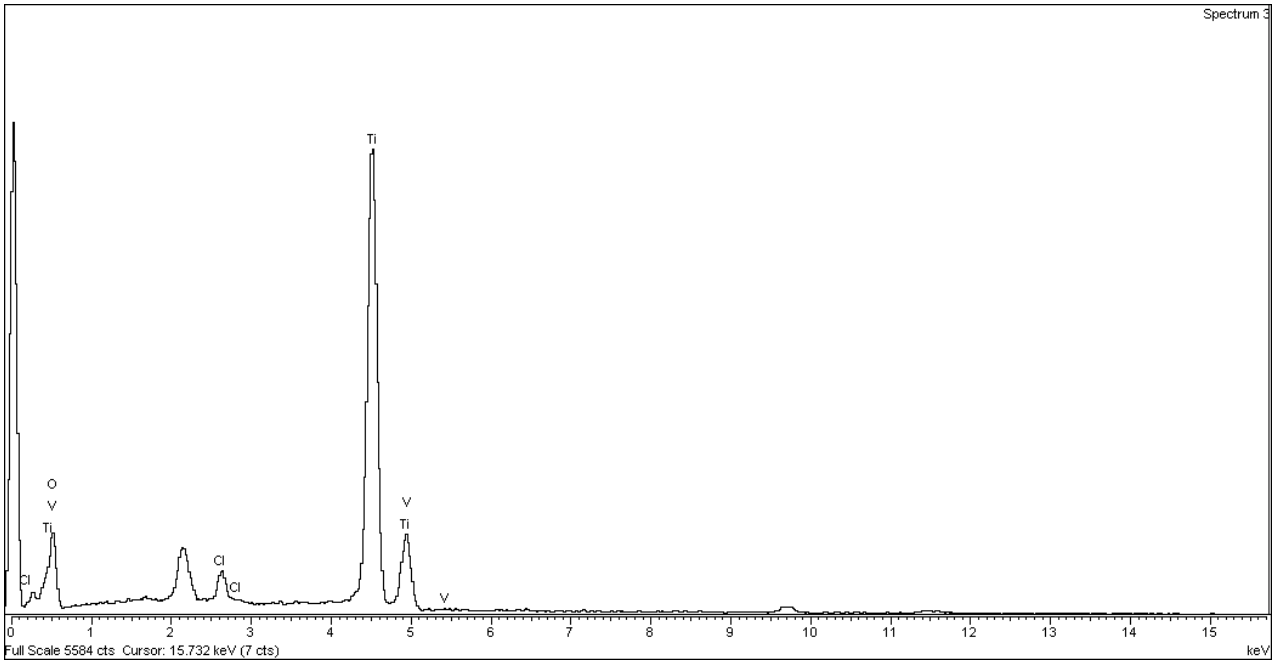

ANOVA interactions for heavy metals reduction

Pb (II) by W-doped titanium dioxide

Level average - Interactions

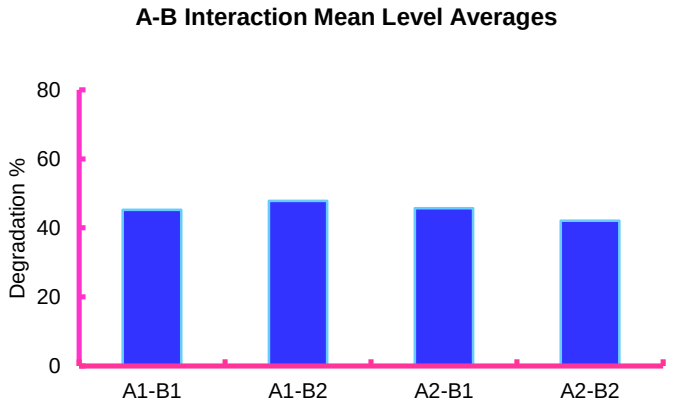

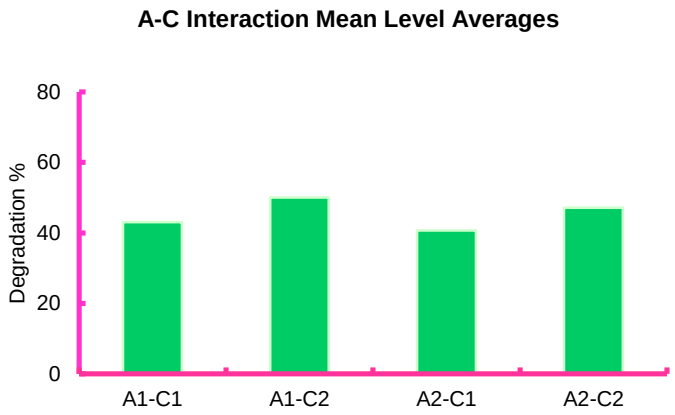

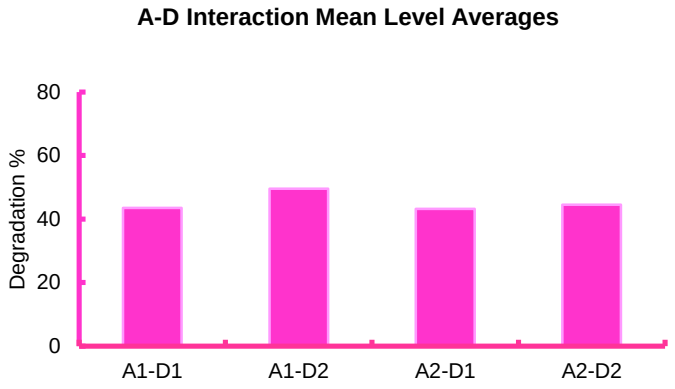

B-C Interaction Mean Level Averages

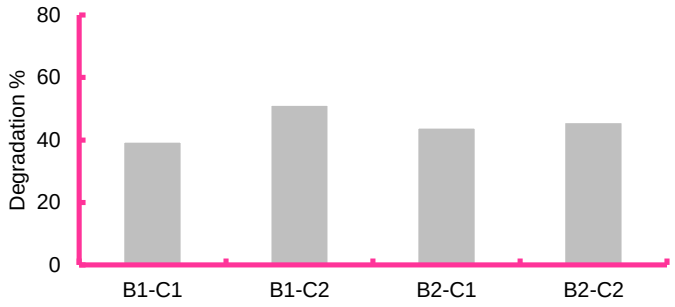

B-D Interaction Mean Level Averages

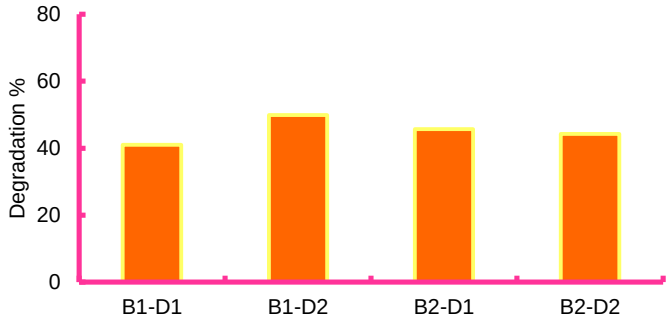

C-D Interaction Mean Level Averages

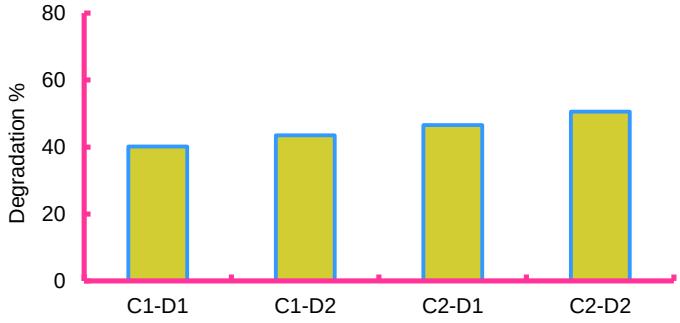

Zn (II) by Fe-doped titanium dioxide

Level average - Interactions

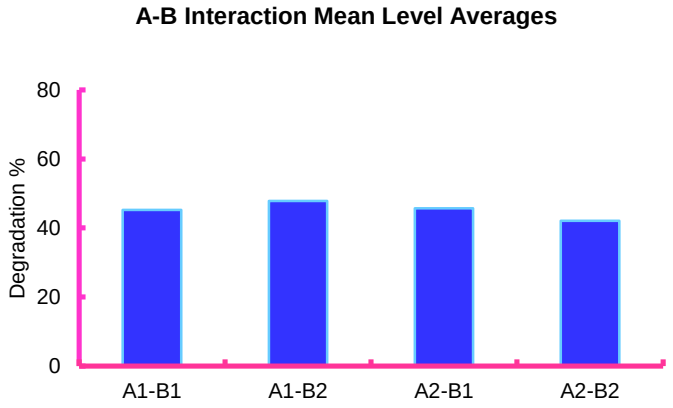

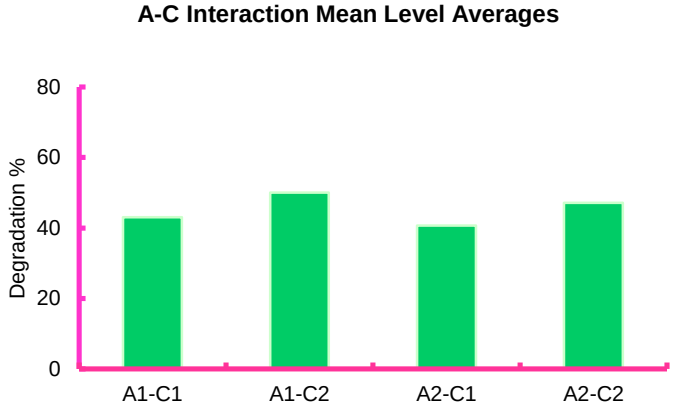

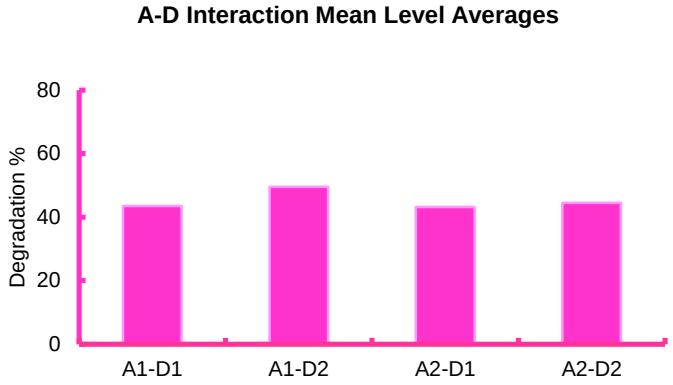

B-C Interaction Mean Level Averages

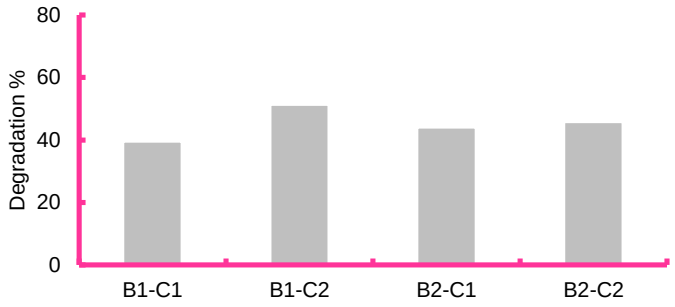

B-D Interaction Mean Level Averages

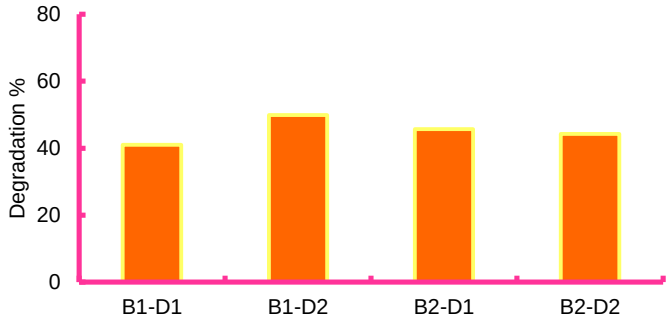

C-D Interaction Mean Level Averages

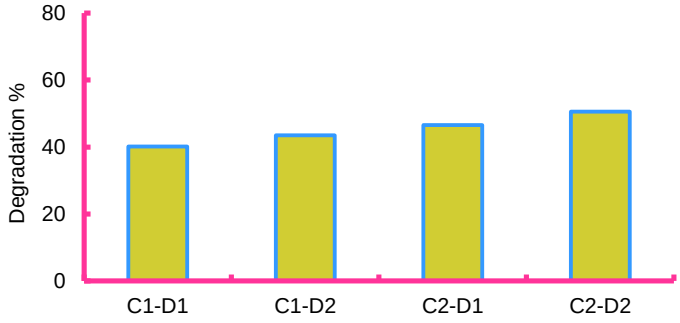

Cd (II) by V-doped titanium dioxide

Level Average - Interactions

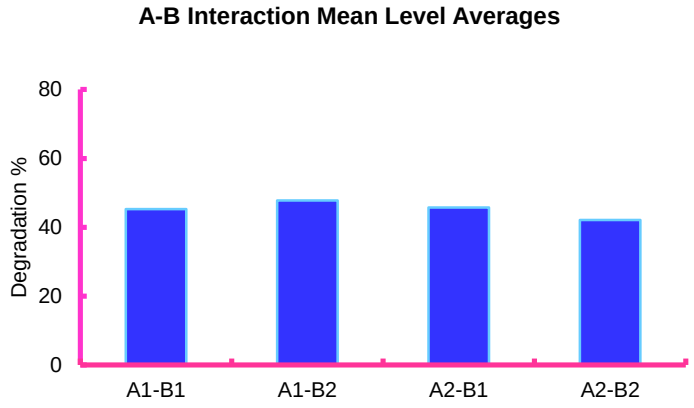

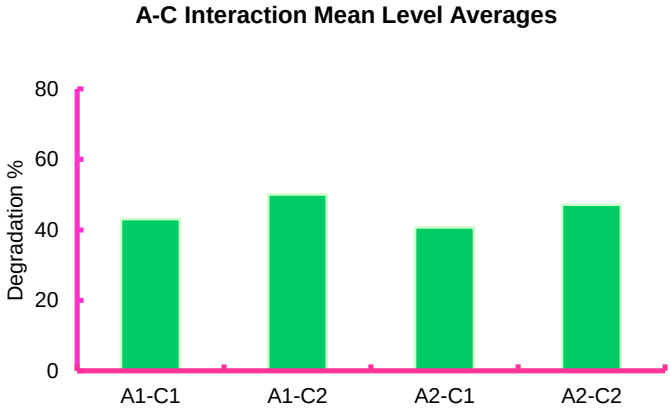

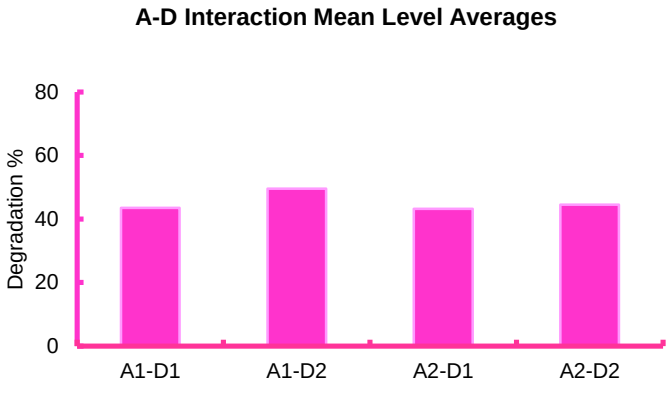

B-C Interaction Mean Level Averages

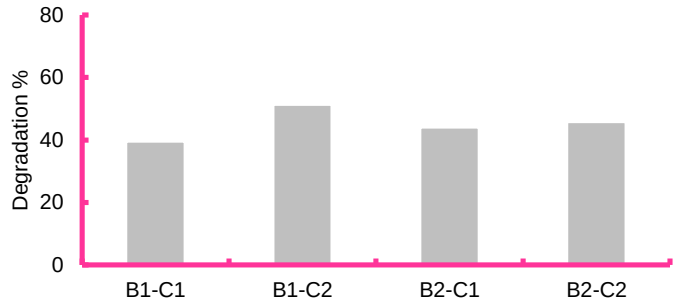

B-D Interaction Mean Level Averages

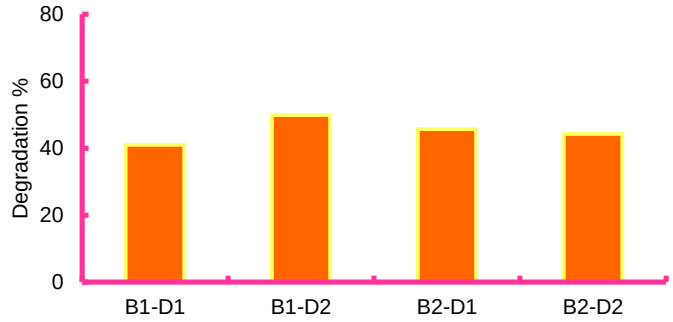

C-D Interaction Mean Level Averages

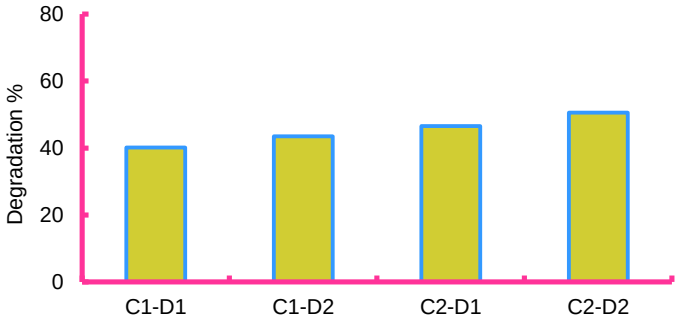

VITAE

Mousab Salah Eldeen Mirghani Mohammed, holds the Sudanese nationality. He graduated in 2005 with a B.Sc. (HONOUR) in Chemical engineering with first class from faculty of Engineering and Technology, Gezira University, Sudan. After graduation, he has been selected to work as a teaching assistant and potential lecturer in petroleum transportation and refining department at Sudan University of Science and Technology (SUST). In 2007, Mousab has attained his Master of Science (MS) degree in chemical engineering from Petronas University of Technology

In October 2008, Mousab joined KFUPM as a Lecturer-B to pursue the Doctor of philosophy (PhD) degree in Chemical engineering. Mousab's research interest includes Catalysis, including synthesis of Nano-sized semiconductors, Photocatalysis, and wastewater treatment.

E-mail: gaily8105@yahoo.com.

Phone: +966 550913463 , +249910515015.